

UC San Diego

UC San Diego Electronic Theses and Dissertations

Title

Intracellular and extracellular interactions of the low density lipoprotein receptor related protein (LRP-1)

Permalink

<https://escholarship.org/uc/item/9f51k7wk>

Author

Guttman, Miklos

Publication Date

2009

Peer reviewed|Thesis/dissertation

UNIVERSITY OF CALIFORNIA, SAN DIEGO

Intracellular and Extracellular Interactions of the Low Density Lipoprotein
Receptor Related Protein (LRP-1)

A dissertation submitted in partial satisfaction of the
requirements for the degree Doctor of Philosophy

in

Chemistry

by

Miklos Guttman

Committee in charge:

Professor Elizabeth Komives, Chair
Professor Tracy Handel
Professor Kim Prather
Professor Susan Taylor
Professor Hector Viadiu-Illaraza

2009

Copyright©

Miklos Guttman, 2009

All rights reserved.

The dissertation of Miklos Guttman is approved, and it is acceptable in
quality and form for publication on microfilm and electronically:

Chair

University of California, San Diego

2009

TABLE OF CONTENTS

Signature Page.....	iii
Table of Contents.....	iv
List of Symbols and Abbreviations.....	vi
List of Figures.....	ix
List of Tables.....	xi
Acknowledgements.....	xii
Vita, Publications, Fields of Study.....	xiv
Abstract of the Dissertation.....	xvi
CHAPTER 1.....	1
Introduction	
The LDL family of receptors.....	2
The LDL-receptor (LDLR).....	5
Apolipoprotein E.....	7
LDL-receptor related protein (LRP-1).....	8
Cytoplasmic interactions of LDLRs.....	11
Goals of dissertation.....	13
References.....	14
CHAPTER 2.....	22
Expression Refolding and Characterization of CR domains	
Introduction.....	23
Materials and Methods.....	25
Results.....	28
Discussion.....	39
References.....	45

CHAPTER 3.....	49
Properties of Ligand Binding Modules Governing the Interaction with ApoE	
Introduction.....	50
Materials and Methods.....	54
Results.....	59
Discussion.....	75
References.....	83
 CHAPTER 4.....	 89
Structure of the Minimum Interface between ApoE and LRP	
Introduction.....	90
Materials and Methods.....	92
Results.....	99
Discussion.....	124
References.....	138
 CHAPTER 5.....	 144
Interactions of the NPXY Microdomains of LRP-1	
Introduction.....	145
Materials and Methods.....	147
Results.....	155
Discussion.....	165
References.....	178

LIST OF SYMBOLS AND ABBREVIATIONS

LDL	Low density lipoprotein
VLDL	Very low density lipoprotein
LDLR	LDL- Receptor
LRP	LDLR-Related Protein
sLRP	soluble LRP
VLDLR	VLDL-Receptor
CR	Complement repeat
LA	Ligand binding module
GST	Glutathione-S-Transferase
RAP	Receptor Associated Protein
α 2M	Alpha-2-macroglobulin
ApoE	Apolipoprotein E
β -VLDL	Beta-very low density lipoprotein
EDTA	Ethylenediaminetetraacetic acid
HEPES	4-(2-Hydroxyethyl)-1-piperazineethanesulfonic acid
TCEP	(tris(2-carboxyethyl)phosphine)
HPLC	High performance liquid chromatography
SDS-PAGE	Sodium dodecyl sulfate-polyacrylamide gel electrophoresis
NMR	Nuclear magnetic resonance
TOCSY	Total correlation spectroscopy
NOE	Nuclear Overhauser effect
NOESY	Nuclear Overhauser effect spectroscopy

COSY	Correlation spectroscopy
HSQC	Heteronuclear single quantum coherence
hNOE	^1H - ^{15}N heteronuclear NOE
R1	Longitudinal relaxation rate
R2	Transverse relaxation rate
ppm	parts per million
HDX	Hydrogen Deuterium exchange
RMSD	Root mean square deviation
MALDI-TOF	Matrix assisted laser desorption ionization- time of flight
AUC	Analytical ultracentrifugation
CD	Circular dichroism
kDa	kiloDalton
SPR	Surface plasmon resonance
K_D	Dissociation equilibrium constant
NC	Negative control
Std	Standard
HMW	High molecular weight
PCR	Polymerase chain reaction
APP	Amyloid precursor protein
CAMKII	Calmodulin-dependent kinase II
CSK	C-src kinase
HA	Influenza hemagglutinin protein

LRP1-CT	LRP1 cytoplasmic domain (amino acids 4745-4807)
MEF	Mouse embryonic fibroblasts
MUDPIT	Multidimensional protein identification technology
PDGF	Platelet-derived growth factor
PI3K	Phosphoinositide-3 kinase
PTB	Phosphotyrosine binding domain
Snx17	Sorting nexin 17

LIST OF FIGURES

Figure 1.1:	Mechanism of receptor mediated endocytosis.....	4
Figure 1.2:	Schematic of three members of the LDL receptor family	6
Figure 1.3:	Crystal structure of Apolipoprotein E.....	10
Figure 2.1:	SDS-PAGE analysis of expression and purification CRs.....	30
Figure 2.2:	^1H , ^{15}N HSQC spectra of each CR/LA.....	35
Figure 2.3:	Analytical RP-HPLC of denaturing vs. native conditions.....	36
Figure 2.4:	^1H , ^{15}N HSQC of LA4 after native HPLC purification.....	37
Figure 2.5:	Calcium binding isotherms of each individual CR/LA	38
Figure 2.6:	Calcium binding of LA45, CR16-18 and LA4 at pH 5.2.....	40
Figure 2.7:	Affinity pulldown assays of CR16-18 with ApoE(130-149).....	42
Figure 3.1:	Schematic diagram of LRP, LDL, and VLDL	52
Figure 3.2:	Binding of smaller units of CR16-18 to ApoE(130-149).....	62
Figure 3.3:	NMR titration of Ub-ApoE(130-149) into each CR/LA.....	63
Figure 3.4:	NMR titration of Ub-ApoE(130-149) into LA4-5 & CR16-18..	64
Figure 3.5:	Amide perturbations and plots of titrations.....	67
Figure 3.6:	NMR titration of Ub-RAPD3 into each CR/LA.....	70
Figure 3.7:	ApoE(130-149) affinity pulldowns with LA/CR constructs.....	72
Figure 3.8:	ApoE(1-191)-DMPC and GST-RAP pulldown assays.....	73
Figure 3.9:	Sequence alignments of LA4/VLA5 and LA5/VLA6 from various species.....	74
Figure 3.10:	Proposed models of how LDL receptors might bind ApoE-containing lipoprotein particles	82

Figure 4.1:	Perturbations of CR17 from binding various ligands.....	101
Figure 4.2:	Perturbations of ApoE(130-149) from CR17 binding.....	102
Figure 4.3:	Chemical shift index plot for ApoE(130-149).....	103
Figure 4.4:	Solution structure of CR17.....	106
Figure 4.5:	Calcium binding of CR17(K5A) and CR17-ApoE(130-149)...	109
Figure 4.6:	HSQC comparison of CR17 to CR17-ApoE(130-149).....	110
Figure 4.7:	Native tryptophan fluorescence of CR17 constructs.....	113
Figure 4.8:	NMR titrations with fusion and CR17(K5A) constructs.....	114
Figure 4.9:	Solution structure of CR17-ApoE(130-149).....	117
Figure 4.10:	Structural and dynamic consequences of ligand binding.....	118
Figure 4.11:	NMR perturbations within CR17-ApoE(130-149).....	119
Figure 4.12:	Relaxation measurements for CR17 constructs.....	123
Figure 4.13:	A different binding mode of ApoE(130-149) on CR17.....	131
Figure 4.14:	Comparison of receptor interactions in ApoE and RAP.....	136
Figure 5.1:	Anti pTyr blots of LRP-1 immuno-precipitates.....	158
Figure 5.2:	SDS-PAGE of proteins binding NPXpY 4507.....	159
Figure 5.3:	Analysis of binding proteins to each microdomain.....	161
Figure 5.4:	Effect of dephosphorylating NPXpY 4507 on binding.....	162
Figure 5.5:	Specific detection of interacting proteins	164
Figure 5.6:	Detection of interactions with recombinant proteins.....	167

LIST OF TABLES

Table 2.1: MALDI TOF analysis of expressed CR constructs.....	31
Table 2.2: Thermodynamics of calcium binding for each CR.....	41
Table 3.1: Binding affinities for various ApoE-LA/CR interactions.....	68
Table 4.1: CR17 & CR17-ApoE(130-149) refinement statistics.....	107
Table 5.1: LRP1 NPXpY ₄₅₀₇ interacting proteins.....	173
Table 5.2: LRP1 NPXpY ₄₅₀₇ interacting proteins.....	175
Table 5.3: LRP1 NPXpY ₄₄₇₃ interacting proteins.....	175
Table 5.4: LRP1 NPXY ₄₅₀₇ interacting proteins.....	176

ACKNOWLEDGEMENTS

First and foremost I would like to thank my advisor, Elizabeth Komives for her mentorship and encouragement throughout my graduate career. My fellow lab members, past and present, have all been tremendously helpful along the way. I would like to especially thank former graduate students J. Helena Prieto, Johnny E. Croy, and Gina Betts for paving the way for this project, and also Mela Mulvihill continuing the research in this area. It was a pleasure to work together with Jonathan Ostrem through the toughest parts of this project. Carla Cervantes has been greatly helpful in designing and analyzing NMR experiments. Thank you Simon Bergqvist, from whom I learned everything about calorimetry and ultracentrifugation, and Stephanie Truhlar who helped me with advice along the way. I would like to thank some of the senior scientists that have aided in my scientific growth. In particular, Justin Torpey and Majid Ghassemian, who maintained the mass spectrometry instrumentation, helped with much of the data collection and processing in this work. Your help was greatly appreciated.

Without the help of Peter J. Dommelle and Tracy M. Handel much of the structural work in the project would not have been possible. Much of the NMR work would also not have been possible without help from Xuemei Huang and Anthony Mrse, who maintain the NMR facilities. In addition Sangwon Lee generously took time to aid the setup of complicated triple resonance experiments. I wish also to thank the co-authors in manuscripts resulting from this work: J. Helena Prieto, Johnny E. Croy, Peter J. Dommelle, Tracy M. Handel, Gina N. Betts, Helen Barnes, Majid Ghassemian, and Peter van der Geer.

The work in this dissertation was funded by the NIH Heme Training Grant.

Chapter 3 is, in part, a reprint of a submitted manuscript in review: Miklos Decoding of lipoprotein – receptor interactions; Properties of ligand binding modules governing interactions with ApoE. Guttman, M., Prieto, J.H., Croy, J.E., Komives, E.A. (2009) *Submitted*. The dissertation author was the primary researcher and author of this manuscript.

Chapter 4 is, in part, a reprint of a submitted manuscript in preparation title: How the ApoE Receptor Binding Sequence binds LRP; Structure of the minimal interface between ApoE and LRP. Guttman, M., Prieto, J.H., Domaille, P. J., Handel, T. M., Komives, E.A. (2009) *manuscript in preparation*. The dissertation author was the primary researcher and author of this manuscript.

Chapter 5 is, in part, a reprint of a submitted manuscript in press: Interactions of the NPXY microdomains of the LDL Receptor-Related Protein 1. Guttman, M., Betts, G.N., Barnes, H., Ghassemian, M., van der Geer, P. and Komives, E.A. (2009) *Proteomics, in press*. The dissertation author was the primary researcher and author of this manuscript.

VITA

Education

B.S. in Biochemistry University of California, Irvine 1999-2003

M.S. in Chemistry University of California, San Diego 2003-2005

Ph.D. in Chemistry University of California, San Diego 2003-2009

Awards and Honors

Heme Training Grant 2005-2008

PUBLICATIONS

How the ApoE Receptor Binding Sequence binds LRP; Structure of the minimal interface between ApoE and LRP. Guttman, M., Prieto, J.H., Domaille, P. J., Handel, T. M., Komives, E.A. (2009) *manuscript in preparation*.

The solution structure of repeats 45 in LDLR reveal more than just beads on a string. Guttman, M., Komives, E.A. (2009) *manuscript in preparation*.

Decoding of lipoprotein – receptor interactions; Properties of ligand binding modules governing interactions with ApoE. Guttman, M., Prieto, J.H., Croy, J.E., Komives, E.A. (2009) *Submitted*.

Interactions of the NPXY microdomains of the LDL Receptor-Related Protein 1. Guttman, M., Betts, G.N., Barnes, H., Ghassemian, M., van der Geer, P. and Komives, E.A. (2009) *Proteomics, in press*.

An unexpected twist in viral capsid maturation. Gertsman I, Gan L, Guttman M, Lee K, Speir JA, Duda RL, Hendrix RW, Komives EA, Johnson JE. *Nature* 2009, 458(7238), 646-50.

FIELDS OF STUDY

Major Field: Biochemistry

Biochemistry: Studies in Biochemistry, Proteomics, and Structural Biology

ABSTRACT OF THE DISSERTATION

Intracellular and Extracellular Interactions of the Low Density Lipoprotein

Receptor Related Protein (LRP-1)

by

Miklos Guttman

Doctor of Philosophy in Chemistry

University of California, San Diego, 2009

Professor Elizabeth Komives, Chair

The LDLR family of receptors mediates the uptake of lipoprotein particles, and is essential for cholesterol homeostasis. The LDL receptor-related protein 1 (LRP-1) mediates internalization of a large number of diverse ligands and is widely implicated in Alzheimer's disease. Clusters of complement-type ligand binding repeats (CRs) in the LDL receptor family are thought to mediate the interactions between these receptors and their various ligands. Apolipoprotein E, a key ligand for cholesterol homeostasis, has been shown to interact with LDLR, LRP and VLDLR, through these clusters. LDLR and VLDLR each contain a single ligand-binding repeat cluster, whereas LRP contains three large clusters of ligand binding repeats, each with ligand binding functions.

In order to study smaller units of these ligand binding clusters we have engineered a new approach to express and refold complement repeat (CR) domains in *E. coli*. This successfully produced high yields of refolded protein with

the benefit of inexpensive isotope labeling for NMR studies. We have expressed a subdomain of sLRP3 (CR16-18) that has previously been shown to recapitulate ligand binding to the isolated receptor binding portion of ApoE (residues 130-149). Binding experiments with the ApoE recognition region of LDLR (LA3-5) and CR16-18 showed that each CR could interact with ApoE(130-149) and that a conserved W25/D30 pair within each repeat appears critical for high affinity. The triple repeat LA3-5 showed the expected interaction with the lipid complexed ApoE(1-191)•DMPC, but surprisingly CR16-18 did not interact with this form of ApoE. To understand these differences in ApoE binding affinity, we introduced mutations of conserved residues from LA5 into CR18, and produced a CR16-18 variant capable of binding ApoE(1-191)•DMPC. This change cannot fully be accounted for by the interaction with ApoE's proposed receptor binding region, therefore we speculate that LA5 is recognizing a distinct epitope on ApoE that may only exist in the lipid bound form. The combination of avidity effects with this distinct recognition process likely governs the ApoE-LDL receptor interaction.

Since even the strongest interaction between ApoE(130-149) and a single repeat (CR17) was relatively weak, we constructed a CR17-ApoE(130-149) fusion protein to stabilize the interface for structural studies. The structure revealed a motif seen previously in all ligand CR interactions, in which lysine residues of the ligand interact with the calcium binding site of the CR. Like many ligands of CRs ApoE(130-149) binds as a helix, but with an unexpected turn at H140. These studies also revealed that little structural rearrangement occurs within CR17 upon binding. In addition, dynamics measurements of the free and

bound CR17 reveal that certain regions become more ordered, while others become less ordered upon binding.

The cytoplasmic tail of LRP, containing two NPXY motifs, has been implicated in the onset of Alzheimer's disease. To examine the intracellular interactions of LRP, as well as to separate which proteins bind to each NPXY motif and their phosphorylation dependence, each NPXY motif microdomain was prepared in both phosphorylated and non-phosphorylated forms and used to probe rodent brain extracts for binding proteins. Proteins that bound specifically to the microdomains were identified by LC-MS/MS, and confirmed by western blot. Recombinant proteins were then tested for binding to each NPXY motif. The NPXY₄₅₀₇ (membrane distal) was found to interact with a large number of proteins, many of which only bound the tyrosine-phosphorylated form. This microdomain also bound a significant number of other proteins in the unphosphorylated state. Many of the interactions were later confirmed to be direct with recombinant proteins. The NPXY₄₄₇₃ (membrane proximal) bound many fewer proteins and only to the phosphorylated form.

Chapter 1
Introduction

1.1 The LDLR family of receptors

Cholesterol transport and homeostasis is a critical function of the circulatory system. Disruption of blood cholesterol levels can lead to several diseases including hypercholesterolemia. Patients with familial hypercholesterolemia develop atherosclerosis early in life. Since cholesterol is only marginally water soluble, it is transported through the blood packaged as lipoprotein particles containing phospholipids and apolipoproteins at the surface. Cell surface receptors of the low density lipoprotein (LDL) receptor family recognize these lipoproteins and mediate the uptake and clearance of the various types of LDL particles. The receptors internalize bound ligands through - mediated endocytosis (Fig. 1.1) (Herz and Strickland 2001). After the clathrin coated pits bud off from the plasma membrane to form endosomes there is a gradual decrease in pH, which is thought to trigger the receptors to release bound ligands (Rudenko and Deisenhofer 2003). Ligands are then trafficked to various cellular compartments, and the receptor is recycled back to the cell surface. This receptor internalization cycle occurs at a constant rate regardless of whether or not ligand is actually bound.

Members of the LDLR family share many structural characteristics and sequence homology including an extracellular ligand binding domain consisting of complement-type repeats (CRs), also called ligand binding modules (LAs), epidermal growth factor precursor homology repeats (EGFs), β -propeller domains, and a single transmembrane segment with an intracellular domain containing NPXY motifs (Fig. 1.2). The clusters of CRs recognize and bind

ligands. Each individual CR/LA is composed of 40-50 amino acids with a well conserved fold stabilized by three disulfide bonds with a C1-C3, C2-C5, C4-C6 disulfide-bonding pattern. A cluster of acidic residues in the C terminal half along with two backbone carbonyls form a high affinity calcium binding site. This calcium binding has been shown to be critical for the folding of each CR and the binding of most ligands. Mutations of disulfide bonding cysteines and residues at the calcium binding site disrupt proper folding and are associated with familial hypercholesterolemia (Blacklow and Kim 1996). Several CR domains have now been solved by both NMR and crystallographic methods (Rudenko and Deisenhofer 2003), and show very little deviation in their overall fold. The high variability in short loops results in different surface contours and electrostatics within each CR, and this is thought to establish ligand specificity (Huang et al. 1999; Blacklow 2007).

The EGF and β -propeller domains have been shown to be critical for ligand release and receptor recycling (Davis 1987). In the case of LDLR at endosomal pH (5.2) the β -propeller domain forms a stable intra-molecular interaction with two CRs, and this process is thought to displace bound ligands (Rudenko et al. 2002). A stable interaction between LA7 and the neighboring EGF repeat in LDLR has been shown to position the β -propeller domain close to the cluster of CRs, also aiding in ligand release (Beglova et al. 2004). It has been speculated that the decrease in calcium concentrations within the endosome plays a role in ligand dissociation as the calcium affinity for certain CRs significantly weakens at lower pH (Simonovic 2001). Very recent evidence

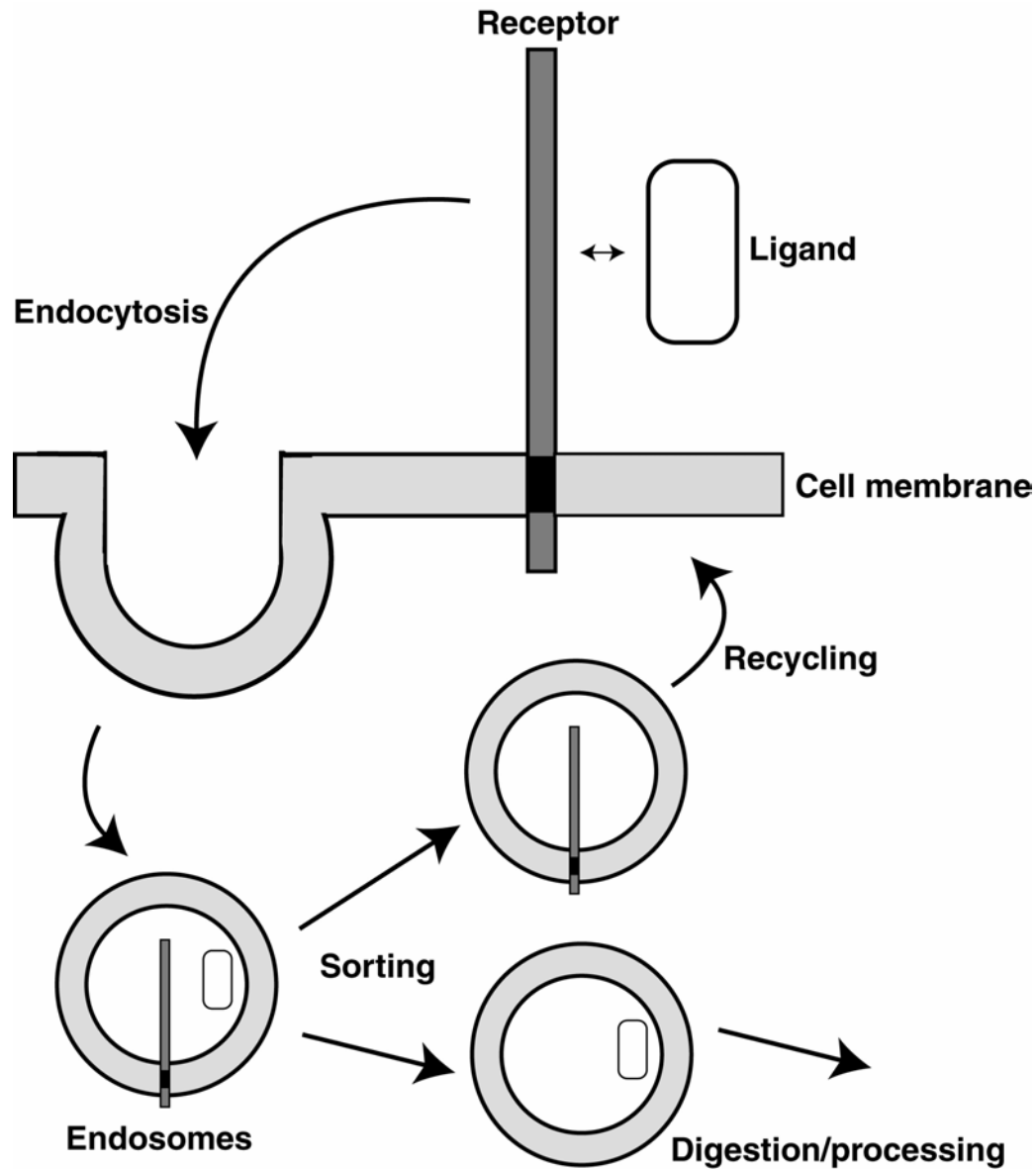


Figure 1.1: Mechanism of receptor mediated endocytosis. Ligands bind to the surface of a receptor and are taken into cells via clathrin coated endocytosis. Within the endosome the ligands dissociate from the receptor and are sorted for digestion while the receptor is recycled back to the cell surface.

suggests that while certain ligands depend on decreasing pH for their release, others are thought to rely on decreasing calcium binding (Zhao and Michaely 2009).

The C-terminal intracellular domain of these receptors interacts with several proteins regulating the function of the receptor. Phosphorylation of residues in the intracellular domain modulates the interactions with various binding partners and regulates internalization (Li et al. 2001; Loukinova et al. 2002; Ranganathan et al. 2004). The NPXY motifs are thought to mediate receptor internalization as mutation of residues within these motifs alters the rate at which receptors are internalized (Lee et al. 2008). The NPXY motifs can also be tyrosine phosphorylated and bind to SH2 and PTB domains, playing a role in signal transduction (Barnes et al. 2003).

1.2 The LDL-Receptor

The most well characterized member of this family is the LDL-Receptor (LDLR) (Blacklow 2007). LDLR is thought to play the largest role in cholesterol uptake (Brown and Goldstein 1986) and over 150 mutations in LDLR have been linked to hypercholesterolemia (Hobbs et al. 1992). Many of these mutations occur in the ligand binding CR/LA cluster disrupting the interaction with lipoprotein ligands (Blacklow and Kim 1996). LDLR is primarily expressed in the liver, where it recognizes and internalizes Apolipoprotein E and B (ApoE/ApoB) containing lipoproteins (Hussain et al. 1999). LDLR contains seven CR/LA domains (denoted LA1-7 from residues 4 to 292), each linked to its neighbor by

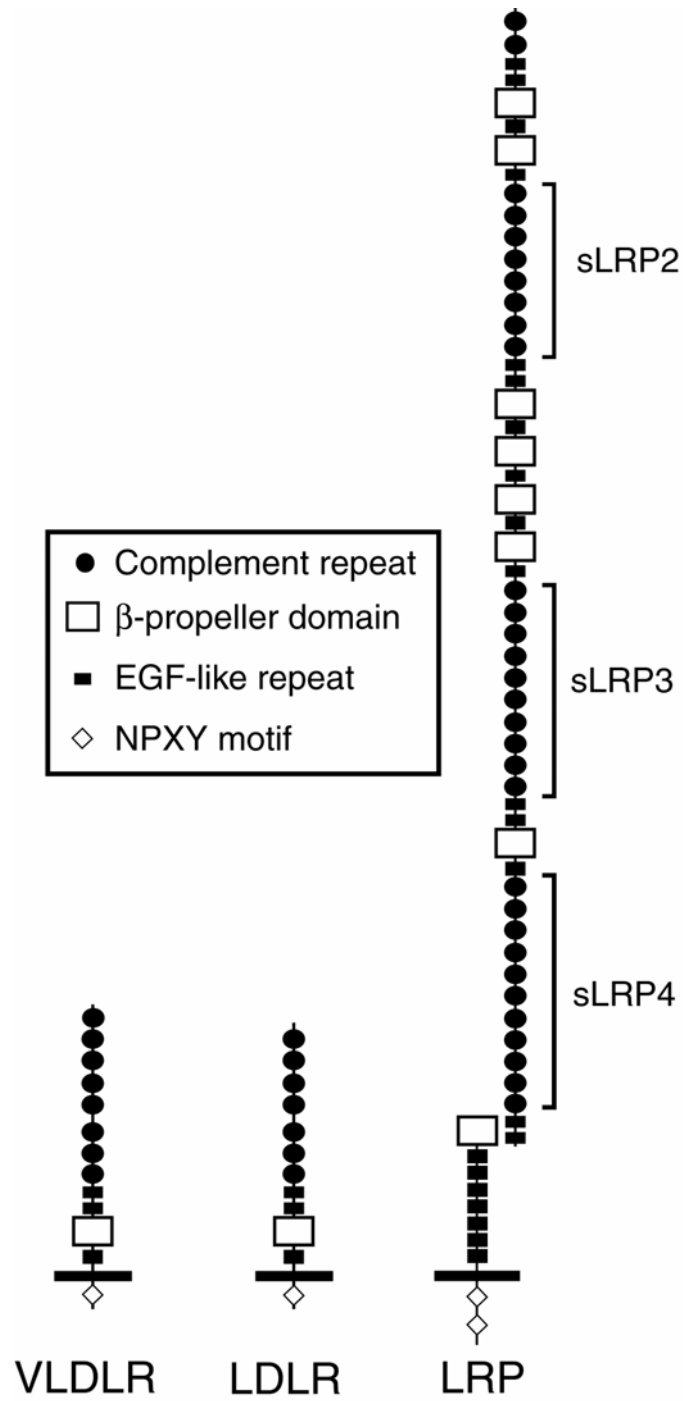


Figure 1.2: Schematic of three members of the LDL receptor family. The large clusters of CRs in LRP (sLRPs) are labeled.

a 4 or 5 residue linker, except for the fourth (LA4) and fifth (LA5) which have a uniquely long 12 residue linker. Low resolution studies showed these modules to form an extended structure with no distinct interdomain structure (Jeon and Shipley 2000). Structural studies with LA1-2 and LA5-6 pairs concluded that each repeat is highly independent of its neighbors and that these repeats act like beads on a string (Kurniawan et al. 2000; Beglova et al. 2001).

1.3 Apolipoprotein E

Apolipoprotein E plays the largest role in receptor mediated lipoprotein uptake (Hui et al. 1984). Common alleles have been associated with type III hyperlipoproteinemia (Rall et al. 1982). ApoE is composed of two domains that both associate with the lipid surface of lipoproteins, but only the N-terminal domain is required for receptor binding (Innerarity et al. 1983). Mutagenesis studies revealed that the critical receptor recognition site is within residues 140-150 (Lalazar et al. 1988; Zaiou et al. 2000). Monoclonal antibodies that recognize this region block receptor binding (Weisgraber 1983). Chimeric lipoproteins in which this segment is spliced into an unrelated lipoprotein have found that residues 131-151 of ApoE are sufficient for receptor recognition (Kiss et al. 2003). Furthermore, when incorporated into lipoprotein particles, peptides from this region of ApoE enhanced uptake both *in vitro* and *in vivo* (Mims et al. 1994; Datta et al. 2000; Datta et al. 2001).

The crystal structure of the N-terminal domain of ApoE in the absence of lipid shows that this domain forms a four helix bundle (Wilson et al. 1991) (Fig.

1.3). Although residues 140-150 form a surface-accessible helix, this lipid-free conformation of the N-terminal domain cannot bind LDL receptors with high affinity. Low resolution structural data indicate that the ApoE helical bundle adopts a new conformation when it is present in lipoprotein particles (Peters-Libeu et al. 2006; Peters-Libeu et al. 2007). Biochemical evidence suggests that the four helix bundle unwinds to wrap around the lipid particle (Fisher and Ryan 1999). NMR studies revealed that region 130-150 still maintains a helical structure when bound to lipid (Raussens et al. 2003). Upon lipid association, two critical lysine residues within this region undergo pKa perturbations and show different susceptibilities for chemical modifications (Lund-Katz et al. 2000). Low resolution crystallographic data on ApoE bound to dipalmitoylphosphatidylcholine (DPPC) particles also suggested that the helices reorient to form high affinity receptor sites (Peters-Libeu et al. 2006). In addition, upon lipid binding, the region downstream of the 140-150 site, which also contains critical residues (Arg 172) for receptor binding, becomes structured (Lalazar and Mahley 1989; Morrow et al. 2000; Gupta et al. 2006). Thus, it is likely that this downstream region is also involved in high affinity receptor recognition in the lipid bound state of ApoE.

1.4 LRP-1

Although LDLR is the primary receptor for cholesterol carrying lipoproteins, studies have shown two other members of the family, the LDL receptor-related protein (LRP) and the very low density lipoprotein receptor (VLDL), can also mediate the uptake of ApoE containing beta-migrating very low

density lipoproteins (β -VLDLs) (Kowal 1989; Hussain et al. 1991; Takahashi et al. 1992; Tacke et al. 2000). VLDLR is primarily expressed in the brain and is highly homologous to LDLR except that it contains 8 rather than 7 LAs. LRP, first identified as the receptor for α -2-macroglobulin (α 2M) (Moestrup and Gliemann 1989), has been shown to play several diverse roles far beyond cholesterol uptake. It is expressed in both the liver and the brain and recognizes at least 30 different ligands including proteases, protease inhibitor complexes, lipoproteins, growth factors, transport proteins and more (Herz and Strickland 2001).

The 600kDa LRP precursor is processed by furin cleavage, into a 515kDa alpha chain and an 85kDa beta chain (Willnow 1996), which remain non-covalently attached at the cell surface. The alpha chain is completely extracellular and contains three large clusters of CRs (sLRPs), and an additional pair of CRs at the far N-terminus. The correct folding and maturation of LRP is dependent on the receptor associated protein (RAP). RAP is an ER resident protein that was first found to co-purify with LRP and was later found critical for proper folding of LRP (Willnow et al. 1995; Bu and Rennke 1996). It is composed of three domains, each of which form a three helix bundle (Lee et al. 2007). Each helical bundle can interact with a pair of CRs (Andersen et al. 2001) and this interaction is thought to also block premature binding of ligands to LRP prior to secretion. RAP has also been shown to block the binding of many ligands of LRP *in vitro* (Herz et al. 1991).

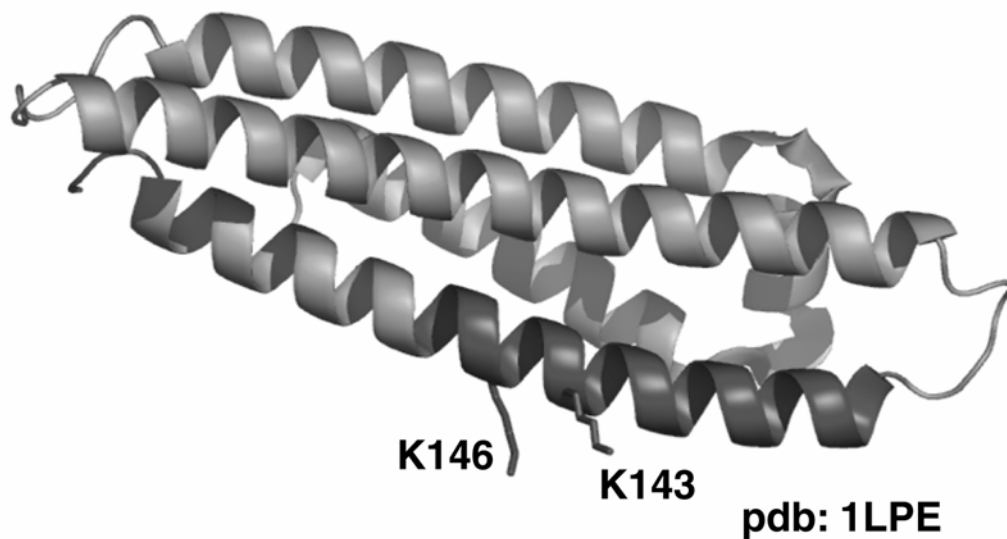


Figure 1.3: Crystal structure of the N terminal domain of Apolipoprotein E. The domain forms a four helix bundle which is thought to unwind upon association with the surface of lipoprotein particles. Residues 130-150, including the critical K143 and K146 for receptor binding are shown in dark grey.

Studies have shown that isolated soluble extracellular regions of LRP (referred to as sLRPs) can interact with many ligands of LRP *in vitro* with variations in their ligand specificity (Willnow et al. 1994; Horn et al. 1997; Neels et al. 1999; Croy et al. 2003). Although sLRP2-4 are thought to be the functional ligand binding regions, sLRP1, containing only 2 CRs, has also been shown to play a role in the binding of α 2M (Mikhailenko et al. 2001). Binding studies with ApoE(130-149) and ApoE(140-151)² have shown that both can directly interact with the three complete sLRPs (2, 3, and 4) of LRP (Croy et al. 2004). Studies aimed at narrowing down the ligand binding region for α 2M have shown that CR3-5 from sLRP2 can interact with the receptor binding domain (RBD) of α 2M with affinity near that of the full sLRP (Dolmer and Gettins 2006). Similar studies aimed at locating the ApoE binding site on LDLR have identified the fourth and fifth repeats (LA4-5) as the critical units (Russell et al. 1989; Fisher et al. 2004).

1.5 Cytoplasmic interactions of LDLRs

Several motifs within the cytoplasmic domains of the receptors interact with proteins regulating their function. The LRP beta chain contains the transmembrane region and a 100 residue intracellular tail (LRP1-CT) containing two NPXY motifs. Both of the NPXY motifs can be phosphorylated by the tyrosine kinase Src. It is now known that phosphorylation of the C terminal NPXY leads to exposure of the N terminal NPXY, which was previously inaccessible (Betts et al. 2008). This indicates that some degree of tertiary structure is present in this cytoplasmic tail. The phosphorylated C-terminal NPXY motif can also

recruit Shc, leading to activation of RAS/MAPK pathway (Barnes et al. 2001). Another motif, the YXXL, was also found to be critical for the regulation of receptor internalization (Li et al. 2000). Proteolytic cleavage of the LRP beta chain releases the intracellular domain, which can then localize to the nucleus potentially regulating transcription (Kinoshita et al. 2003) similarly to what was seen for activation of Notch (Artavanis-Tsakonas et al. 1999).

LRP is linked to Alzheimer's disease (AD) on several levels. Studies indicate a genetic link between LRP and early onset AD (Arelin et al. 2002). One of the phenotypes of AD is the buildup of amyloid plaques within brain tissue, formed by the amyloidogenic A β 40/A β 42 peptides resulting from secretase cleavage of the Amyloid Precursor Protein (APP) (King and Scott Turner 2004). LRP and APP have been shown to interact both extracellularly and intracellularly (Kinoshita et al. 2001). LRP can internalize A β 40/42 complexed with α 2M or ApoE (Haas et al. 1997; LaDu et al. 1997; Narita et al. 1997). Mutations within the C-terminal NPXY domain in LRP have been shown to affect APP processing and A β production (Pietrzik et al. 2002). It was also found that the adaptor protein Fe65, also implicated in AD, could interact with both LRP's and APP's intracellular domains linking the two (Pietrzik et al. 2004). Despite all of these data, how LRP affects the onset of AD remains unclear.

Goals of Dissertation

Previous studies have attempted to locate ApoE binding regions within sLRPs of LRP by homology to the ApoE binding region in LDLR. CR3-5 (sLRP2), CR16-18 (sLRP3) and CR25-27 (sLRP4) were selected based on homology to LA3-5 from LDLR. Each of these were expressed and purified from *P. pastoris* and assayed for binding the receptor binding region of ApoE (residues 130-149). Only CR16-18 displayed an affinity near that of the entire sLRP (200nM). Work described here examines this ApoE-LRP interaction in greater detail. The many interactions of LRP through its cytoplasmic NPXY motifs were also of interest as it is still unclear how this region affects the onset of AD. The overall goals of the project are:

- I. Develop an *E. coli* based expression system capable of high yields of active sLRP subdomains and compatible with isotope labeling for NMR studies.
- II. Assess whether smaller units of CR16-18 are capable of a strong interaction with ApoE(130-149).
- III. Compare the LRP interaction with ApoE(130-149) to the full N-terminal domain of ApoE complexed with lipid and verify critical residues involved in this interaction by mutagenesis.
- IV. Use NMR titrations, and NMR structural determination to solve the interface between ApoE(130-149) and the minimal binding portion of CR16-18.

- V. Examine binding interactions at the C-terminal NPXY motifs of LRP, along with the dependence on tyrosine phosphorylation, by directed proteomics using peptides from these regions as affinity reagents.

References

- Andersen, O.M., Schwarz, F.P., Eisenstein, E., Jacobsen, C., Moestrup, S.K., Etzerodt, M., and Thøgersen, H.C. 2001. Dominant thermodynamic role of the third independent receptor binding site in the receptor-associated protein RAP. *Biochem J* 40: 15408-15417.
- Arelin, K., Kinoshita, A., Whelan, C.M., Irizarry, M.C., Rebeck, G.W., Strickland, D.K., and Hyman, B.T. 2002. LRP and senile plaques in Alzheimer's disease: colocalization with apolipoprotein E and with activated astrocytes. *Brain Res Mol Brain Res* 104: 38-46.
- Artavanis-Tsakonas, S., Rand, M.D., and Lake, R.J. 1999. Notch signaling: cell fate control and signal integration in development. *Science* 284: 770-776.
- Barnes, H., Ackermann, E.J., and van der Geer, P. 2003. v-Src induces Shc binding to tyrosine 63 in the cytoplasmic domain of the LDL receptor-related protein 1. *Oncogene* 22: 3589-3597.
- Barnes, H., Larsen, B., Tyers, M., and van der Geer, P. 2001. Tyrosine-phosphorylated low density lipoprotein receptor-related protein 1 (LRP1) associates with the adaptor protein SHC in SRC-transformed cells. *Journal of Biological Chemistry* 276: 19119-19125.
- Beglova, N., Jeon, H., Fisher, C., and Blacklow, S.C. 2004. Cooperation between fixed and low pH-inducible interfaces controls lipoprotein release by the LDL receptor. *Mol Cell* 16.
- Beglova, N., North, C.L., and Blacklow, S.C. 2001. Backbone dynamics of a module pair from the ligand-binding domain of the LDL receptor. *Biochemistry* 40: 2808-2815.
- Betts, G.N., van der Geer, P., and Komives, E.A. 2008. Structural and Functional Consequences of Tyrosine Phosphorylation in the LRP1 Cytoplasmic Domain. *J. Biol. Chem.* 283: 15656-15664.

- Blacklow, S.C. 2007. Versatility in ligand recognition by LDL receptor family proteins: advances and frontiers. *Curr Opin Struct Biol* 17: 419-426.
- Blacklow, S.C., and Kim, P.S. 1996. Protein folding and calcium binding defects arising from familial hypercholesterolemia mutations of the LDL receptor. *Nat Struct Biol* 3: 758-762.
- Brown, M.S., and Goldstein, J.L. 1986. A receptor-mediated pathway for cholesterol homeostasis. *Science* 232: 34-47.
- Bu, G., and Rennke, S. 1996. Receptor-associated protein is a folding chaperone for low density lipoprotein receptor-related protein. *Journal of Biological Chemistry* 271: 22218-22224.
- Croy, J.E., Brandon, T., and Komives, E.A. 2004. Two apolipoprotein E mimetic peptides, apoE(130-149) and apoE(141-155)₂, bind to LRP1. *Biochemistry* 34: 7328-7335.
- Croy, J.E., Shin, W.D., Knauer, M.F., Knauer, D.J., and Komives, E.A. 2003. All three LDL receptor homology regions of the LDL receptor-related protein (LRP) bind multiple ligands. *Biochemistry* 42: 13049-13057.
- Datta, G., Chaddha, M., Garber, D.W., Chung, B.H., Tytler, E.M., Dashti, N., Bradley, W.A., Gianturco, S.H., and Anantharamaiah, G.M. 2000. The receptor binding domain of apolipoprotein E, linked to a model class A amphipathic helix, enhances internalization and degradation of LDL by fibroblasts. *Biochem J* 39: 213-220.
- Datta, G., Garber, D.W., Chung, B.H., Chaddha, M., Dashti, N., Bradley, W.A., Gianturco, S.H., and Anantharamaiah, G.M. 2001. Cationic domain 141-150 of apoE covalently linked to a class A amphipathic helix enhances atherogenic lipoprotein metabolism in vitro and in vivo. *J Lipid Res* 42: 959-966.
- Davis, C.G., Goldstein, J. L., Sudhof, T. C., Anderson, R. G. W., Russell, D. W., and Brown, M. S. 1987. Acid-dependant ligand dissociation and recycling of LDL receptor mediated by growth factor homology region. *Nature* 326: 760-765.
- Dolmer, K., and Gettins, P.G. 2006. Three complement-like repeats compose the complete alpha2-macroglobulin binding site in the second ligand binding cluster of the low density lipoprotein receptor-related protein. *J Biol Chem* 281: 34189-34196.

- Fisher, C., Abdul-Aziz, D., and Blacklow, S.C. 2004. A two-module region of the low-density lipoprotein receptor sufficient for formation of complexes with apolipoprotein E ligands. *Biochem J* 43: 1037-1044.
- Fisher, C.A., and Ryan, R.O. 1999. Lipid binding-induced conformational changes in the N-terminal domain of human apolipoprotein E. *J Lipid Res* 40: 93-99.
- Gupta, V., Narayanaswami, V., Budamagunta, M.S., Yamamoto, T., Voss, J.C., and Ryan, R.O. 2006. Lipid-induced extension of apolipoprotein E helix 4 correlates with low density lipoprotein receptor binding ability. *J Biol Chem* 281: 39294-39299.
- Haas, C., Cazorla, P., Miguel, C.D., Valdivieso, F., and Vazquez, J. 1997. Apolipoprotein E forms stable complexes with recombinant Alzheimer's disease beta-amyloid precursor protein. *Biochem J* 325 (Pt 1): 169-175.
- Herz, J., Goldstein, J.L., Strickland, D.K., Ho, Y.K., and Brown, M.S. 1991. 39-kDa protein modulates binding of ligands to low density lipoprotein receptor-related protein/alpha 2-macroglobulin receptor. *Journal of Biological Chemistry* 266: 21232-21238.
- Herz, J., and Strickland, D.K. 2001. LRP: A multifunctional scavenger and signaling receptor. *J. Clin. Invest.* 108: 779-784.
- Hobbs, H.H., Brown, M.S., and Goldstein, J.L. 1992. Molecular genetics of the LDL receptor gene in familial hypercholesterolemia. *Human mutation* 1: 445-466.
- Horn, I.R., van den Berg, B.M.M., van der Meijden, P.Z., Pannekoek, H., and van Zonneveld, A.J. 1997. Molecular analysis of ligand binding to the second cluster of complement-type repeats of the low density lipoprotein receptor-related protein. *J Biol Chem* 272: 13608-13613.
- Huang, W., Dolmer, K., and Gettins, P.G. 1999. NMR solution structure of complement-like repeat CR8 from the low density lipoprotein receptor-related protein. *J Biol Chem* 274: 14130-14136.
- Hui, D.Y., Innerarity, T.L., and Mahley, R.W. 1984. Defective hepatic lipoprotein receptor binding of B-very low density lipoproteins from type 111 hyperlipoproteinemic patients: importance of apolipoprotein E. *J Biol Chem* 259.
- Hussain, M.M., Maxfield, F.R., Más-Oliva, J., Tabas, I., Ji, Z.S., Innerarity, T.L., and Mahley, R.W. 1991. Clearance of chylomicron remnants by the low

- density lipoprotein receptor-related protein/alpha 2-macroglobulin receptor. *J Biol Chem* 266: 13936-13940.
- Hussain, M.M., Strickland, D.A., and Bakillah, A. 1999. The mammalian low-density lipoprotein receptor family. *Annu Rev Nutr* 19: 141-172.
- Innerarity, T.L., Friedlander, E.J., Rall, S.C.J., Weisgraber, K.H., and Mahley, R.W. 1983. The Receptor Binding Domain of Human Apolipoprotein E. Binding Of Apolipoprotein E fragments. *J Biol Chem.* 258: 12341-12347.
- Jeon, H., and Shipley, G.G. 2000. Vesicle-reconstituted low density lipoprotein receptor. Visualization by cryoelectron microscopy. *J Biol Chem.* 275: 30458-30464.
- King, G.D., and Scott Turner, R. 2004. Adaptor protein interactions: modulators of amyloid precursor protein metabolism and Alzheimer's disease risk? *Experimental neurology* 185: 208-219.
- Kinoshita, A., Shah, T., Tangredi, M.M., Strickland, D.K., and Hyman, B.T. 2003. The intracellular domain of the low density lipoprotein receptor-related protein modulates transactivation mediated by amyloid precursor protein and Fe65. *J Biol Chem* 278: 41182-41188.
- Kinoshita, A., Whelan, C.M., Smith, C.J., Mikhailenko, I., Rebeck, G.W., Strickland, D.K., and Hyman, B.T. 2001. Demonstration by fluorescence resonance energy transfer of two sites of interaction between the low-density lipoprotein receptor-related protein and the amyloid precursor protein: role of the intracellular adapter protein Fe65. *J Neurosci* 21: 8354-8361.
- Kiss, R.S., Weers, P.M., Narayanaswami, V., Cohen, J., Kay, C.M., and Ryan, R.O. 2003. Structure-guided protein engineering modulates helix bundle exchangeable apolipoprotein properties. *J Biol Chem* 278: 21952-21959.
- Kowal, R.C., Herz, J, Goldstein, J. L., Esser, V., and Brown, M. S. 1989. Low density receptor-related protein mediates uptake of cholesteryl esters derived from apolipoprotein E-enriched lipoproteins. *Proc. Natl. Acad. Sci. USA* 86: 5810-5814.
- Kurniawan, N.D., Atkins, A.R., Bieri, S., Brown, C.J., Brereton, I.M., Kroon, P.A., and Smith, R. 2000. NMR structure of a concatemer of the first and second ligand-binding modules of the human low-density lipoprotein receptor. *Protein Sci* 9: 1282-1293.

- LaDu, M.J., Lukens, J.R., Reardon, C.A., and Getz, G.S. 1997. Association of human, rat, and rabbit apolipoprotein E with beta-amyloid. *Journal of neuroscience research* 49: 9-18.
- Lalazar, A., and Mahley, R.W. 1989. Human apolipoprotein E. Receptor binding activity of truncated variants with carboxyl-terminal deletions. *J Biol Chem* 264: 8447-8450.
- Lalazar, A., Weisgraber, K.H., Rall, S.C.J., Gilad, H., Innerarity, T.L., Levanon, A.Z., Boyles, J.K., Amit, B., Gorecki, M., Mahley, R.W., et al. 1988. Site-specific Mutagenesis of human apolipoprotein E. Receptor binding activity of variants with single amino acids substitutions. *J Biol Chem.* 263: 3542-3545.
- Lee, D., Walsh, J.D., Migliorini, M., P., Y., Cai, T., Schwieters, C.D., Krueger, S., Strickland, D.K., and Wang, Y.X. 2007. The structure of receptor-associated protein (RAP). *Protein Sci* 16: 1628-1640.
- Lee, J., Retamal, C., Cuitiño, L., Caruano-Yzermans, A., Shin, J.E., van Kerkhof, P., Marzolo, M.P., and Bu, G. 2008. Adaptor protein sorting nexin 17 regulates amyloid precursor protein trafficking and processing in the early endosomes. *J Biol Chem* 283: 11501-11508.
- Li, Y., Marzolo, M.P., van Kerkhof, P., Strous, G.J., and Bu, G. 2000. The YXXL motif, but not the two NPXY motifs, serves as the dominant endocytosis signal for low density lipoprotein receptor-related protein. *J. Biol. Chem.* 275: 17187-17194.
- Li, Y., van Kerkhof, P., Marzolo, M.P., Strous, G.J., and Bu, G. 2001. Identification of a major cyclic AMP-dependent protein kinase A phosphorylation site within the cytoplasmic tail of the low-density lipoprotein receptor-related protein: implication for receptor-mediated endocytosis. *Mol. Cell. Biol.* 21: 1185-1195.
- Loukinova, E., Ranganathan, S., Kuznetsov, S., Gorlatova, N., Migliorini, M.M., Loukinov, D., Ulery, P.G., Mikhailenko, I., Lawrence, D.A., and Strickland, D.K. 2002. Platelet-derived growth factor (PDGF)-induced tyrosine phosphorylation of the low density lipoprotein receptor-related protein (LRP). Evidence for integrated co-receptor function between LRP and the PDGF. *J Biol Chem* 277: 15499-15506.
- Lund-Katz, S., Zaiou, M., Wehrli, S., Dhanasekaran, P., Baldwin, F., Weisgraber, K.H., and Phillips, M.C. 2000. Effects of lipid interaction on the lysine microenvironments in apolipoprotein E. *J Biol Chem* 275: 34459-34464.

- Mikhailenko, I., Battey, F.D., Migliorini, M., Ruiz, J.F., Argraves, K., Moayeri, M., and Strickland, D.K. 2001. Recognition of α 2-macroglobulin by the low density lipoprotein receptor-related protein requires the cooperation of two ligand binding cluster regions. *J. Biol. Chem.* 276: 39484-39491.
- Mims, M.P., Darnule, A.T., Tovar, R.W., Pownall, H.J., Sparrow, D.A., Sparrow, J.T., Via, D.P., and Smith, L.C. 1994. A nonexchangeable apolipoprotein E peptide that mediates binding to the low density lipoprotein receptor. *J Biol Chem* 269: 20539-20547.
- Moestrup, S.K., and Gliemann, J. 1989. Purification of the rat hepatic α 2-macroglobulin receptor as an approximately 440-kDa single chain protein. *J Biol Chem.* 264: 15574-15577.
- Morrow, J.A., Arnold, K.S., Dong, J., Balesta, M.E., and Innerarity, T.L. 2000. Effect of Arginine 172 on the Binding of Apolipoprotein E to the Low Density Lipoprotein Receptor. *J Biol Chem* 275: 2576-2580.
- Narita, M., Holtzman, D.M., Schwartz, A.L., and Bu, G. 1997. α 2-macroglobulin complexes with and mediates the endocytosis of beta-amyloid peptide via cell surface low-density lipoprotein receptor-related protein. *Journal of neurochemistry* 69: 1904-1911.
- Neels, J.G., van den Berg, B.M.M., Lookene, A., Olivecrona, G., Pannekoek, H., and van Zonneveld, A.J. 1999. The second and fourth cluster of class A cysteine-rich repeats of the low density lipoprotein receptor-related protein share ligand binding properties. *J. Biol. Chem.* 274: 31305-31311.
- Peters-Libeu, C.A., Newhouse, Y., Hall, S.C., Witkowska, H.E., and Weisgraber, K.H. 2007. Apolipoprotein E.dipalmitoylphosphatidylcholine particles are ellipsoidal in solution. *J Lipid Res* 48: 1035-1044.
- Peters-Libeu, C.A., Newhouse, Y., Hatters, D.M., and Weisgraber, K.H. 2006. Model of biologically active apolipoprotein E bound to dipalmitoylphosphatidylcholine. *J Biol Chem* 281: 1073-1079.
- Pietrzik, C.U., Busse, T., Merriam, D.E., Weggen, S., and Koo, E.H. 2002. The cytoplasmic domain of the LDL receptor-related protein regulates multiple steps in APP processing. *The EMBO journal* 21: 5691-5700.
- Pietrzik, C.U., Yoon, I.S., Jaeger, S., Busse, T., Weggen, S., and Koo, E.H. 2004. FE65 constitutes the functional link between the low-density lipoprotein receptor-related protein and the amyloid precursor protein. *J Neurosci.*: 4259-4265.

- Rall, S.C.J., Weisgraber, K.H., Innerarity, T.L., and Mahley, R.W. 1982. Structural basis for receptor binding heterogeneity of apolipoprotein E from type III hyperlipoproteinemic subjects. *Proc Natl Acad Sci* 79: 4696-4700.
- Ranganathan, S., Liu, C.X., Migliorini, M.M., Von Arnim, C.A., Peltan, I.D., Mikhailenko, I., Hyman, B.T., and Strickland, D.K. 2004. Serine and threonine phosphorylation of the low density lipoprotein receptor-related protein by protein kinase Calpha regulates endocytosis and association with adaptor molecules. *J Biol Chem* 279: 40536-40544.
- Raussens, V., Slupsky, C.M., Sykes, B.D., and Ryan, R.O. 2003. Lipid-bound structure of an apolipoprotein E-derived peptide. *J Biol Chem* 278: 25998-26006.
- Rudenko, G., and Deisenhofer, J. 2003. The low-density lipoprotein receptor: ligands, debates and lore. *Curr Opin Struct Biol* 13: 683-689.
- Rudenko, G., Henry, L., Henderson, K., Ichtchenko, K., Brown, M.S., Goldstein, J.L., and Deisenhofer, J. 2002. Structure of the LDL receptor extracellular domain at endosomal pH. *Science* 298: 2353-2358.
- Russell, D.W., Brown, M.S., and Goldstein, J.L. 1989. Different combinations of cysteine-rich repeats mediate binding of low density lipoprotein receptor to two different proteins. *J Biol Chem* 264: 21682-21688.
- Simonovic, M., Dolmer, K., Huang, W., Strickland, D. K., Volz, K., Gettins, P. G. W. 2001. Calcuim Coordination and pH dependence of the calcium affinity of ligand-binding repeat CR7 from the LRP. Comparision with related domains from the LRP and the LDL receptor. *Biochemistry* 40: 15127-15134.
- Tacken, P.J., Teusink, B., Jong, M.C., Harats, D., Havekes, L.M., van Dijk, K.W., and Hofker, M.H. 2000. LDL receptor deficiency unmasks altered VLDL triglyceride metabolism in VLDL receptor transgenic and knockout mice. *J Lipid Res* 41: 2055-2062.
- Takahashi, S., Kawarabayasi, Y., Nakai, T., Sakai, J., and Yamamoto, T. 1992. Rabbit very low density lipoprotein receptor: a low density lipoprotein receptor-like protein with distinct ligand specificity. *Proc Natl Acad Sci* 89: 9252-9256.
- Weisgraber, K.L., Innerarity, T. L., Harder, K. J., Mahley, R. W., Milne, R. W., Marcel, Y. L., Sparrow, J. T. 1983. The Receptor Binding Domain Of Human Apolipoprotein E. *J. Biol. Chem* 258: 12348-12354.

- Willnow, T.E., and Moehring, J. M., Inocencio, N. M., Moehring, T. J., and Herz, J. 1996. The low-density-lipoprotein receptor-related protein (LRP) is processed by furin in vivo and in vitro. *Biochem. J.* 313: 71-76.
- Willnow, T.E., Armstrong, S.A., Hammer, R.E., and Herz, J. 1995. Functional expression of low density lipoprotein receptor-related protein is controlled by receptor-associated protein in vivo. *Proc Natl Acad Sci* 92: 4537-4541.
- Willnow, T.E., Orth, K., and Herz, J. 1994. Molecular dissection of ligand binding sites on the low density lipoprotein receptor-related protein. *Journal of Biological Chemistry* 269: 15827-15832.
- Wilson, C., Wardell, M.R., Weisgraber, K.H., Mahley, R.W., and Agard, D.A. 1991. Three-dimensional structure of the LDL receptor-binding domain of human apolipoprotein E. *Science* 252: 1817-1822.
- Zaiou, M., Arnold, K.S., Newhouse, Y.M., Innerarity, T.L., Weisgraber, K.H., Segall, M.L., Phillips, M.C., and Lund-Katz, S. 2000. Apolipoprotein E₃-low density lipoprotein receptor interaction. Influences of basic residue and amphipathic alpha-helix organization in the ligand. *J Lipid Res* 41: 1087-1095.
- Zhao, Z., and Michaely, P. 2009. The Role of Calcium in Lipoprotein Release by the Low-Density Lipoprotein Receptor. *Biochemistry* 48: 7313–7324.

Chapter 2

Expression and Refolding and Characterization of CR domains

Introduction

The low density lipoprotein receptor is a major receptor for cholesterol containing lipoprotein particles, and is the most studied in this family of receptors (Brown and Goldstein 1986; Blacklow 2007). Seven LDL-A (LA) modules also known as complement type repeats (CRs) in the extracellular domain of this receptor mediate ligand interactions. Natural mutations in the LA modules lead to familial hypercholesterolemia (FH) (Fass 1997). The structures of several LA modules from LDLR and other receptors have been solved both by X-ray crystallography and NMR. All of these share a conserved disulfide-bonding pattern and a calcium binding site (Guo et al. 2004). Several of the mutations associated with FH have been shown to affect disulfide bonding cysteines or correspond to residues involved in calcium binding (Blacklow and Kim 1996). This region of LDLR has been found to have a high affinity for several natural ligands including Apolipoprotein E (ApoE)-containing β -VLDL particles (Esser et al. 1988).

Ligand binding assays with recombinant LDLR lacking single modules showed that LA5, and to a lesser extent LA4, were the key modules for mediating β -VLDL binding (Russell et al. 1989). The LA45 module pair was later shown to be able to bind β -VLDL mimicking apoE•dimyristoyl-phosphatidylcholine (DMPC) particles *in vitro* (Fisher et al. 2004). The LDL receptor-related protein (LRP) was also shown to interact with ApoE containing lipoprotein particles (Kowal 1989; Hussain et al. 1991). Binding studies with ApoE(130-149) and ApoE(140-151)², which are thought to represent the receptor binding site (Weisgraber et al. 1983;

Zaiou et al. 2000; Kiss et al. 2003), have shown that both can directly interact with the three complete ligand binding clusters (sLRP2, 3, and 4) of LRP (Croy et al. 2004).

Upon internalization to the endosome the bound ligands must dissociate from the receptor and be trafficked to various cellular compartments. This process is thought to be driven by the gradual decrease in pH within the endosome (Davis 1987). It has also been hypothesized that the drop in calcium concentrations within the endosome plays a role in ligand release (Simonovic et al. 2001). The structure of the entire LDLR at endosomal pH showed self-interaction with the β -propeller domain, consistent with LDL release at low pH (Rudenko et al. 2002). However recent evidence suggests that both calcium dependent and pH dependent mechanisms govern ligand release (Zhao and Michaely 2009).

Based on homology to the ApoE binding site on LDLR, a three repeat segment (CR16-18) of sLRP3 was found to have binding affinity to ApoE(130-149) equal to that of the full sLRP3 (Croy et al., unpublished observations). In order to examine the structural and dynamic properties of this three repeat construct further and to compare it to LA3-5 of the LDLR, as well as to examine the details behind the interface with ApoE(130-149), it was necessary to establish an expression and purification protocol capable of high yields and the possibility for inexpensive isotopic labeling for NMR studies.

Materials and Methods

Cloning. Full length human LRP-1 cDNA was a generous gift of Dr. Joachim Herz (Herz et al. 1988). Human LDLR cDNA was obtained from ATTC (10658357). The expression vector encoding the TrpLE sequence behind the T7 promoter, pMMHb, was a kind gift from S. Blacklow (Fass 1997; North and Blacklow 1999). This vector was modified by introduction of a thrombin cleavage site (GGLVPR) by PCR just after the TrpLE sequence and before the BamH1 site. Residues 88-126 (LA3), 123-167 (LA4), 171-214 (LA5), 88-167 (LA34), 123-214 (LA45) and 88-235 (LA35) of the mature form of human LDLR, and CR16 (2712-2754), CR17 (2751-2798) CR18 (2794-2838), CR1617, CR1718, and CR16-18 of mature human LRP1 were amplified by PCR and cloned via BamH1 and EcoR1 sites into the modified pMMHb vector. DNA oligonucleotides were inserted at the 3' BamH1 site to yield a C-terminal FLAG-tag (KDDDDKYD).

Expression/purification. Each CR fragment was expressed in *E. coli* strain BL21-DE3 cells. Cultures were grown in M9 minimal media supplemented with NZ amine at 37°C to OD₆₀₀ 1.0 and induced with 0.5mM IPTG. For NMR samples M9 media was used with ¹⁵NH₄Cl (1g/L) and ¹³C glucose (3g/L) (Cambridge Isotope Labs). After 12 hrs of expression, cells were harvested and lysed by sonication. Inclusion bodies were isolated by centrifugation and resuspended in resolubilizing buffer (8M Urea, 50mM Tris (pH 8.0), 150mM NaCl, 1mM β-mercaptoethanol). Proteins were captured with Ni-NTA (Qiagen) and washed with a gradient (50 ml to 50 ml) of resolubilizing buffer to refolding buffer (50mM Tris (pH 8.2), 400mM NaCl, 10mM CaCl₂ and 1.5mM/0.4mM reduced/oxidized

glutathione). Columns were sealed and the resin was allowed to mix continuously by rocking in refolding buffer at 4°C for three days after which they were washed with 50mM Tris (pH 8.0), 150mM NaCl, 10mM CaCl₂ and treated with active bovine thrombin (40µg/L expressed protein) for 12 hrs at 25°C. Refolded, cleaved CRs were then purified by C18 reverse phase HPLC (Waters, Milford, MA, USA) in 10mM NH₄OAc pH 5.5, 5mM CaCl₂ with a linear acetonitrile gradient (10-50%). Proteins were dried and further purified with the same gradient on C18 HPLC (300mm x 19mm I.D., Waters), but in 0.1% trifluoroacetic acid (TFA). Active bovine thrombin was purified as described previously (Koeppel et al. 2005).

Mass Spectrometry. Masses of the final proteins were confirmed by MALDI-TOF (Voyager DESTRA) mass spectrometry. Purified protein eluted from the HPLC, in 0.1% TFA, was mixed 1:1 with sinnapinic acid matrix (Agilent).

Disulfide Bond Mapping. Purified LA4 was partially reduced with 20mM Tris(2-carboxyethyl)phosphine (TCEP) (Sigma-Aldrich) in 170mM Citrate (pH 3) to avoid disulfide shuffling. The reaction was quenched with rapid injection of 2.2M iodoacetamide in 500mM Tris pH 8.0, vortexed for 30 seconds, and subsequently quenched with 0.5M citrate pH 3.0 (Gray 1993). Partially reduced fragments were separated by C18 analytical HPLC. Tryptic and chymotryptic fragments of these partially reduced species were analyzed by MALDI TOF-TOF on an ABI 4800 (Applied Biosystems) with α -Cyano-4-hydroxycinnamic acid

matrix (Agilent).

Isothermal titration calorimetry. Calcium binding titrations were performed on a MicroCal VP-ITC calorimeter at 35°C. Lyophilized protein was resuspended (50-300µM) in Chelex (BioRad)-treated buffer (20mM Hepes (pH 7.4), 150mM NaCl, 0.02% azide). Each single CR/LA was titrated with 10 fold molar excess of CaCl₂ in the same buffer except LA4 which was titrated using a 20 fold molar excess of CaCl₂. Data were fit to single binding site models in Origin 6.0 except CR16-18 and LA45 which were fit to a two site binding model (OriginLab). Titrations with LA4 were repeated the same way using 20mM Hepes, 20mM NaOAc pH 5.2, 150mM NaCl, 0.02% azide.

NMR. NMR spectra were collected on a Bruker Avance III 600 MHz spectrometer equipped with a cryoprobe. ¹⁵N labeled CRs (0.2-0.5mM) were resuspended in 20mM Hepes (pH 7.4), 150mM NaCl, 5mM CaCl₂, 10% D₂O and 0.02% sodium azide. ¹H-¹⁵N HSQC spectra were collected at 307°K. The data were processed using Azara (Wayne Boucher and the Department of Biochemistry, University of Cambridge) and visualized in Sparky (T. D. Goddard and D. G. Kneller, SPARKY 3, University of California, San Francisco).

ApoE binding assay. ApoE(130-149) was synthesized with N-terminal biotinylation on a 9050 peptide synthesizer (Applied Biosystems). A scrambled ApoE(130-149) was also synthesized with the sequence

LREKKLRVVSALRTHRLELRL. All pulldown reactions were carried out in HBST (20mM Hepes pH 7.4, 150mM NaCl 0.02% sodium azide, 0.1% Tween-20 (Biorad)) containing either 2mM CaCl₂ or 2mM EDTA. ApoE peptide (130-149) with an N-terminal biotin was immobilized onto streptavidin agarose (Fluka) at saturating concentrations as described previously (Croy et al. 2004). Either uncoupled beads or scrambled ApoE(130-149) peptide was used as a negative control. FLAG-tagged complement repeat constructs were added (500nM), reactions were left rocking at 25°C for 2 hours, then washed twice with the same buffer, resolved by SDS-PAGE, probed with anti-SLRP3 (Croy et al. 2003) or anti-FLAG antibody (a generous gift from P. van der Geer) and detected by chemiluminescence (Western Lightening Plus kit, Perkin Elmer). GST-RAP (6µM) and high molecular weight (HMW) heparin (5mg/mL) (Sigma-Aldrich) were tested as inhibitors. Purification of GST-RAP has been described previously (Croy et al. 2003).

Results

Vector Modification and Expression. Initial attempts to express single, double, or triple CR constructs with a His8 tag, or with GST, and Ubiquitin as fusion proteins failed to generate high yields. The pMMHb vector had previously been used to express high amounts of LA5 of LDLR in *E. coli* as inclusion bodies (Fass 1997). Since within this vector the TrpLE fusion protein was designed to be cleaved off after the linking methionine residue by cyanogen bromide, and CR18 contained a native methionine, modification of this step was necessary. Insertion

of a thrombin cleavage site instead of the labile methionine was ideal, as thrombin is a highly specific protease, and was readily available in the lab. Each single double and triple CR in LA3-5 and CR16-18 was cloned into this modified pMMHb vector and successfully overexpressed as inclusion bodies in *E. coli*. Overexpression was also possible in M9 minimal media making it suitable for isotope labeling. A C-terminal FLAG tag was inserted into each construct, and did not interfere with high yield expression.

Purification and refolding of CR constructs. After resolubilization of inclusion bodies, proteins were successfully captured by nickel affinity chromatography under denaturing conditions. Initial attempts to purify the protein from the nickel resin and refold by dialysis led to solubility problems, likely resulting from the poor solubility of the TrpLE fusion protein. We therefore attempted to cleave the protein from the TrpLE fusion prior to refolding of disulfide bonds, however thrombin cleavage was very poor under these reducing conditions. In order to circumvent both of these problems we attempted refolding the disulfides while the protein was still immobilized on nickel resin. Using a mixture of reduced and oxidized glutathione supplemented with calcium chloride which favors the formation of the native disulfide pattern (Blacklow and Kim 1996) was successful. After disulfide oxidation the nickel column was washed and treated with thrombin to cleave off the refolded CR construct, leaving the TrpLE fusion peptide immobilized (Fig 2.1).

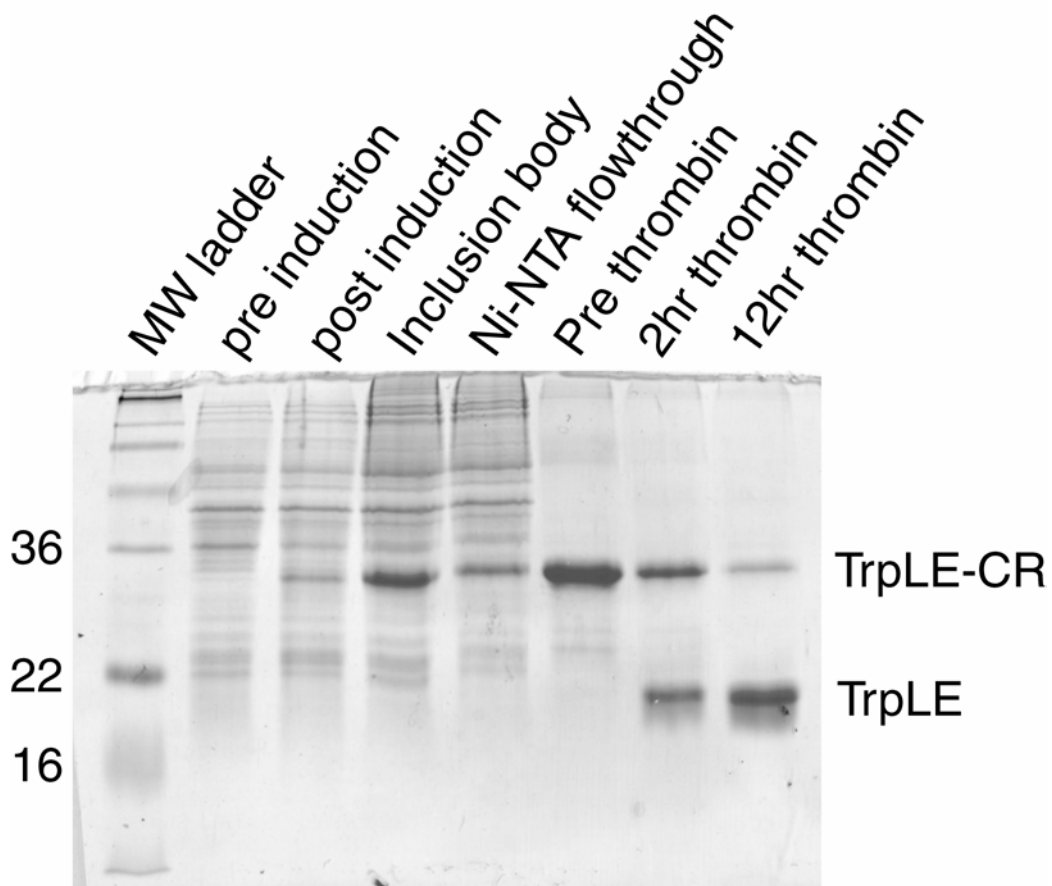


Figure 2.1: SDS-PAGE analysis of expression and purification of CR17-18 from *E. coli*. Samples for the last three lanes are of immobilized protein on Ni-NTA beads.

Table 2.1: Average mass (Da) obtained from MALDI-TOF mass spectrometric analysis of each expressed CR construct compared to the theoretical masses correcting for the loss of six ^1H 's from the disulfide bonds.

	Expected	experimental
LA3	4480.9	4480.9
LA4	5120.9	5118.7
LA5	4764.1	4764.2
LA4-5	10153.43	10151.17
LA3-5	14067.72	14058.42
LA3-5FLAG	15553.8	15552.96
CR16	4890.0	4893.3
CR17	5095.3	5093.6
CR18	5656.8	5655.2
CR16-17	9413.6	9408.3
CR17-18	9764.2	9765.72
CR16-18	14076.2	14080.41
CR16-18	14323.7	14321.74
CR16-17FLAG	10890.1	10902.84
CR16-18FLAG	15574.3	15574.95
CR17-18FLAG	11257.7	11260.27

Cleaved protein was then purified over reverse phase high performance liquid chromatography (RP-HPLC) (C18 preparatory column (Waters) with a gradient of 10% to 50% acetonitrile) to separate various disulfide isomers. This approach yielded a sharp peak with several lower abundance, later eluting peaks as seen before with successful refolding (Blacklow and Kim 1996). Each CR had the correct mass as assessed by mass spectrometry (Table 2.1). The protocol successfully generated several mgs of purified, refolded protein per liter of M9 minimal media for single module constructs and nearly one mg/L for double and triple constructs.

Characterization of individual CRs. In order to prepare samples for NMR studies each single CR domain was expressed using this protocol with ^{15}N supplemented minimal media. All constructs could be freeze dried after HPLC and resuspended for NMR studies. ^1H , ^{15}N heteronuclear single quantum coherence (HSQC) spectra of each CR showed well dispersed resonance shifts in the presence of calcium (Fig. 2.2). Each CR had close to the number of expected cross peaks except for CR18 and LA4. Although mass spectrometry showed CR18 was not truncated it only showed 30 of the 44 expected peaks, possibly indicating conformational exchange rendering certain regions invisible. LA4 showed far more than the expected number of peaks (56/41) indicating multiple species or multiple conformations were present within the sample. Size exclusion chromatography showed LA4 to be monomeric indicating that no higher order oligomers were present. Analytical RP-HPLC of LA4 showed only a

single peak and no other mass besides full LA4 was observed by mass spectrometry.

Partial reduction coupled to mass spectrometry was used to map the disulfide bonding pattern of LA4. Isolation of partially reduced fragments purified by HPLC were digested by trypsin and chymotrypsin and peptides sequenced by MALDI TOF-TOF mass spectrometry. Within the isolated species with only a single disulfide reduction and alkylation the two alkylated cysteines reveal the broken disulfide bond. For LA4 it was observed that the C-terminal cysteine had this alkylation pattern with three different cysteines, indicating the presence of several disulfide isoforms. We therefore speculated that multiple disulfide isomers of LA4 were co-eluting by RP-HPLC. Since only the correct disulfide isomer should have a high affinity for calcium we attempted RP-HPLC of the calcium bound LA4. Using 10mM NH₄OAc pH 5.5 with 5mM CaCl₂ as the aqueous phase instead of 0.1% TFA we were able to resolve three species that previously co-eluted as one (Fig. 2.3). The first peak yielded an HSQC spectrum that had uniform peak intensities and now had 37 of the 43 expected cross peaks (Fig. 2.4). This same problem was also seen with LA3-5 and LA4-5 therefore all constructs containing LA4 were purified using this “native” HPLC purification, which was also very effective at separating disulfide isomers even at preparatory scale HPLC (Fig 2.3).

Calcium binding of each CR. Refolded CRs were titrated with calcium, and binding was monitored by isothermal titration calorimetry (ITC). Binding isotherms of CR16, CR17, CR18, LA3 and LA5 showed that each could bind one calcium ion with thermodynamic properties similar to previous reports for LA5 (Simonovic et al. 2001) (Fig. 2.5). LA4 reproducibly yielded a hyperbolic curve, indicating a significantly weaker calcium binding. Measured calcium affinities are listed in Table 2.2. To assess whether low pH or the presence of LA5 would enhance the weak calcium affinity of LA4, the same titrations were conducted at pH 5.2 and with LA45. LA4 showed an even weaker affinity for calcium at low pH ($>500\mu\text{M}$). The binding isotherm of LA45 showed the strong interaction but with a stoichiometry of 1, indicating that LA5 is still binding one calcium ion tightly but LA4 still has a weak binding affinity.

Calcium titration of the three repeat CR16-18 showed multiple binding events, and the data were fit to a two-site binding model (Fig. 2.6). Although the first site has relatively few data points, the thermodynamic parameters are congruent with CR16 binding initially with high affinity, followed by CR17 and CR18 binding with weaker affinity, but higher enthalpy. The thermodynamic properties of this second binding site are in good agreement with the average between CR17 and CR18.

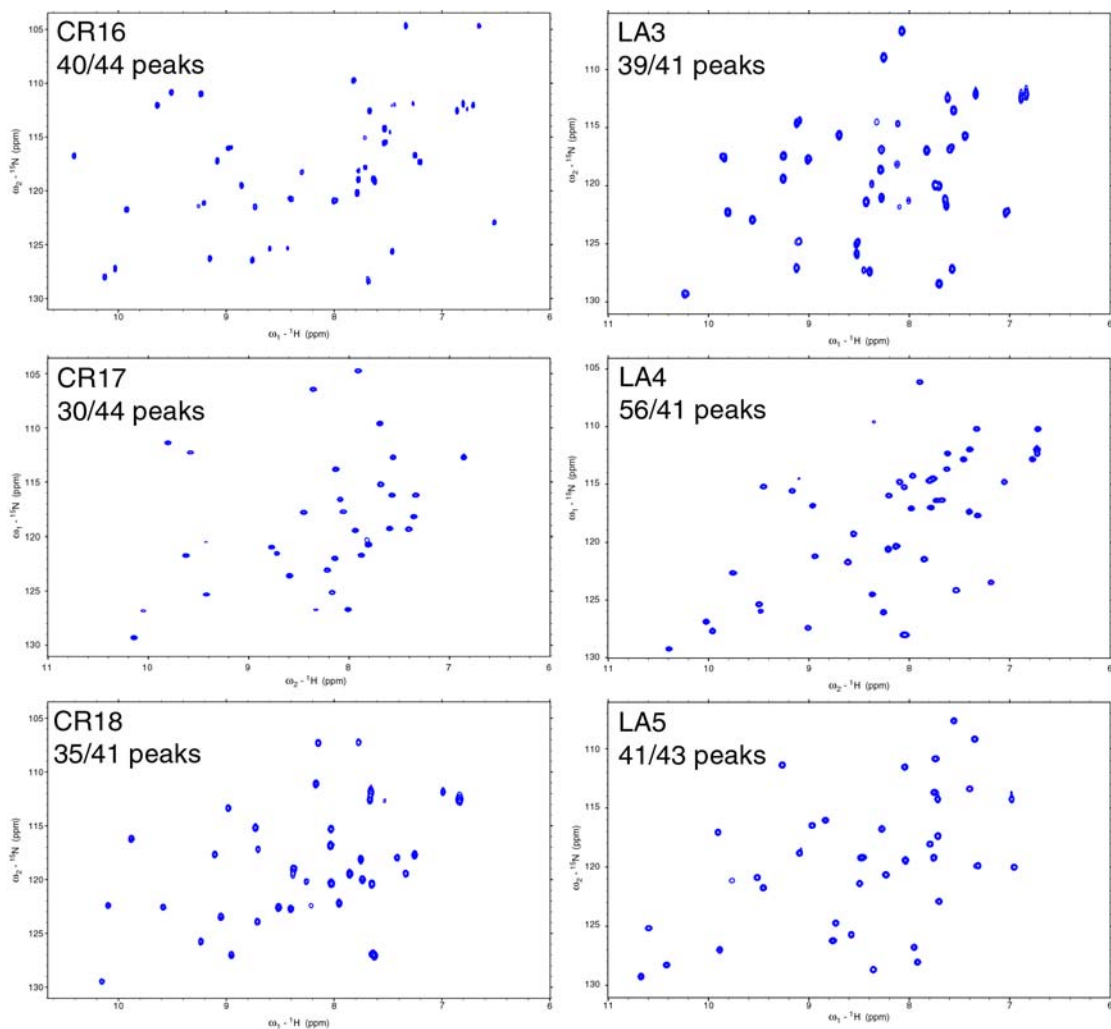


Figure 2.2: ^1H , ^{15}N HSQC spectra of each CR/LA from LA3-5 and CR16-18. The spectrum of LA4 has more, while CR17 has significantly fewer than expected number of cross peaks.

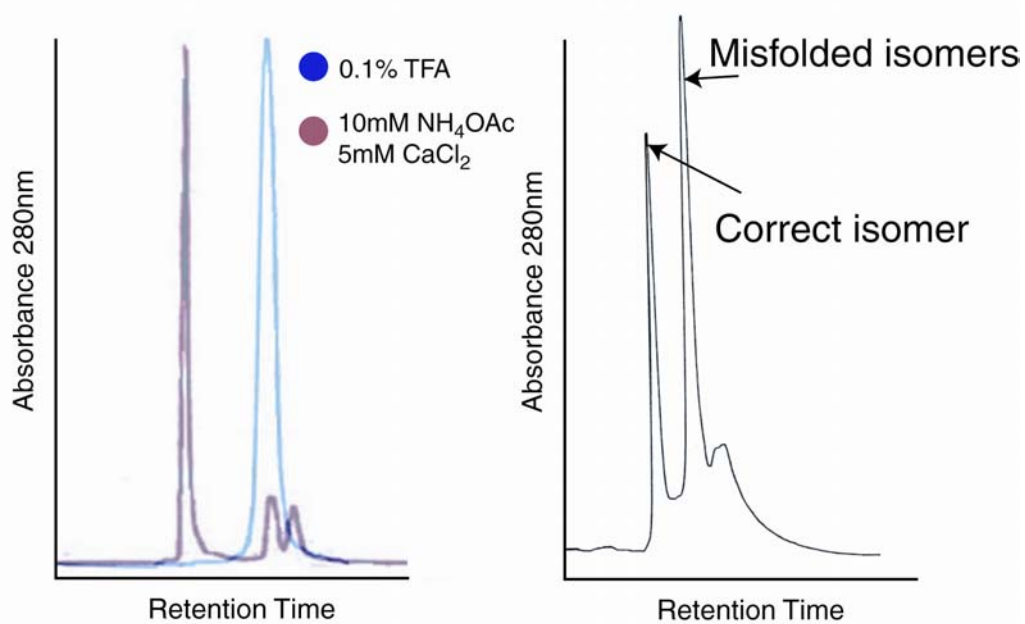


Figure 2.3: Left: Analytical RP-HPLC of LA4 with either denaturing (0.1%TFA) (blue) or native (10mM NH₄OAc pH 5.5, 5mM CaCl₂) buffer as the mobile aqueous phase. Right: Preparatory HPLC of LA45 using the same native RP-HPLC.

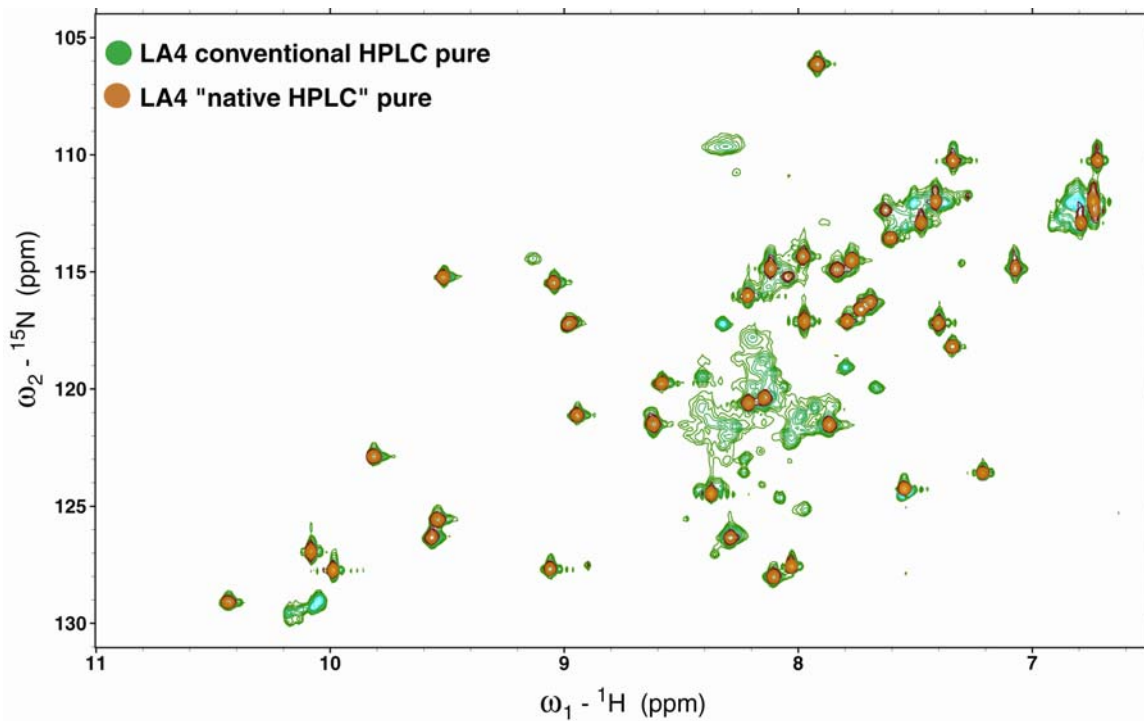


Figure 2.4: ${}^1\text{H}, {}^{15}\text{N}$ HSQC spectra of LA4 after conventional (0.1% TFA) HPLC purification (green), and further purification with HPLC run in 10mM NH_4OAc and 5mM CaCl_2 (orange).

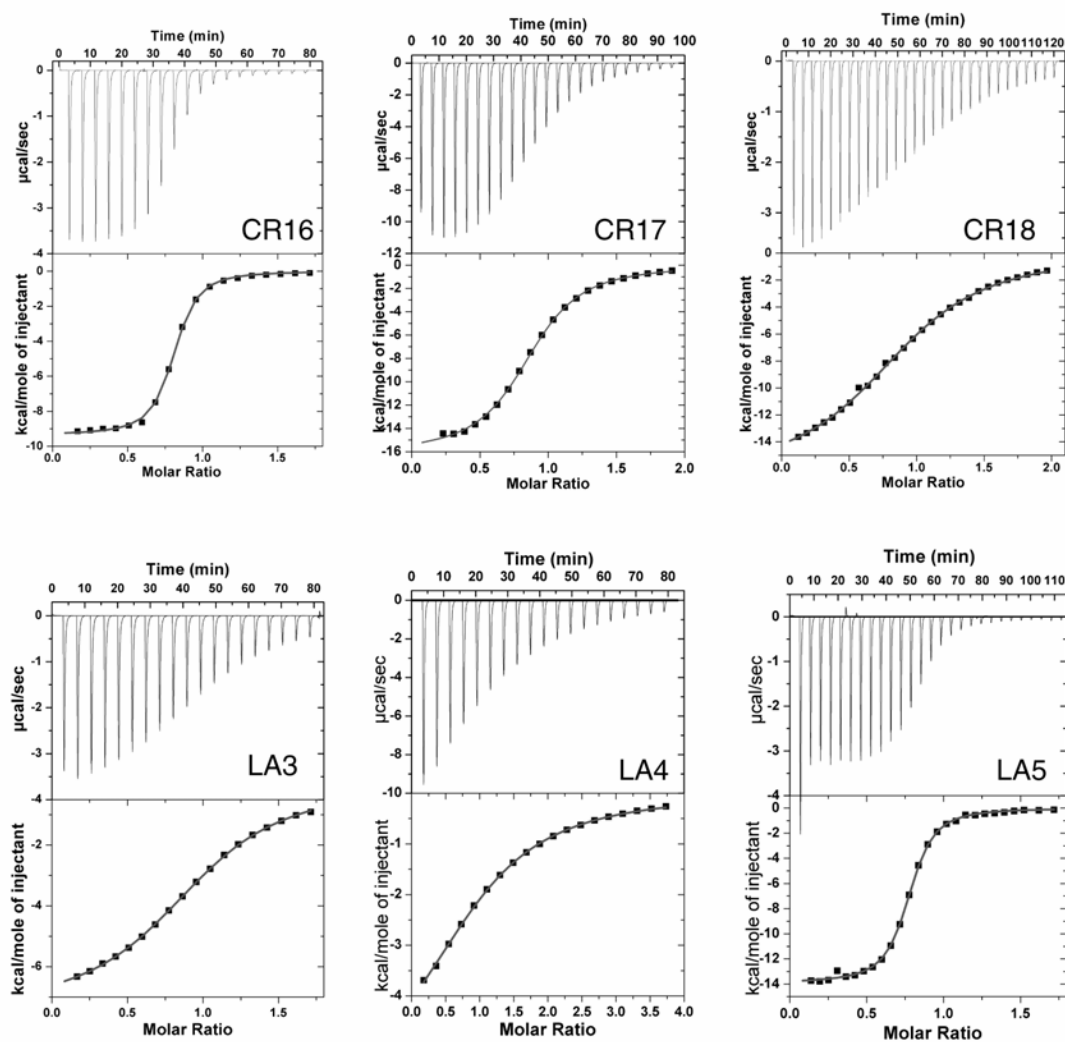


Figure 2.5: Calcium binding isotherms of each individual CR/LA monitored by isothermal titration calorimetry at pH 7.4. Unlike the others LA4 has a hyperbolic curve indicating weak binding.

Binding assays with ApoE(130-149). To ensure that CR16-18 refolded from *E. coli* inclusion bodies could still interact with ApoE(130-149), pulldown assays were conducted side by side with active CR16-18 derived from *P. pastoris*. Immobilized ApoE(130-149) was able to interact with CR16-18 from both sources. The polyclonal antibody raised against sLRP3 was able to recognize *E. coli* derived CR16-18 (Fig. 2.7). Pulldown assays revealed a much weaker interaction with the scrambled ApoE peptide. This interaction was also calcium dependent and inhibited by heparin, and RAP (Fig. 2.7), in agreement with previous results (Croy et al. 2004; Fisher et al. 2004).

Discussion

An efficient technique for expression/purification of CR domains.

Expression of CR constructs in *E. coli* as inclusion bodies is an effective way of obtaining large quantities of protein with the possibility of inexpensive isotopic labeling. The expression from the pMMHb vector to produce a TrpLE fusion that is thrombin-cleavable allows CR domains to remain immobilized for on-column refolding and proteolytic cleavage from the fusion protein. The on-column approach minimizes solubility problems encountered during refolding. The modified vector also uses thrombin cleavage instead of cyanogen bromide therefore sequences with native methionines can be expressed without the occurrence of secondary cleavages.

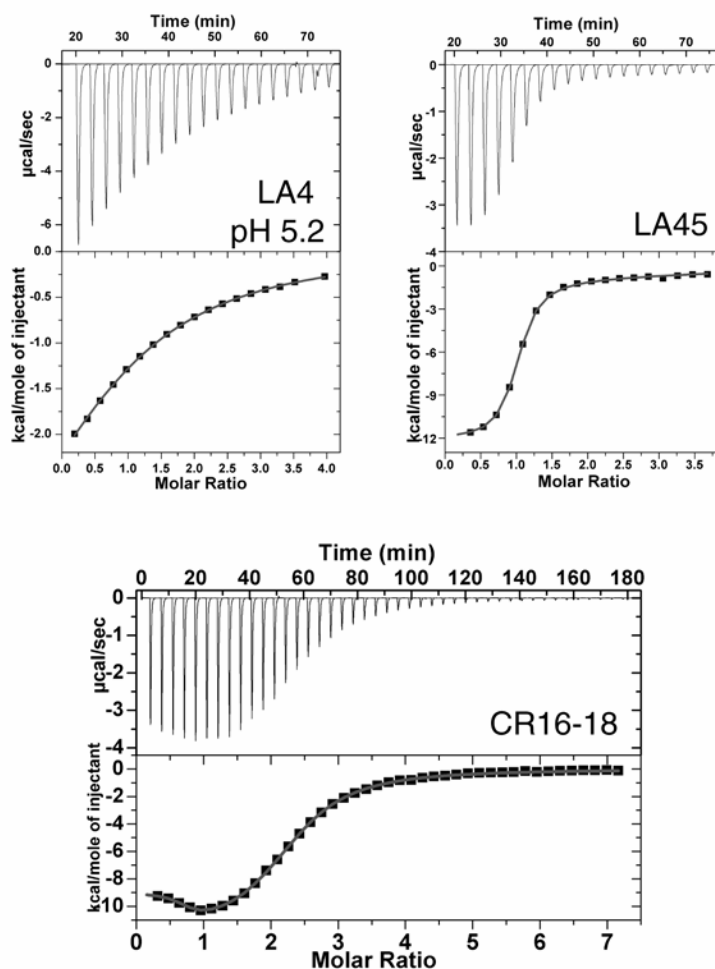


Figure 2.6: Calcium binding isotherms of LA4 at pH 5.2, and LA4-5 and CR16-18 at pH 7.4. LA4 still shows a weak affinity calcium at low pH and when covalently attached to LA5. The triple repeat CR16-18 can be fit two a two binding site model in which CR16 binds first with higher affinity but lower enthalpy, followed by CR17 and CR18 binding weaker but with higher enthalpy.

Table 2.2: Binding stoichiometries (N) affinities (K_D) and enthalpies (ΔH) of each CR construct as measured by isothermal titration calorimetry. LA45 and CR16-18 were fit to a two site model. In LA45 the first site is congruent with LA5 binding, masking the weaker affinity of LA4 which could not be fit with high certainty. CR16-18 could be fit two a two site model in which the first site is congruent with CR16 binding, followed by CR17 and CR18 binding with similar thermodynamic properties.

CR domain	N	K_D (μM)	ΔH (Kcal/mol)
LA3	0.978	16	-7.4
LA4	1.03	163	-6.1
LA5	0.755	0.79	-14
LA4 pH 5.2	1.12	546	-4.5
LA45 1st site	0.95	-	-7.2
LA45 2nd site	0.95	0.962	12.1
CR16	0.776	0.7	-9.4
CR17	0.87	6	-7.7
CR18	0.946	13.7	-16.4
CR16-18 1st site	0.74	0.18	-9
CR16-18 2nd site	1.77	7.5	-12.2
average (16 & 17)	1.816	9.85	-12.05

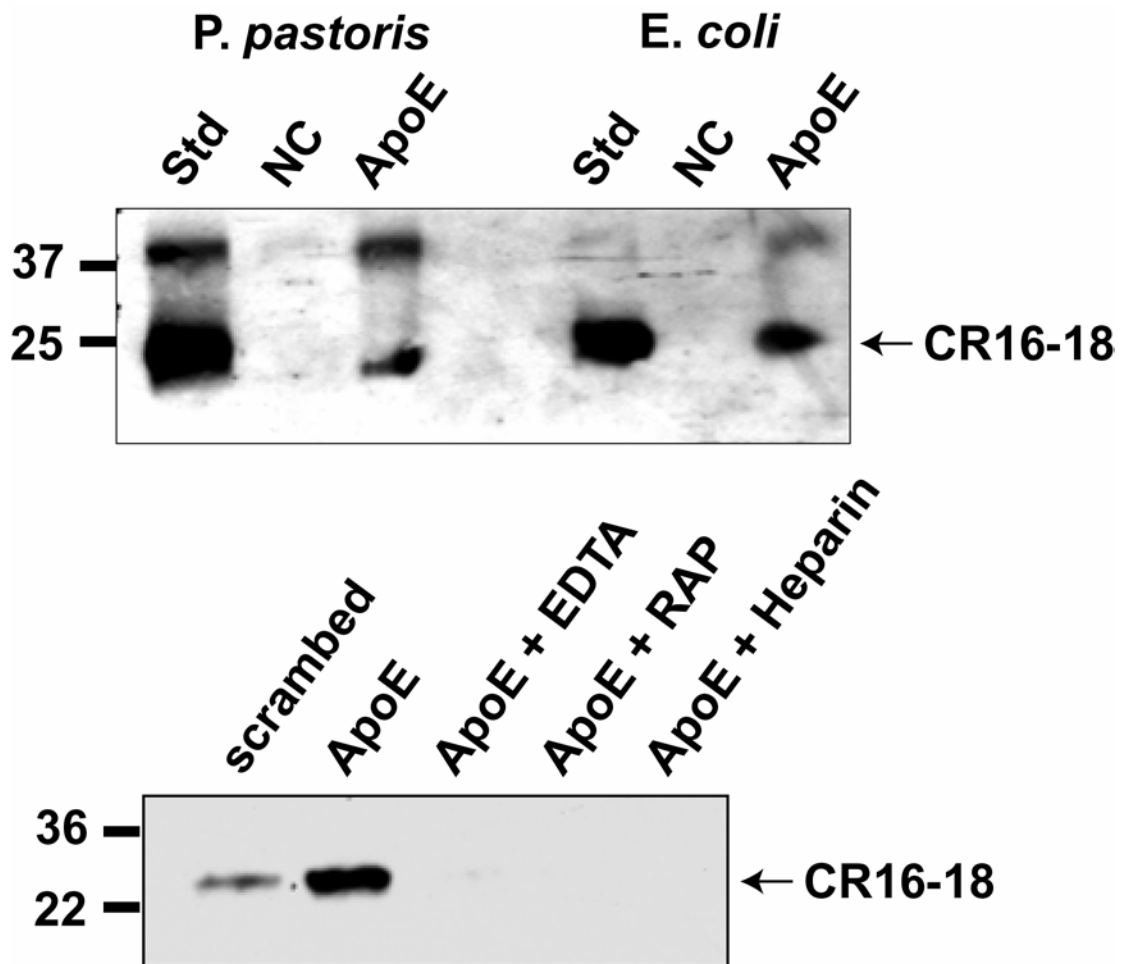


Figure 2.7: Top: Affinity pull-down assays of CR16-18 from either *P. pastoris* or *E. coli* with immobilized ApoE(130-149) peptide or unconjugated beads (NC). Bound CR16-18 was detected by immunoblotting with a polyclonal anti-sLRP3 antibody. Bottom: Same ApoE(130-149) affinity assay comparing binding to scrambled ApoE(130-149) peptide, and inhibition by EDTA, RAP, and Heparin, detected by anti-FLAG immunoblotting.

Addition of calcium in the refolding buffer favors high efficiency of correct refolding for most CRs. The poor refolding efficiency of LA4 was previously observed (Bieri et al. 1998) using very different refolding techniques, indicating that this is not a result of our immobilized refolding strategy. These previous studies have speculated that the presence of neighboring CRs may be required for efficient folding of this LA4. However even in the context of LA45 and LA3-5 the same multiple isomers of LA4 were still present.

Our “native” RP-HPLC is a very effective way to purify correctly refolded CR isomers even at preparatory scale. The observation that multiple isomers of LA4 coeluted perfectly in conventional HPLC may raise alarm as several studies examining refolded domains of LDLR containing LA4 have used this approach to purify the constructs (Simmons et al. 1997; Fisher et al. 2004; Abdul-Aziz et al. 2005).

LA4 has an unusually weak affinity for calcium. Calcium binding monitored by ITC show each refolded CR can interact with a single calcium ion. For the most part, the measured affinities are similar to previously published values for CR/LA domains (North and Blacklow 1999; Simonovic et al. 2001; Andersen et al. 2003; Rudenko and Deisenhofer 2003), except that of LA4. Calcium binding of LA4 has only previously been tested using a four repeat construct LA3-6 (Fisher et al. 2004), in which the weak binding isotherm of this repeat may not be distinguishable. This weak affinity may be the reason we, and others, have seen poor refolding efficiency of this repeat (Bieri et al. 1998).

LA4's weak calcium affinity may have functional relevance for LDLR. At serum calcium levels of around 2mM (Marshall 1995) both LA4 and LA5 would be over 90% calcium bound. As calcium concentrations fall to 10 μ M in the endosome (Gerasimenko et al. 1998), LA4 would only be 2% calcium bound, thus serving as a potential calcium dependent ligand release trigger. It is still not known how much ligand binding affects calcium affinity, therefore it is possible that if LA4 were bound to ligand, the calcium binding site may be stabilized interfering with this triggering mechanism.

Previously it has been concluded that the decrease in calcium concentrations only marginally effects the amount of calcium-bound conformers, however none of the modules in LDLR, and only one in LRP showed calcium affinity as weak as LA4 (Simonovic et al. 2001). These results are consistent with the recent model that both the low pH and the low Ca⁺² ion concentration in the endosome trigger LDL release (Zhao and Michaely 2009) but suggest a revision to the proposal that LA5 is the module triggering ligand release in the endosome (Arias-Moreno et al. 2008).

Refolded CR16-18 is structured and capable of binding ApoE(130-149). In the presence of calcium each purified CR yielded well dispersed spectra as seen for previously for LA1, LA2 and CR8 (Daly 1995; Daly et al. 1995; Huang et al. 1999). The interaction between ApoE(130-149) was still observed with CR16-18 refolded from *E. coli*, also indicating correct refolding. The results also indicate that the native N-linked glycosylation between CR17 and CR18, which is present

in *P. pastoris* derived CR16-18, is not involved in ApoE binding.

References

- Abdul-Aziz, D., Fisher, C., Beglova, N., and Blacklow, S.C. 2005. Folding and binding integrity of variants of a prototype ligand-binding module from the LDL receptor possessing multiple alanine substitutions. *Biochem J* 44: 5075-5085.
- Andersen, O.M., Vorum, H., Honoré, B., and Thøgersen, H.C. 2003. Ca²⁺ binding to complement-type repeat domains 5 and 6 from the low-density lipoprotein receptor-related protein. *BMC Biochemistry* 4.
- Arias-Moreno, X., Velazquez-Campoy, A., Rodríguez, J.C.P., M., and Sancho, J. 2008. Mechanism of low density lipoprotein (LDL) release in the endosome: implications of the stability and Ca²⁺ affinity of the fifth binding module of the LDL receptor. *J Biol Chem* 283: 22670-22679.
- Bieri, S., Atkins, A.R., Lee, H.T., Winzor, D.J., Smith, R., and Kroon, P.A. 1998. Folding, Calcium Binding, and Structural Characterization of a Concatemer of the First and Second Ligand-Binding Modules of the Low-Density Lipoprotein Receptor. *Biochemistry* 37: 10994-11002.
- Blacklow, S.C. 2007. Versatility in ligand recognition by LDL receptor family proteins: advances and frontiers. *Curr Opin Struct Biol* 17: 419-426.
- Blacklow, S.C., and Kim, P.S. 1996. Protein folding and calcium binding defects arising from familial hypercholesterolemia mutations of the LDL receptor. *Nat Struct Biol* 3: 758-762.
- Brown, M.S., and Goldstein, J.L. 1986. A receptor-mediated pathway for cholesterol homeostasis. *Science (New York, N.Y)* 232: 34-47.
- Croy, J.E., Brandon, T., and Komives, E.A. 2004. Two apolipoprotein E mimetic peptides, apoE(130-149) and apoE(141-155)₂, bind to LRP1. *Biochemistry* 34: 7328-7335.
- Croy, J.E., Shin, W.D., Knauer, M.F., Knauer, D.J., and Komives, E.A. 2003. All three LDL receptor homology regions of the LDL receptor-related protein (LRP) bind multiple ligands. *Biochemistry* 42: 13049-13057.
- Daly, N.L., Djordjevic, J.T., Kroon, P.A., and Smith, R. 1995. Three-dimensional structure of the second cysteine-rich repeat from the human low-density

- lipoprotein receptor. *Biochemistry* 34: 14474-14481.
- Daly, N.L., Scanlon, M. J., Djordijevic, J. T., Kroon, P.A., and Smith, R. 1995. Three-dimensional structure of a cysteine-rich repeat from the low-density lipoprotein receptor. *Proc. Natl. Acad. Sci. USA* 92: 6334-6338.
- Davis, C.G., Goldstein, J. L., Sudhof, T. C., Anderson, R. G. W., Russell, D. W., and Brown, M. S. 1987. Acid-dependant ligand dissociation and recycling of LDL receptor mediated by growth factor homology region. *Nature* 326: 760-765.
- Esser, V., Limbird, L.E., Brown, M.S., Goldstein, J.L., and Russell, D.W. 1988. Mutational analysis of the ligand binding domain of the low density lipoprotein receptor. *J Biol Chem* 263: 13282-13290.
- Fass, D., Blacklow, S., Kim, P. S., and Berger, J. M. 1997. Molecular basis of familial hypercholesterolaemia from structure of LDL receptor module. *Nature* 388: 691-693.
- Fisher, C., Abdul-Aziz, D., and Blacklow, S.C. 2004. A two-module region of the low-density lipoprotein receptor sufficient for formation of complexes with apolipoprotein E ligands. *Biochem J* 43: 1037-1044.
- Gerasimenko, J.V., Tepikin, A.V., Petersen, O.H., and Gerasimenko, O.V. 1998. Calcium uptake via endocytosis with rapid release from acidifying endosomes. *Curr Biol* 8: 1335-1338.
- Gray, W.R. 1993. Disulfide structures of highly bridged peptides: a new strategy for analysis. *Protein Sci* 2: 1732-1748.
- Guo, Y., Yu, X., Rihani, K., Wang, Q.Y., and Rong, L. 2004. The role of a conserved acidic residue in calcium-dependent protein folding for a low density lipoprotein (LDL)-A module: implications in structure and function for the LDL receptor superfamily. *J Biol Chem* 279: 16629-16637.
- Herz, J., Hamann, U., Rogne, S., Myklebost, O., Gausepohl, H., and Stanley, K.K. 1988. Surface location and high affinity for calcium of a 500-kd liver membrane protein closely related to the LDL-receptor suggest a physiological role as lipoprotein receptor. *Embo Journal* 7: 4119-4127.
- Huang, W., Dolmer, K., and Gettins, P.G. 1999. NMR solution structure of complement-like repeat CR8 from the low density lipoprotein receptor-related protein. *J Biol Chem* 274: 14130-14136.
- Hussain, M.M., Maxfield, F.R., Más-Oliva, J., Tabas, I., Ji, Z.S., Innerarity, T.L.,

- and Mahley, R.W. 1991. Clearance of chylomicron remnants by the low density lipoprotein receptor-related protein/alpha 2-macroglobulin receptor. *J Biol Chem* 266: 13936-13940.
- Kiss, R.S., Weers, P.M., Narayanaswami, V., Cohen, J., Kay, C.M., and Ryan, R.O. 2003. Structure-guided protein engineering modulates helix bundle exchangeable apolipoprotein properties. *J Biol Chem* 278: 21952-21959.
- Koeppel, J.R., Seitova, A., Mather, T., and Komives, E.A. 2005. Thrombomodulin Tightens the Thrombin Active Site Loops To Promote Protein C Activation. *Biochemistry* 44: 14784-14791.
- Kowal, R.C., Herz, J., Goldstein, J. L., Esser, V., and Brown, M. S. 1989. Low density receptor-related protein mediates uptake of cholesteryl esters derived from apolipoprotein E-enriched lipoproteins. *Proc. Natl. Acad. Sci. USA* 86: 5810-5814.
- Marshall, W.J. 1995. *Clinical Chemistry*. Mosby, London.
- North, C.L., and Blacklow, S.C. 1999. Structural independence of ligand-binding modules five and six of the LDL receptor. *Biochem J* 38: 3926-3935.
- Rudenko, G., and Deisenhofer, J. 2003. The low-density lipoprotein receptor: ligands, debates and lore. *Curr Opin Struct Biol* 13: 683-689.
- Rudenko, G., Henry, L., Henderson, K., Ichtchenko, K., Brown, M.S., Goldstein, J.L., and Deisenhofer, J. 2002. Structure of the LDL receptor extracellular domain at endosomal pH. *Science (New York, N.Y)* 298: 2353-2358.
- Russell, D.W., Brown, M.S., and Goldstein, J.L. 1989. Different combinations of cysteine-rich repeats mediate binding of low density lipoprotein receptor to two different proteins. *J Biol Chem* 264: 21682-21688.
- Simmons, T., Newhouse, Y.M., Arnold, K.S., Innerarity, T.L., and Weisgraber, K.H. 1997. Human low density lipoprotein receptor fragment. Successful refolding of a functionally active ligand-binding domain produced in *Escherichia coli*. *J Biol Chem* 272: 25531-25536.
- Simonovic, M., Dolmer, K., Huang, W., Strickland, D.K., Volz, K., and Gettins, P.G.W. 2001. Calcium Coordination and pH dependence of the calcium affinity of ligand-binding repeat CR7 from the LRP. Comparison with related domains from the LRP and the LDL receptor. *Biochemistry* 40: 15127-15134.
- Weisgraber, K.L., Innerarity, T.L., Harder, K.J., Mahley, R.W., Milne, R.W.,

- Marcel, Y.L., and Sparrow, J.T. 1983. The Receptor Binding Domain Of Human Apolipoprotein E. *J. Biol. Chem* 258: 12348-12354.
- Zaiou, M., Arnold, K.S., Newhouse, Y.M., Innerarity, T.L., Weisgraber, K.H., Segall, M.L., Phillips, M.C., and Lund-Katz, S. 2000. Apolipoprotein E;-low density lipoprotein receptor interaction. Influences of basic residue and amphipathic alpha-helix organization in the ligand. *J Lipid Res* 41: 1087-1095.
- Zhao, Z., and Michaely, P. 2009. The Role of Calcium in Lipoprotein Release by the Low-Density Lipoprotein Receptor. *Biochemistry* 48: 7313–7324.

Chapter 3
Properties of Ligand Binding Modules
Governing Interactions with ApoE

Introduction

As mentioned in Chapter One, the low density lipoprotein receptor (LDLR) mediates cholesterol uptake into cells (Blacklow 2007). Two other members of this receptor family, the LDL receptor-related protein (LRP) and the very low density lipoprotein receptor (VLDLR) have also been shown to internalize lipoprotein particles (Kowal 1989; Hussain et al. 1991; Takahashi et al. 1992; Tacke et al. 2000). All three receptors share many structural characteristics including clusters of complement-type repeats (CRs), also called ligand binding modules (LAs), epidermal growth factor precursor homology repeats (EGFs), β -propeller domains, and a single transmembrane region (Fig. 3.1). These clusters of CRs alone can recognize and bind various ligands (Simmons et al. 1997; Croy et al. 2003). The most well characterized of these receptors, LDLR, is genetically linked to familial hypercholesterolemia (FH) (Brown 1986). Several of the mutations causing FH have been shown to wreck proper folding of these CRs (Blacklow and Kim 1996). Several CR domains have now been solved by both NMR and crystallographic methods (Rudenko and Deisenhofer 2003), and show very little deviation in their overall fold. It is believed that high variability in short loops of these repeats results in different surface contours and electrostatics, which establish ligand specificity (Huang et al. 1999; Blacklow 2007).

Much like LDLR, LRP was shown to bind and internalize β -VLDLs, but only if the VLDLs were enriched with ApoE (Kowal 1989). Other distinctions between the two receptors have been observed including calcium dependence (Beisiegel et al. 1989; Mokuno 1991), and RAP inhibition of ligand binding (Herz

et al. 1991; Croy et al. 2003). The receptor associated protein (RAP) is an ER resident protein, serving as a chaperone for the maturation of LRP (Willnow et al. 1995; Bu and Rennke 1996). RAP can interact with ligand binding clusters of this family of receptors, blocking the binding of certain ligands (Herz et al. 1991). Each of the three helical bundle domains of RAP can interact with receptors, but the third domain (RAPD3) has the highest affinity for these ligand binding clusters (Andersen et al. 2001). It was shown that RAPD3 displayed high affinity for nearly all CR pairs with a conserved DXDXD motif between the 4th and 5th cysteines (Andersen et al. 2000).

LDLR family members recognize apolipoproteins on the surface of lipoprotein particles, particularly Apolipoprotein E, which plays the largest role in receptor mediated cholesterol uptake (Hui et al. 1984). ApoE is a constituent of several lipoprotein particles, and common alleles affecting receptor binding, are associated with type III hyperlipoproteinemia (Rall et al. 1982). Several studies agree that the critical receptor recognition site is within residues 140-150 of the N-terminal domain (Innerarity et al. 1983; Weisgraber 1983; Lalazar et al. 1988; Zaiou et al. 2000; Kiss et al. 2003). Peptides from this region of ApoE incorporated into lipoprotein particles, enhanced uptake both *in vitro* and *in vivo* (Mims et al. 1994; Datta et al. 2001). Studies have also shown that ApoE(130-149) can directly interact with the three complete sLRPs (2, 3, and 4) of LRP (Croy et al. 2004).

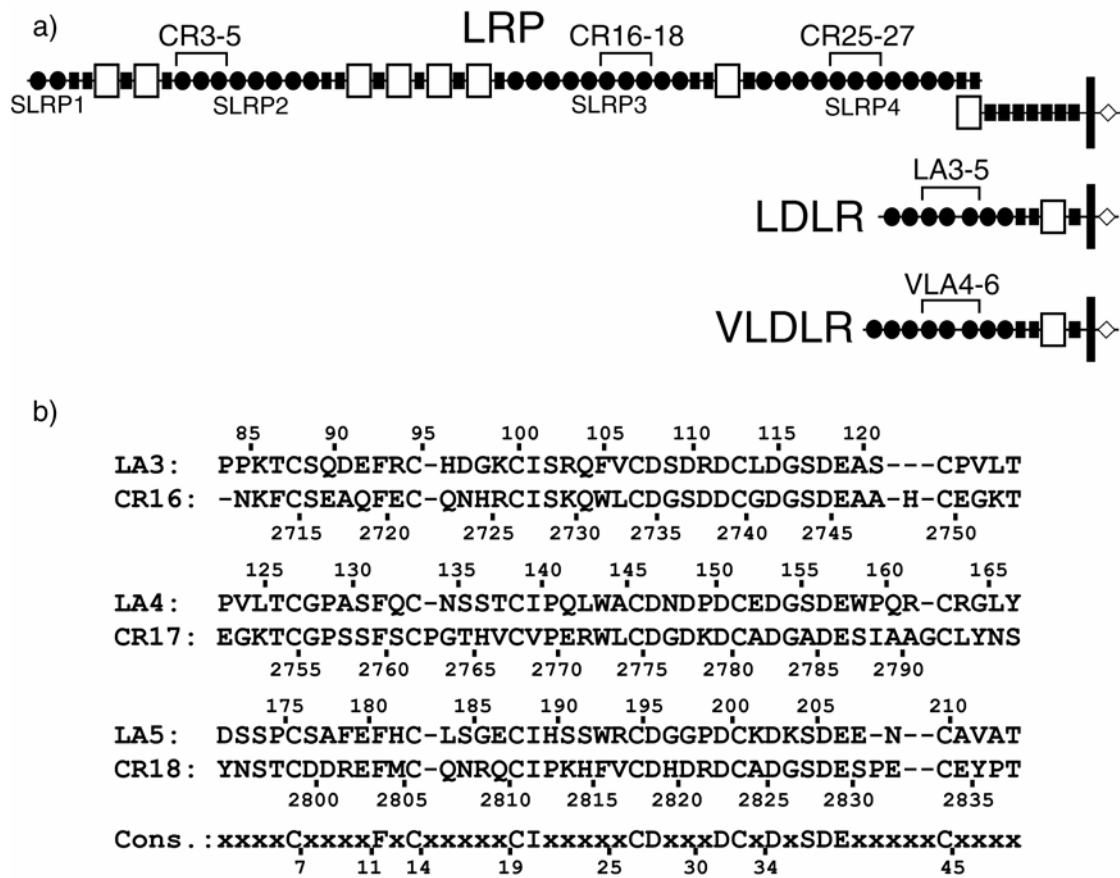


Figure 3.1: **a)** Schematic diagram of LRP, LDL, and VLDL showing CR/LA modules (circles), EGF domains (black rectangles), β -propeller domains (clear rectangles), and intracellular domain (diamonds). **b)** Sequence alignment of LA3-5 with CR16-18 with overall consensus for complement repeats (Blacklow and Kim 1996).

The crystal structure of the N terminal domain of ApoE has been solved (Wilson et al. 1991), and although residues 131-151 form a surface-accessible helix in the structure, the N-terminal domain alone cannot bind LDL receptors with high affinity. Low resolution structural information indicates that the ApoE helical bundle adopts a new conformation when it is present in lipoprotein particles (Fisher and Ryan 1999; Peters-Libeu et al. 2006; Peters-Libeu et al. 2007). Evidence suggests that upon lipid association this region of ApoE becomes more accessible (Lund-Katz et al. 2000). In addition, upon lipid binding, the region downstream of the 140-150 site, which also contains critical residues for receptor binding, becomes structured (Rall et al. 1982; Lalazar and Mahley 1989; Morrow et al. 2000; Gupta et al. 2006). Thus, it is also possible that this downstream region forms a high affinity receptor recognition site in the lipid bound state of ApoE.

Studies aimed at narrowing down the exact binding modules involved in recognizing ApoE have found minimal units in LDLR (Russell et al. 1989; Fisher et al. 2004) and VLDLR (Ruiz et al. 2005). Deletion studies in LDLR have implicated LA5 as the critical repeat for β -VLDL binding (Russell et al. 1989). LA45 was shown to be the minimal unit of LDLR capable of binding ApoE(1-191)•dimyristoyl-phosphatidylcholine (DMPC) particles *in vitro*, which are thought to mimic the lipid bound conformer of ApoE (Fisher et al. 2004). Similar studies have implicated repeats 5 and 6 (VLA56) of VLDLR in ApoE binding (Ruiz et al. 2005). Interestingly both LA45 and VLA56 have a uniquely long linker sequence

connecting the two repeats. We have previously observed that CR16-18 from sLRP3 of LRP was capable of binding ApoE(130-149) with high affinity. In order to better understand what properties of CRs govern ApoE recognition, the interaction was examined with this fragment of LRP, along with repeats from LDLR. Together, the results reveal specific regions within LDLRs that are critical for the recognition of ApoE containing lipoproteins.

Materials and Methods

Protein expression and purification. CR16-18, LA3-5 and all smaller domains were expressed and purified as described in Chapter Two. All mutants were made using either inverse PCR (Clackson et al. 1991) or Quickchange (Stratagene, La Jolla, CA, USA) mutagenesis, and verified by DNA sequencing. A triple tandem CR17 (CR17³) was constructed by inserting CR17 with identical sticky ends into the BamH1 site of CR17 in the pMMHb vector, and screening for multiple insertions with correct orientation. Inverse PCR mutagenesis was used to remove CR17 from CR16-18 yielding a two repeat CR16(Δ 17)18.

ApoE(130-149) and ApoE(141-155)² were synthesized with N terminal biotinylation on a 9050 peptide synthesizer (Applied Biosystems). A scrambled ApoE(130-149) was also synthesized with the sequence LREKKLRVSALRTHRLELRL. Purification of GST-RAP has been described previously (Croy et al. 2003). All of the LDLR ligands were prepared as ubiquitin fusions because this aided in solubility of the ApoE(130-149). A Ubiquitin (Ub)

fusion vector was generated by cloning the DNA sequence for Ubiquitin into the Nco1 and BamH1 sites of vector pHis8 (Jez et al. 2000). RAPD3 (residues 218-323) was introduced between the BamH1 and Not1 sites to generate a His8-Ub-RAPD3 construct. The same strategy was used to generate His8-Ub-ApoE(130-149). A stop codon was inserted at the C terminal end of Ub to generate a His8-Ub construct that was used to prepare free Ub as a negative control ligand. Expression vectors were introduced into BL21-DE3 cells, grown in LB to OD₆₀₀ 0.5, induced with 0.1mM IPTG isopropyl-beta-D-thiogalactopyranoside (IPTG) for 4 hrs at 37°C. Cells were harvested, resuspended in TBS (50mM Tris pH 8.0 500mM NaCl), lysed by sonication, and the protein was purified by Ni-NTA (Qiagen), followed by gel filtration through Sephadex 75 (GE healthcare) in MB150 (20mM Hepes pH 7.45, 150mM NaCl, 10mM CaCl₂, and 0.02% azide.). Ub-ApoE(130-149) was further purified with an additional cation exchange (monoS) (GE healthcare) step prior to gel filtration.

An expression vector for ApoE 1-191 was a kind gift from S. Blacklow. His tagged ApoE 1-191 was expressed in BL21-DE3, purified and complexed with dimyristoyl-phosphatidylcholine (DMPC) (Avanti Polar Lipids, Alabaster, AL, USA) as described previously (Fisher et al. 2004). Expressed proteins were analyzed by MALDI-TOF on a Voyager DE-STR (Applied Biosystems, Foster City, CA, USA) with sinnapinic acid (Agilent, Santa Clara, CA, USA) as the matrix.

ApoE (130-149) Pulldowns. All reactions were carried out in HBST (20mM HEPES pH 7.4, 150mM NaCl 0.02% sodium azide, 0.1% Tween-20 (Biorad, Hercules, CA, USA)) containing either 2mM CaCl₂ or 2mM EDTA. ApoE peptide (130-149) with an N-terminal biotin was immobilized onto streptavidin agarose (Fluka, Buchs, Switzerland) at saturating concentrations as described previously (Croy et al. 2004). Either uncoupled beads or scrambled ApoE(130-149) peptide was used as a negative control. FLAG-tagged complement repeat constructs were added (500nM), reactions were left rocking at 25°C for 2 hours, then washed twice with the same buffer, resolved by SDS-PAGE, probed with anti-FLAG antibody (a generous gift from P. van der Geer) and detected by chemiluminescence (Western Lightning Plus kit, Perkin Elmer, Waltham, MA, USA). For comparisons of CR16-18, CR1617, CR1718, and CR16(Δ17)18, 500nM and 5μM concentrations were used in pulldown binding assays.

GST-RAP and ApoE-DMPC pulldowns. GST-RAP (1μM) or ApoE(1-191)•DMPC (2μM) was mixed with various FLAG-tagged LA/CR constructs (1μM), at 25°C for 1 hour, in HBST with either 1mM calcium or 1mM EDTA. The LA/CR constructs were then captured with anti-FLAG agarose (Sigma-Aldrich, ST. Louis, MO, USA) for 30 minutes, washed 3 times in the same HBST buffer, resolved by SDS-PAGE and probed by western blot with antibodies anti-ApoE (Millipore, Billerica, MA, USA), anti-GST (GE Healthcare, Uppsala, Sweden) and anti-FLAG rabbit serum. In order to avoid the high background caused by minor

precipitation of ApoE-DMPC, reactions were centrifuged for 5 minutes after the incubation step, and the supernatant was added to anti-FLAG agarose.

NMR titrations. All titrations of CR/LA(s) with various ligands were performed in 20mM Hepes (pH 7.45), 150mM NaCl, 10mM CaCl₂, and 0.02% azide in 10% D₂O at 307°K. Due to self association of CR17, all CR concentrations were kept under 100μM, which became problematic at large excess of titrated ligands due to the appearance of peaks from natural abundance ¹⁵N from the ligand. Identical aliquots of ¹⁵N labeled CR/LAs were resuspended in either Ub-fused ligand or Ub, adjusted to pH 7.45, and mixed in various ratios to yield samples with varying concentrations of ligand but identical total protein concentration. Only well resolved peaks in all titrations were used for affinity calculations. Slow exchange binding kinetics were seen for CR18-RAPD3 titrations (Fig. 3.6), thus only shifts showing fast exchange kinetics were used for affinity measurements. For some titrations, the highest ligand concentration could not be included in the fit due to poor signal to noise and broadening of peaks. ¹⁵N shifts were normalized by a factor of 9.8, and the net shift for every cross peak in both ¹H and ¹⁵N was calculated. A global fit of all perturbations (>0.015ppm) was implemented as described previously (Hoffman et al. 2005). Titration curves were also fit to measurements of the largest cross peak perturbation and the sum of all individual perturbations. Overall K_Ds are reported as the average from these three methods, with the standard deviation of all measurements.

NMR assignments. NMR spectra were collected on a Bruker Avance 800 MHz, or a Bruker Avance III 600 MHz spectrometer equipped with a cryoprobe. ^{15}N , ^{13}C labeled CR16-18 (0.5mM) was resuspended in 20mM Hepes (pH 6.6), 150mM NaCl, 5mM CaCl_2 , 50mM Arginine, 50mM Glutamic acid, 10% D_2O and 0.02% sodium azide. Amide assignments were made with ^1H - ^{15}N HSQC, HNC0, HNCA, HN(CO)CA, HNCACB collected at 307K. Assignments for CR17 were also made using a 0.7mM sample of ^{15}N , ^{13}C labeled CR17 at pH 7.45 in the same buffer, with HSQC, CBCANH, CBCANNH experiments. ^{15}N labeled CR16 (0.4mM) and CR18 (0.6mM) were titrated from pH 6.6 to pH 7.45 to monitor pH-dependent chemical shift changes and to transfer the assignments from CR16-18 at pH 6.6. LA45 was assigned in the same buffer without the 50mM Arg/Glu, with the same set of experiments used for CR17, and assignments were transferred to LA4 and LA5. The data were processed using Azara (Wayne Boucher and the Department of Biochemistry, University of Cambridge) and analyzed in Sparky (T. D. Goddard and D. G. Kneller, SPARKY 3, University of California, San Francisco). All assignment data for CR16-18, CR17, and LA45 have been deposited to the BMRB (IDs 16509, 16482 and 16480).

Alignments. To further analyze the sequences for unique residues that might be involved in ApoE binding, alignments of LA45 from LDLR and VLA56 from VLDLR from various species were made with genedoc 2.6 (Nicholas and Jr. 1997) (uniprot accession numbers: P01130, P98155, P35951, P98156, P35952, P98166, Q28832, P35950, Q99087, Q6NS01, Q99088, O77505, P20063, P35953, P98165, Q7ZZT0, Q6S4M2).

Results

Two-domain fragments of CR16-18 bind ApoE(130-149) more weakly than CR16-18. FLAG-tagged CR16-18 and smaller constructs lacking a single repeat were assayed side by side for binding ApoE(130-149). Although CR16-17 showed no binding, CR17-18 and to a lesser degree CR16(Δ 17)18 showed weaker affinity (Fig. 3.2). It took ten fold higher concentrations of CR17-18 to observe the same signal as that of CR16-18 indicating that there is roughly an order of magnitude difference in their affinities.

Titrations of ApoE(130-149) binding to LRP1 CR(s). NMR titrations were used to examine the binding of CR16-18 to ApoE(130-149). Initial titration experiments with ApoE(130-149) peptide resulted in solubility problems, so ApoE(130-149) was expressed as a ubiquitin (Ub) fusion protein, and this alleviated the solubility problems even at concentrations above 1mM. Binding of

Ub-ApoE(130-149) caused specific perturbations in each repeat (Fig. 3.3). The most notable perturbation was a strong downfield ^1H shift for the indole of W2773 in CR17. The same was true for the indole of W2732 in CR16, and W144 in LA4. F2816, which is in the same position in CR18, showed the largest perturbation in this repeat. Other amides showing large perturbations included: K2730, W2732, D2735, G2736, S2737, A2746, in CR16; F2760, C2768, V2769, R2772, W2773, D2776, A2790, in CR17; and R2809, C2818, D2829, E2833, in CR18; D149 in LA4; S192 and G198 in LA5. Titrations of Ub-ApoE(130-149) with individual CRs showed identical shifts to those observed in CR16-18 (Fig 3.4), and the same similarity was observed for LA45. Plots of relative perturbations in each repeat show the majority of large shifts are located in two loops between the third and fifth Cys (residues 23-32 according to consensus numbering in Fig. 3.1), but there was also significant variability of which residues shifted more among the three repeats (Fig. 3.6a). Some amide cross peaks which were nearly invisible in CR17 (C2762, C2768) became well resolved upon addition of ApoE(130-149) hinting that slow dynamics in unbound CR17 are alleviated in the ApoE(130-149)-bound form.

Due to the weak binding and small shifts, three different fitting methods were implemented to calculate K_D s from these titrations, giving remarkably similar results for most cases (Table 3.1) (Fig. 3.6b). These calculations revealed that CR17 had the highest affinity for ApoE(130-149) with a K_D of $930\mu\text{M}$, similar to the value measured for LA4, $1092 \pm 91\mu\text{M}$. In the context of CR16-18 and LA45, both CR17 and LA4 showed tighter binding to ApoE(130-

149) ($650 \pm 94 \mu\text{M}$ and $380 \pm 41 \mu\text{M}$ respectively). CR18 had a significantly weaker affinity (1.6mM) as both the isolated domain and in the context of CR16-18. CR16 had a very weak affinity as an isolated repeat ($\sim 3.2 \text{mM}$) but a much stronger affinity in the context of CR16-18 ($730 \pm 47 \mu\text{M}$), and a similar enhancement was seen for LA5 ($3.9 \pm 0.29 \text{mM}$ to $640 \pm 16 \mu\text{M}$). Although amides in LA3 were not assigned, titrations showed an extremely weak affinity ($>5 \text{mM}$) for ApoE(130-149).

To ensure the observed affinity was purely the result of interaction with the ApoE(130-149), CR17 was also titrated with two variants of ApoE; Ub-ApoE(130-149)(K143/146A) and Ub-ApoE(130-140). These titrations showed that the double mutation of the critical lysines, K143 and K146 to Ala significantly weakened binding ($K_D = 3.5 \text{mM}$), and truncation of the last nine residues (ApoE(130-140)) nearly abolished it ($K_D > 5 \text{mM}$). Similarly, mutation of D2778 in CR17 (D2778A), that has been shown to be important for RAP binding, decreased the affinity for ApoE(130-149) significantly ($K_D = 3.5 \text{mM}$) (Andersen et al. 2000).

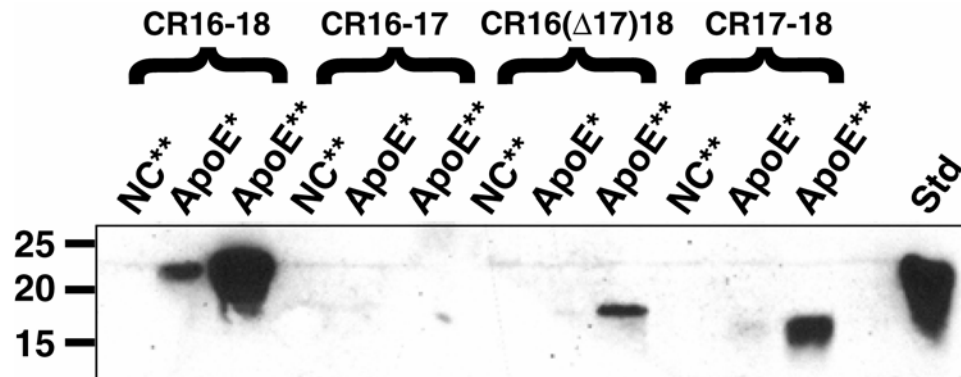


Figure 3.2: FLAG-tagged CR16-18 and smaller repeats were tested for binding ApoE(130-149) with (*) 2.0 μ M CR domain and unconjugated beads, (**) 100nM CR domain and immobilized ApoE(130-149), or (*) 2.0 μ M CR domain and immobilized ApoE(130-149). The bound subdomains were visualized by anti-FLAG immunoblotting.

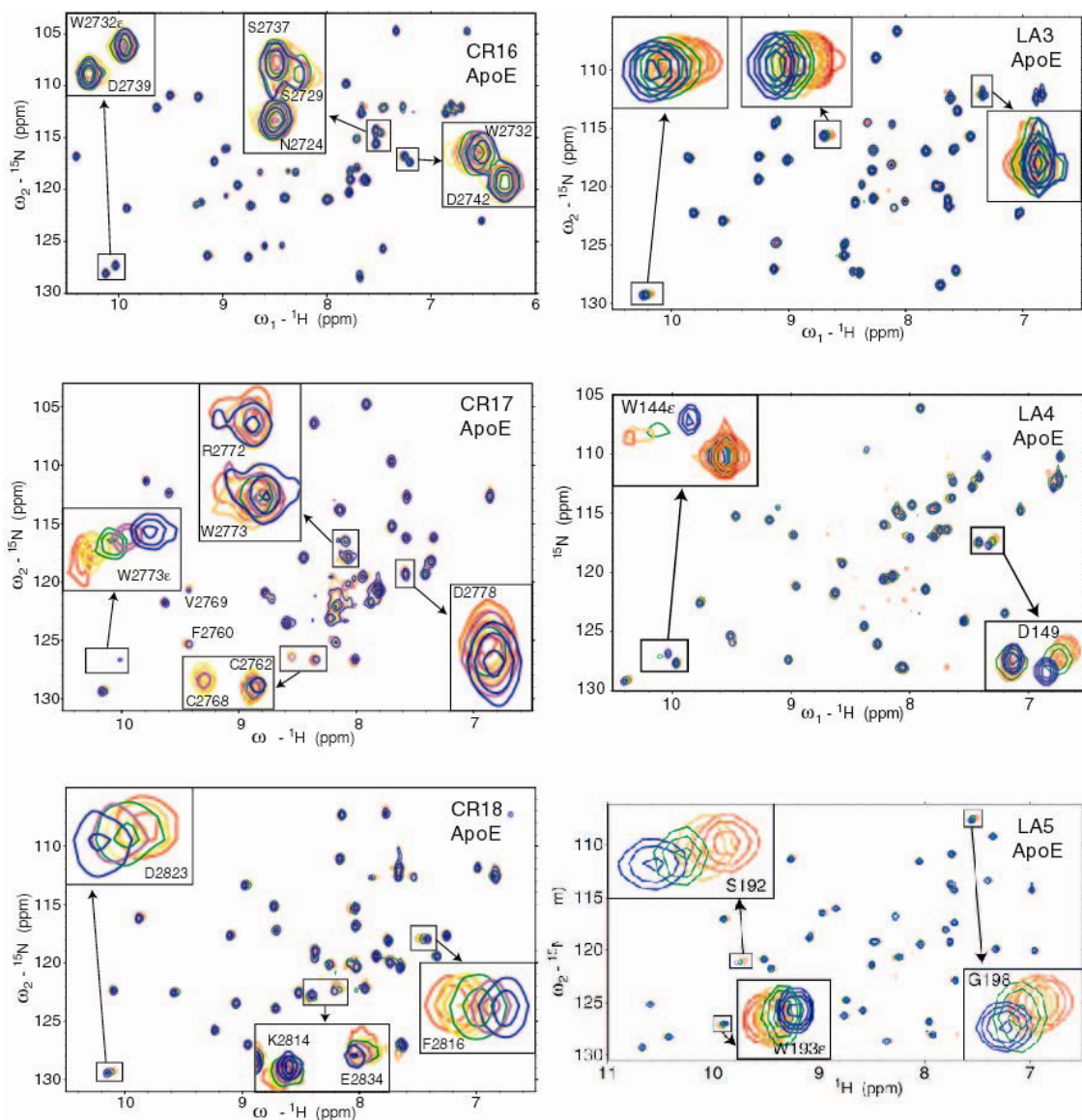


Figure 3.3: NMR titration of Ub-ApoE(130-149) into each CR/LA, from zero ligand (blue) to green, orange, and final ligand concentration (red). Strong perturbations are labeled, and some are expanded for clarity.

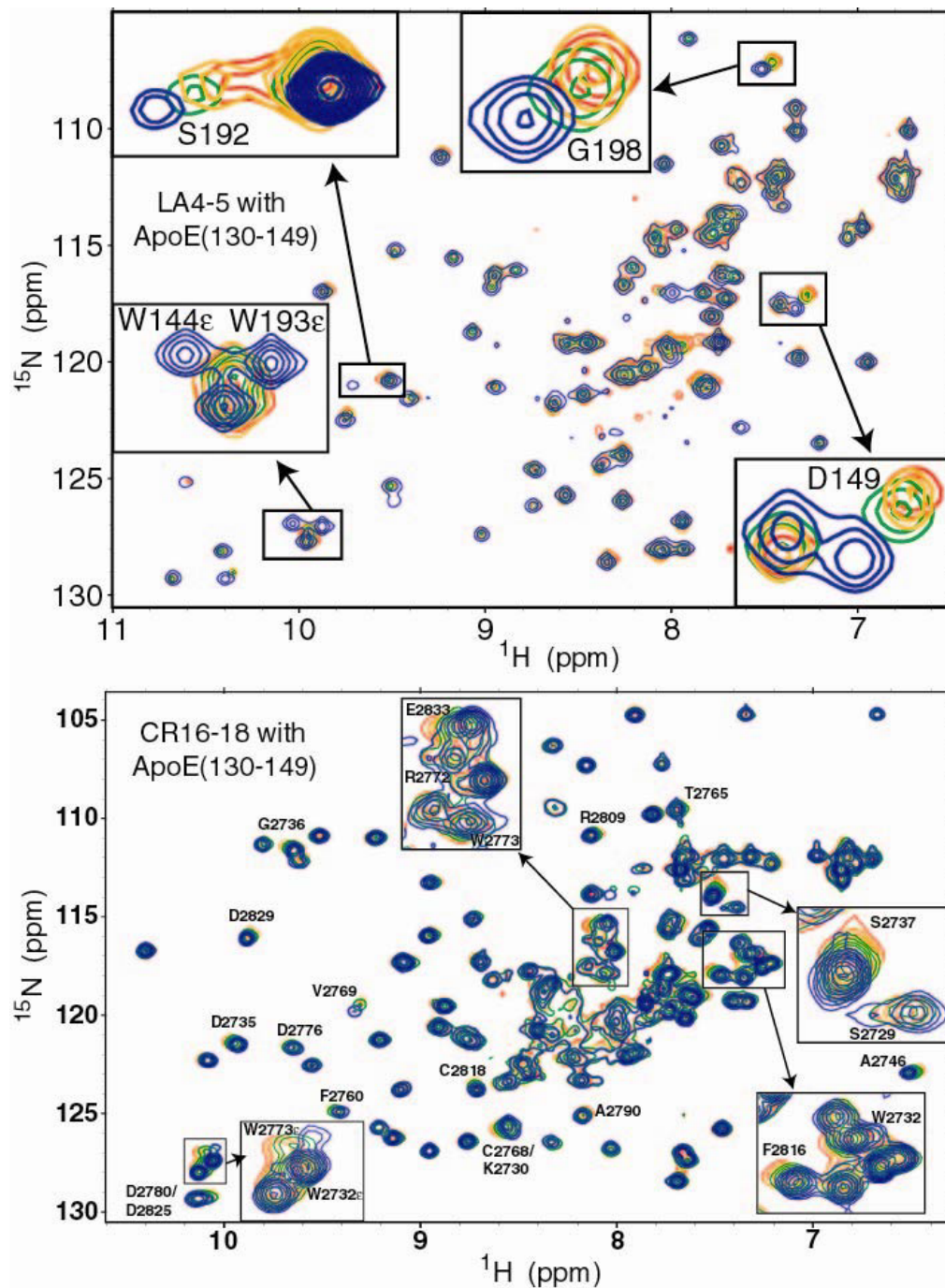


Figure 3.4: NMR titration of Ub-ApoE(130-149) into LA4-5 and CR16-18, from zero ligand (blue) to green, orange, and final ligand concentration (red). Strong perturbations are labeled, and some are expanded for clarity.

The results from titrations of the LRP CRs with ApoE(130-149) indicated that individual CRs could each bind ApoE(130-149). To see whether RAP might elicit similar chemical shift perturbations in the CRs, we titrated the individual CRs with RAPD3. Although two CRs are known to be required for high affinity binding of RAPD3 (Andersen et al. 2000), strong chemical shift perturbations were observed with single CRs (Fig. 3.6). In LA4 and CR17, the largest perturbation was a downfield ^1H shift for the indole of W144 and W2773, exactly as seen with ApoE(130-149). The overall pattern of residues shifted in CR17 was similar to that observed upon ApoE(130-149) binding, with notable differences in the direction of shifts for R2772, W2773, and D2778. C2781 also showed a large perturbation, and the two crosspeaks that became visible upon ApoE(130-149) binding (C2762, C2768) showed the opposite effect with RAPD3. Cross peaks in CR18 showed both fast and slow exchange kinetics when perturbed by RAPD3 binding. C2806, N2808, D2821, and D2823, showed the largest perturbations with fast exchange, of which D2823 shows the same shift it did upon ApoE(130-149) binding (Fig. 3.6). Cross peaks for D2800, D2812, K2814, and F2816 could not be followed due to the slow kinetics of exchange. The fast exchanging chemical shift perturbations were fit to titration curves in the same manner as was done for ApoE (Table 3.1). Each of the individual CRs bound RAPD3 roughly ten-fold tighter than ApoE(130-149). LA4, CR17 and CR18 showed the strongest affinity (49 μM , 35 μM and 58 μM respectively) (Fig. 3.5). LA3 and LA5 had much weaker affinities (490 μM , 670 μM respectively), and the mutation of the

critical Asp in CR17, (D2778A) again showed a drastic decrease in K_D for RAPD3 (K_D increased from 35 to 720 μ M).

Binding to ApoE(1-191)•DMPC. To examine the interaction with the full receptor binding site of lipid-complexed ApoE, Flag-tagged LA3-5 and CR16-18 were used for pulldown assays with ApoE(1-191)•DMPC. As expected, both constructs could interact with GST-RAP in a calcium dependent manner (Fisher et al. 2004), but only LA3-5 showed binding to ApoE(1-191)•DMPC. This was a surprising result considering that CR16-18 bound ApoE(130-149) with similar properties and was discovered by sequence similarity to LA3-5. To test whether multiple copies of a CR with high ApoE(130-149) affinity could interact with lipid complexed ApoE, a triple CR17 (CR17³) was constructed. Despite a strong interaction with ApoE(130-149) and GST-RAP, CR17³ showed no interaction with ApoE(1-191)•DMPC (Fig. 3.7, 3.8).

D149 in LA4, D2778 in CR17 and D2821 in CR18 (all equivalent to D30 in the consensus) showed chemical shift perturbation upon RAPD3 binding in our NMR titrations, and mutation of this residue in CR17 disrupted binding of ApoE(130-149) and RAPD3 (see above). We mutated each of these to Ala in LA3-5 and CR16-18 to test for effects on ApoE(1-191)•DMPC binding. Mutation of D149A(D30A) in LA4 weakened binding to ApoE(130-149) and GST-RAP, and completely abolished ApoE(1-191)•DMPC binding (Fig. 3.7, 3.8). Similarly, alanine mutation of the critical D2778 and D2821 (both D30) in CR17 and CR18

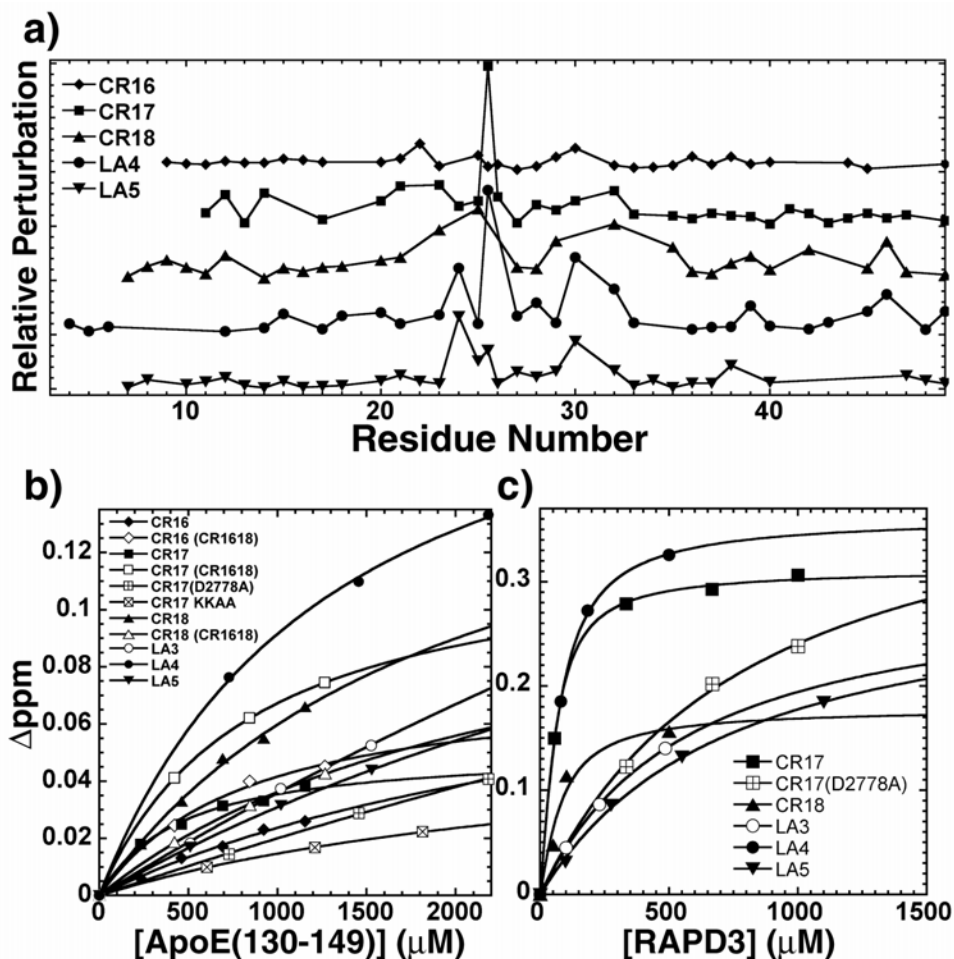


Figure 3.5: **a)** Plot of relative amide perturbation for each residue in CR16 (◆), CR17 (■), CR18 (▲), LA4 (●), and LA5 (▼). CRs are each renumbered for alignments shown in Fig. 1b, and indole sidechains of W25 are plotted at the x-axis value of 25.5. **b)** NMR titration plots for Ub-ApoE(130-149) with: CR16 (◆), CR16 in CR16-18 (◇), CR17 (■), CR17 in CR16-18 (□), CR17(D2778A) ([+]), CR17 with ApoE(130-149) (K143/146A) ([X]), CR18 (▲), CR18 in CR16-18 (Δ), LA3 (○), LA4 (●), and LA5 (▼). **c)** NMR titration plots for Ub-RAPD3 with the same symbols from b). For both plots the largest resolvable amide perturbation was plotted against the ligand concentration.

Table 3.1: Binding affinities for various ApoE-LA/CR interactions

ND, certain titrations could not be fit, or yielded K_D values $>5\text{mM}$ with large uncertainty.

	K_D (Global)	K_D (Largest)	K_D (Sum)	K_D (Overall)
<u>(μM)</u>				
Ub-RAPD3 binding				
CR17	33 ± 8	33 ± 3	40 ± 6	35 ± 4
CR17 (D2778A)	710 ± 62	770 ± 130	680 ± 95	720 ± 46
CR18	55 ± 5	57 ± 30	62 ± 33	58 ± 4
LA3	460 ± 22	530 ± 4	480 ± 40	490 ± 36
LA4	52 ± 5	50 ± 2	46 ± 4	49 ± 3
LA5	650 ± 35	700 ± 70	660 ± 52	670 ± 26
Ub-ApoE(130-149) binding				
CR16	ND	3176 ± 1050	ND	$3176 \pm \text{ND}$
CR17	1027 ± 284	852 ± 334	912 ± 205	930 ± 89
CR17 (D2778A)	3496 ± 729	ND	3545 ± 250	3521 ± 35
CR18	1441 ± 266	1975 ± 381	1349 ± 163	1588 ± 338
CR16 (in 16-18)	774 ± 102	744 ± 183	681 ± 67	733 ± 47
CR17 (in 16-18)	581 ± 92	757 ± 7	610 ± 19	649 ± 94
CR18 (in 16-18)	1194 ± 239	2249 ± 220	1289 ± 90	1577 ± 584
LA3	8509 ± 3018	ND	9961 ± 160	9235 ± 1027
LA4	1031 ± 73	1197 ± 106	1049 ± 26	1092 ± 91
LA5	3822 ± 433	4189 ± 538	3622 ± 167	3878 ± 288
LA4 (in 4-5)	395 ± 16	410 ± 69	332 ± 11	379 ± 41
LA5 (in 4-5)	700 ± 1	753 ± 116	454 ± 48	636 ± 160
UbApoE (130-149) (K143/146A) binding				
CR17	3840 ± 801	2761 ± 361	3776 ± 375	3459 ± 605
UbApoE (130-140) binding				
CR17	ND	ND	ND	$>5\text{mM}$

dramatically weakened GST-RAP binding and abolished ApoE(130-149) binding. Just like wild-type this double-mutant also did not bind ApoE(1-191)•DMPC.

LA5, which bound ApoE(130-149) weakly, has a Gly at position 30 instead of an Asp. To test the importance of this site further, we mutated G198D(G30D)/P199A(P31A) in LA5 to introduce this missing Asp. Surprisingly this substitution in LA5 dramatically enhanced both ApoE(130-149) and ApoE(1-191)•DMPC binding (Fig. 3.7, 3.8). This mutation also increased binding to the scrambled peptide indicating an increase in non-specific binding of the ApoE(130-149). Thus, D30 is an important residue for ApoE binding, but there must be other key determinants for binding ApoE(1-191)•DMPC that are missing from CR16-18.

To investigate other properties of LA3-5 that promoted interaction with ApoE, sequences of LA45 from several species were aligned, along with the corresponding repeats VLA56 in VLDLR (Fig. 3.9). Beyond residues conserved in all CR/LA repeats, LA4 and VLA5 showed complete conservation of a Trp at position 25 and an acidic residue at position 30 (cf Fig. 3.1). These residues, however, are also present in CR17 and thus, no uniquely conserved residues were found in LA4/VLA5 that might account for enhanced binding of ApoE(1-191)•DMPC. However, alignments of LA5 and VLA6 showed a different set of highly conserved residues: E11, S17, E19, H22, W25, and K34 that were not all present in any of the CRs in LRP. While E11, S17 and W25 are quite common among all CRs in several receptors, E19 and H22 along with K34 are very rare.

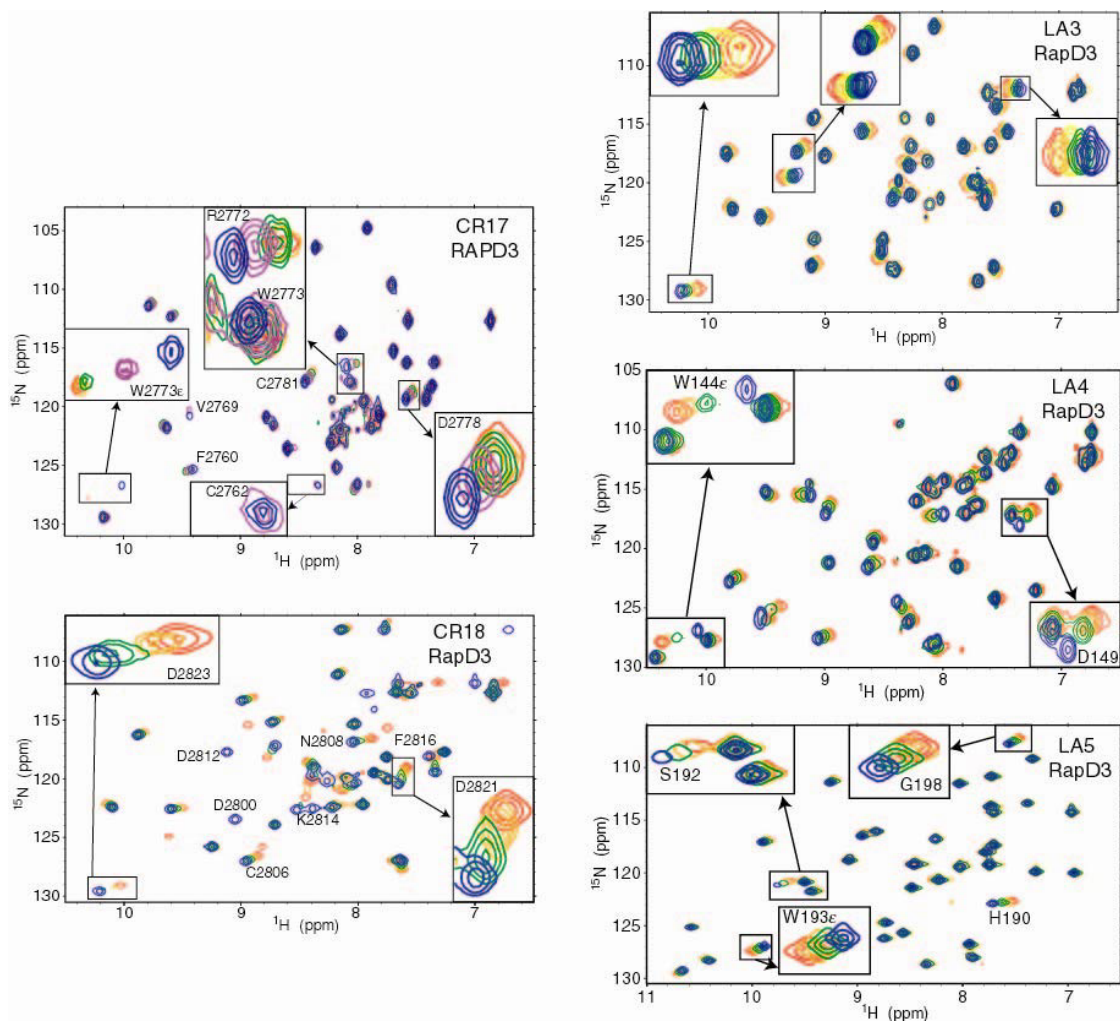


Figure 3.6: NMR titration of Ub-RAPD3 into LA4, LA5, CR16, CR17 and CR18 from zero ligand (blue) to green, orange, and final ligand concentration (red). Strong perturbations are labeled, and some are expanded for clarity.

To probe the importance of these residues, mutations E180A(E11A), E187A(E19A), H190A(H22A) in LA5 were made in LA3-5. HPLC analysis of the refolded mutants showed that E180A(E11A) and E187A(E19A) mutants did not refold to a single isoform. Further mutants E187Q(E19Q) and E187A(E19A)/K202L(K34L) also were not able to properly refold. Mutation of H190A(H22A) in LA5 had little effect on RAP binding, but weakened overall ApoE(1-191)•DMPC binding (Fig. 3.7). Similar to the G198D/P199A mutant, the H190A mutation also increased binding to the scrambled peptide indicating an increase in non-specific binding of the ApoE(130-149) (Fig. 3.8). Since we had no way of testing the importance of E187 (E19) because these mutations did not refold correctly, we instead attempted to substitute the entire beta strand (residues 186-193 of LA5) into CR18 to create a possible gain-of-function CR18 variant; CR18(β 2swap). This swap introduced three substitutions of residues we hypothesized are critical for binding ApoE(1-191)•DMPC; Q19E, and K22H, and F25W. To test the importance of lysine at position 34 we also introduced the A2825K(A34K) mutation into the CR16-18(β 2swap) variant. Fortunately both CR16-18(β 2swap) variants refolded correctly, and could interact with GST-RAP (Fig. 3.8). These mutants bound more strongly to ApoE(130-149) and more importantly, unlike wild type, could now interact with ApoE(1-191)•DMPC (Fig. 3.7, 3.8).

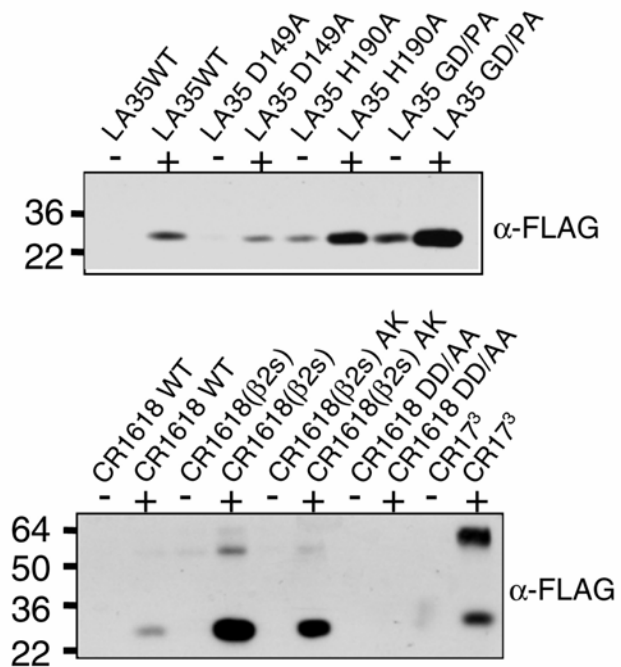


Figure 3.7: Affinity pull-downs of various LA/CR constructs to scrambled peptide (-) or ApoE(130-149) (+), visualized by anti-FLAG immunoblotting. LA35 GD/PA refers to G198D/P199A, CR1618(β 2s) refers to the β 2swap mutant, AK is the A2825K mutation in CR18(β 2swap), and CR1618 DDAA is the D2778A/D2821A double mutant.

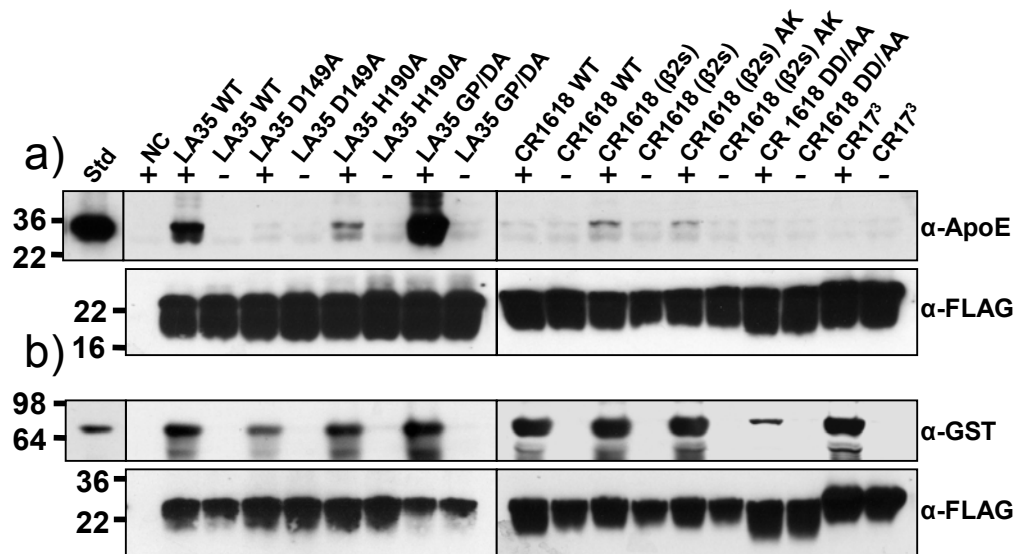


Figure 3.8: **a)** Various LA/CR constructs and mutants were assayed for binding ApoE(1-191)•DMPC particles in the presence of calcium (+) or EDTA (-). Blots were visualized by α-ApoE (top) and anti-FLAG (bottom) immunoblotting. **b)** Same CR/LA constructs assayed for GST-RAP binding, visualized by anti-GST (top) and anti-FLAG (bottom) immunoblotting. LA35 GD/PA refers to G198D/P199A, CR1618(β2s) refers to the β2swap mutant, AK is A2825K mutation in CR18(β2swap), CR1618 DDAA the D2778A/D2821A double mutant.

```

LA4 (LDLR)
Human: TCGPASFCNS-STCIPQLWACDNDPDCEDGSDEWPQRCR
Monkey: TCGPASFCNS-STCIPQLWACDNDPDCEDGSDEWPQHCCQ
Pig: TCGPASFCNS-STCIPQLWACDNDPDCEDGSDEWPQHCCR
Mouse: TCGPAHFRCNS-SICIPSLWACDGDVDCVDSHEWPQNCQ
Rat: TCGPAHFRCNS-SSCIPSLWACDGDRCDDGSDEWPQNCG
Rabbit: TCGPAHFRCNS-SSCVPALWACDGEPCDDGSDEWPARGC
Hamster: TCGPAHFRCNS-WCIPSLWACDGDGDDCEDGSDEWPQNCG
Frog1: TCNPAMFQCKDKGICIPKLWACDGDVDCVDSHEWPEEH--CE
Frog2: TCNPAMFQCKDKGICIPKLWACDGDRCDDGSDEWPEEH--CE
Zebrafish: TCGSSSFRCNN-AQCVPRLVWCDGDADCADNSDELPEKCG
VLA5 (VLDLR)
Human: TCGAHEFQCST-SSCIPISWVCDDDADCSDSDESLEQCG
Mouse: TCGAHEFQCST-SSCIPISWVCDDDADCSDSDESLEQCG
Rat: TCGAHEFQCST-SSCIPISWVCDDDADCSDSDESLEQCG
Rabbit: TCGAHEFQCST-SSCIPISWVCDDDADCSDSDESLEQCG
Cow: TVGPTSSSAAP-PCIPISWVCDDDADCSDSDESLEQCG
Chicken: TCGVHEFQCKS-STCIPISWVCDDDADCSDSDESLEQCG
Frog: TCGAHEFQCKN-FSCIPISWVCDDEPCADHSDDESLEQCG
Consensus: TCGAHEFQCKN-FSCIPISWVCDDEPCADHSDDESLEQCG

LA5 (LDLR)
Human: PCSAFEFHCLSGECIHSSWRCDGGPDCCKDKSDEENCA
Monkey: PCSAFEFHCRSGECIHSGWRCDGGPDCCKDKSDEENCP
Pig: PCSALEFHCHSGECIHSSWRCDGDTDCCKDKSDEENCD
Mouse: PCSSLEFHCGSSECIHRSWVCDGEADCKDKSDEEHCA
Rat: PCSSLEFHCGSSECIHRSWVCDGAADCKDKSDEENCA
Rabbit: PCSRHEFHCGSGECVHASWRCDGDADCRDGSDEERDCA
Hamster: PCSSLEFHCGSSECIHRSWVCDGSADCKDKSDEEHCV
Frog (1): PCAPLEFHCGSGECIHMSWKCDAGYDCKHKSDDKDCV
Frog (2): PCSPLEFHCGSGECIHMSWKCDGGFDCKDKSDEKDCV
Zebrafish: PCTSMEFHCGSGECIHGSWKCDGGADCLDHSDEQNCs
VLA6 (VLDLR)
Human: KCPASEIQCGSGECIHKKWRCDGDPDCCKDGSDEVNCP
Mouse: KCPTSEIQCGSGECIHKKWRCDGDPDCCKDGSDEVNCP
Rat: KCPTSEIQCGSGECIHKKWRCDGDPDCCKDGSDEVNCP
Rabbit: KCPASEIQCGSGECIHKKWRCDGDPDCCKDGSDEVNCP
Cow: RCPASEIQCGSGECIHKKWRCDGDPDCCKDGSDEVNCP
Chicken: KCSTSEVQCGSGECIHKKWRCDGDPDCCKDGSDEVNCP
Frog: RCSANEMPCGSGECIHKKWRCDGDADCKDKSDEVNCP
Consensus: KCPASEIQCGSGECIHKKWRCDGDPDCCKDGSDEVNCP

```

Figure 3.9: Sequence alignments of LA4/VLA5 and LA5/VLA6 from various species. Consensus for these specific repeats is listed as completely conserved (upper case) and mostly conserved (lower case). Highlights show residues conserved in all complement repeats (light) and residues only conserved in these specific repeats (dark).

Discussion

Overall sequence similarity does not reveal ApoE binding capability.

Much is known about the context in which ApoE binds LDLR receptor family members, but little is known about which specific regions within the receptors bind to which specific sequences in ApoE. The dearth of information is partly due to the inability to prepare monomeric binding active ApoE so that single specific binding events can be examined. We used sequence alignments to identify regions within the sLRPs of LRP potentially capable of binding ApoE based on sequence similarity to an ApoE binding region (LA3-5) of LDLR. We had previously shown that residues 130-149, a critical receptor binding region in ApoE, could interact with each sLRP of LRP (Croy et al. 2004). Despite their similarity to LA3-5, neither CR3-5 from sLRP2 nor CR25-27 from sLRP4 showed significant affinity for ApoE(130-149). In contrast, CR16-18 in sLRP3 was able to recapitulate the full binding affinity for this portion of ApoE that was observed for full sLRP3. It remains possible that other effects such as glycosylation, misfolding, or proteolytic clipping may have prevented CR3-5 and CR25-27 from binding. Regardless of this caveat, CR16-18 remained the focus of the rest of the work presented here.

Importance of the ApoE(130-149) receptor binding region and resemblance to RAP. NMR perturbations for ApoE(130-149) binding show variance between repeats, but overall the biggest changes are between the third and fifth cysteines (Fig. 3.5). Comparisons of ApoE(130-149) and RAPD3 titrations with single repeats indicated that the interfaces, to some extent, were

similar. For both ligands, the largest perturbation in CR17 was seen in the indole of a semi-conserved tryptophan at position 25 (cf Fig. 3.1, 3.3). In addition, the amide of the W25 and several nearby residues were highly shifted with both RAPD3 and ApoE(130-149) indicating that this region is involved in both interfaces. CR18 also showed similar perturbations from binding these two ligands, but upon titration certain residues disappeared and reappeared indicating slow kinetics of binding.

Although ApoE(130-149) NMR titrations resulted in high uncertainty for the measured K_D , the multiple calculation methods ensured that overall trends were consistent (Table 3.1). The data indicate that each CR can bind Ub-ApoE(130-149) with a relatively weak affinity (high μM to low mM). CR17 had the strongest affinity for both ApoE(130-149) and RAPD3, with K_D s similar to those seen for LA4. Both of these repeats have a Trp at position 25 and an Asp at position 30. NMR titrations and pulldown assays agree that mutation of D30 ruins the interaction with RAP in agreement with previous studies (Andersen et al. 2000). We now show that this particular Asp is also critical for the binding of ApoE(1-191)•DMPC. Both CR18 and LA3 have this critical Asp at position 30 but lack a Trp at position 25, which can explain their weaker affinity for ApoE(130-149). However, CR18 retains affinity for RAPD3 whereas LA3 has a very weak affinity for RAPD3, indicating that the RAP interaction is also dependent on residues beyond this W25/D30 pair.

The importance of D30 and W25 is in strong agreement with the crystal structure of RAPD3 bound to LA34, in which W144(W25) and D149(D30) in LA4

are at the center of the interface making contacts with lysines of RAP (Fisher et al. 2006). CR17 probably binds RAPD3 with the same interface as seen in the crystal structure with LA4, as the largest perturbations W2778, R2777, C2781, and D2778 are at this interface. Two lysines from RAP are buried in this interface, and it is thought that lysines 143 and 146 of ApoE are similarly involved in receptor binding (Zaiou et al. 2000; Prévost and Raussens 2004; Fisher et al. 2006). Consistent with this, our ApoE(130-149; K143/146A) mutant showed significantly decreased affinity for CR17.

Unlike CR17 and CR18, CR16 had a much stronger affinity for ApoE(130-149) in the context of CR16-18 (3.2mM vs. 730 μ M). This could be an effect of structural and dynamic perturbations from the presence of the neighboring CR17. LA5 showed a similar increase in ApoE(130-149) affinity upon linkage to LA4 (3.9mM to 640 μ M). The similar binding affinities of CR16 and CR17 when in the context of CR16-18 may lead to the speculation that only one ApoE(130-149) is binding both repeats. We think this is very unlikely because the chemical shift changes observed in the single domains are identical to those observed when the domains are in the context of CR16-18. As for LA45, the affinities of each repeat are well outside of the error, indicating isolated binding events. The perturbations in LA45 are also identical to those seen for isolated LA4 and LA5 upon ApoE(130-149) titrations further arguing that there is an intrinsic change to certain repeats when bound to its neighbor affecting its ligand binding properties.

Avidity may account for much of the observed binding. Initial SPR experiments with CR16-18 gave K_D s in the high nM range (Croy et al.,

unpublished observations), whereas NMR perturbation experiments with ubiquitin-fused ApoE(130-149) showed each repeat of CR16-18 binding ApoE with only high μM affinity. The high affinity measured for CR16-18 by SPR and pulldown assay was therefore likely caused by an avidity effect in which multiple repeats simultaneously engage immobilized ApoE(130-149) molecules. This also explains the significant decrease in affinity observed upon removal of any of the three CRs.

It has previously been proposed that avidity effects, in which several interactions occur simultaneously with many copies of ApoE on LDL particle surfaces, govern the binding to the receptor (Mahley et al. 1984). Modified ApoE-DMPC particles which contain only a single copy of active ApoE showed a 26 fold decrease in affinity for receptors compared to those with 4 active copies (Pitas et al. 1980). Native lipoprotein particles can contain many copies of ApoE, so it is possible that much like in our ApoE(130-149) studies, multiple weak interactions would account for tight binding (Fig. 3.10a). A similar avidity effect was also seen for the interaction between VLDLR repeats and human rhinovirus capsid (Verdaguer et al. 2004). The observation that incorporation of ApoE(129-169) into lipoprotein particles enhances receptor-mediated particle uptake (Mims et al. 1994) can also be explained by this avidity mechanism.

A distinct binding site on lipid-bound ApoE for LA5. Despite the interactions that were seen with ApoE(130-149), CR16-18 failed to show any interaction with ApoE(1-191)•DMPC (Fig. 3.7, 3.8). CR17³ which has an even higher affinity for ApoE(130-149) was also unable to interact with lipid bound

ApoE(1-191). Since all the constructs were correctly folded as assessed by HPLC and GST-RAP binding, these results strongly suggest that ApoE(1-191)•DMPC interactions involve additional features within the CR repeats beyond those required for binding ApoE(130-149). Alignments of LA45 and VLA56, thought to be the crucial repeats in their receptors for ApoE binding (Fisher et al. 2004; Ruiz et al. 2005), show high conservation of the critical W25/D30 pair in LA4 and VLA5. However LA5, which is the most critical repeat for β -VLDL binding (Russell et al. 1989), does not have this Asp. Introduction of an Asp at position 30 in LA5 unexpectedly improved the binding to ApoE•DMPC (Fig. 3.8). This Asp in LA5 is not required for ApoE•DMPC binding but additional acidic residues may be enhancing electrostatic interactions with ApoE, which also explain the increased binding to both ApoE(130-149) and the scrambled ApoE peptide.

Since ApoE undergoes structural rearrangement upon incorporation into lipid particles (Fisher and Ryan 1999; Lund-Katz et al. 2000; Peters-Libeu et al. 2006) we speculated that this form of ApoE has an additional binding site which is recognized by LA5. Examination of conserved residues in LA5 and VLA6 showed a novel set of conserved residues (Fig. 3.9). H190(H22) and E187(E19) were particularly interesting as they are very rare among these repeats but completely conserved in LA5 and VLA6 among several species. In addition to being involved in the intra-molecular interface with LDLR's β -propeller domain at endosomal pH (Rudenko et al. 2002), our pulldown assays show that the conserved H190(H22) in LA5 is also important for ApoE(1-191)•DMPC binding.

Mutation of E180(E11) and E187(E19) yielded misfolded protein, indicating that these residues are necessary for proper refolding of LA5. Previous Ala saturation mutagenesis also implicated H190(H22) in ApoE binding and could not test E187(E19) due to similar refolding problems (Abdul-Aziz et al. 2005).

When E187 (E19) along with H190 (H22) was introduced into CR18, it produced a CR16-18 variant that could bind to ApoE(1-191)•DMPC albeit with weaker affinity than LA3-5 (Fig. 3.8). Lysine 202, which is semi-conserved in LA5/VLA6, was also introduced into this CR16-18 construct but had little effect on ApoE binding. Since CR18 has a native E11 its role was not tested, thus it is still unclear whether it is critical. These CR18 mutations also enhanced the interaction with ApoE(130-149), which can be explained by the substitution of the native Phe at position 25 with a Trp, forming the critical W25/D30 pair. The weaker affinity of the CR16-18(β 2swap) for ApoE(1-191)•DMPC compared to LA3-5 indicates that residues beyond the β -swap region contribute to the binding affinity. It is possible that the uniquely long linker between LA4 and LA5, which has been shown to modulate ApoE affinity, and is absent from CR16-18, contributes to this difference in observed affinities.

Taken together, these results suggest that two distinct binding events are occurring between ApoE and the LA4-5 repeats of LDLR (Fig. 3.10b). The first repeat (LA4) containing the W25/D30 pair, likely interacts with the 140-150 site, and the second repeat (LA5) containing an E19, H22, and possibly E11 and W25, recognizes the second site that is revealed when ApoE associates with lipid particles. It is possible that helical extension of the region following residue

160 of ApoE forms this second site (Gupta et al. 2006), and that it involves the critical R172 (Morrow et al. 2000).

Comparison of LDLR and LRP. In the full native interaction between LDL particles and receptors, high affinity recognition could stem from both avidity effects and lipid-induced reorganization of ApoE. This can explain the differences observed for LDLR/VLDLR and LRP internalization of ApoE containing lipoproteins. LDLR can clear several classes of ApoE containing lipoproteins but LRP has only been shown to internalize ApoE enriched β -VLDLs (Kowal 1989). LRP lacks a repeat with the critical residues in LA5, but has many repeats with the critical W25/D30 pair, so it can still form many weak interactions with lipoprotein particles rich in ApoE (Fig. 3.10). The observation that sLRPs 2 and 4 of LRP had higher affinities for β -VLDL (Neels et al. 1999) is also in agreement with this model as these sLRPs contain more repeats with the critical W25/D30 pair (7/8 in SLRP2, 7/11 in SLRP4, only 3/10 in SLRP3). Thus lipoprotein uptake and cholesterol homeostasis may be regulated by both of these mechanisms.

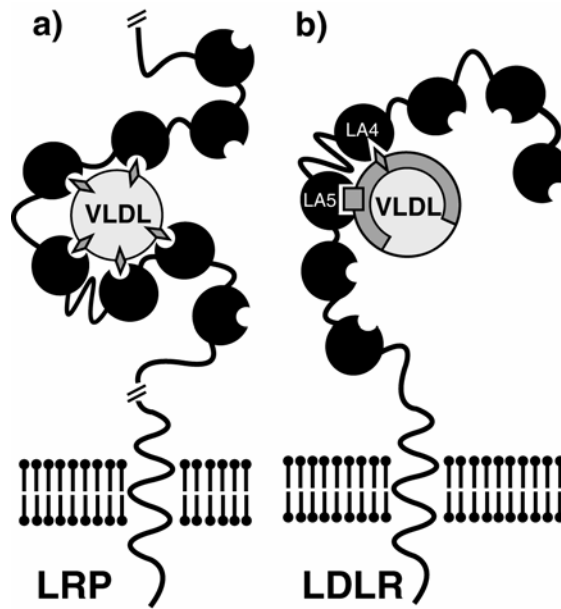


Figure 3.10: Proposed models of how LDL receptors might bind ApoE-containing lipoprotein particles. **a)** Avidity model in which multiple copies of ApoE (grey diamonds) exposed on the particle surface combine many weak interactions with ligand binding repeats (black circles) on the receptor into one strong interaction. **b)** The lipoprotein bound form of ApoE present epitopes which are recognized by specific repeats of LDLR. In this case LA4 is recognizing one epitope on an ApoE molecule (grey diamond), and LA5 is recognizing a different epitope (grey square).

References

- Abdul-Aziz, D., Fisher, C., Beglova, N., and Blacklow, S.C. 2005. Folding and binding integrity of variants of a prototype ligand-binding module from the LDL receptor possessing multiple alanine substitutions. *Biochem J* 44: 5075-5085.
- Andersen, O.M., Christensen, L.L., Christensen, P.A., Sørensen, E.S., Jacobsen, C., Moestrup, S.K., Etzerodt, M., and Thøgersen, H.C. 2000. Identification of the minimal functional unit in the low density lipoprotein receptor-related protein for binding the receptor-associated protein (RAP). A conserved acidic residue in the complement-type repeats is important for recognition of RAP. *J Biol Chem* 275: 21017-21024.
- Andersen, O.M., Schwarz, F.P., Eisenstein, E., Jacobsen, C., Moestrup, S.K., Etzerodt, M., and Thøgersen, H.C. 2001. Dominant thermodynamic role of the third independent receptor binding site in the receptor-associated protein RAP. *Biochem J* 40: 15408-15417.
- Beisiegel, U., Weber, W., Ihrke, G., Herz, J., and Stanley, K.K. 1989. The LDL-receptor-related protein, LRP, is an apolipoprotein E-binding protein. *Nature* 341: 162-164.
- Blacklow, S.C. 2007. Versatility in ligand recognition by LDL receptor family proteins: advances and frontiers. *Curr Opin Struct Biol* 17: 419-426.
- Blacklow, S.C., and Kim, P.S. 1996. Protein folding and calcium binding defects arising from familial hypercholesterolemia mutations of the LDL receptor. *Nat Struct Biol* 3: 758-762.
- Brown, M.S., and Goldstein, J. L. 1986. A receptor-mediated pathway for cholesterol homeostasis. *Science* 232: 34-47.
- Bu, G., and Rennke, S. 1996. Receptor-associated protein is a folding chaperone for low density lipoprotein receptor-related protein. *Journal of Biological Chemistry* 271: 22218-22224.
- Clackson, T., Detlef, G., and Jones, P. 1991. PCR, a Practical Approach. (eds. M. McPherson, P. Quirke, and G. Taylor), pp. 202. IRL Press, Oxford.
- Croy, J.E., Brandon, T., and Komives, E.A. 2004. Two apolipoprotein E mimetic peptides, apoE(130-149) and apoE(141-155)₂, bind to LRP1. *Biochemistry* 34: 7328-7335.

- Croy, J.E., Shin, W.D., Knauer, M.F., Knauer, D.J., and Komives, E.A. 2003. All three LDL receptor homology regions of the LDL receptor-related protein (LRP) bind multiple ligands. *Biochemistry* 42: 13049-13057.
- Datta, G., Garber, D.W., Chung, B.H., Chaddha, M., Dashti, N., Bradley, W.A., Gianturco, S.H., and Anantharamaiah, G.M. 2001. Cationic domain 141-150 of apoE covalently linked to a class A amphipathic helix enhances atherogenic lipoprotein metabolism in vitro and in vivo. *J Lipid Res* 42: 959-966.
- Fisher, C., Abdul-Aziz, D., and Blacklow, S.C. 2004. A two-module region of the low-density lipoprotein receptor sufficient for formation of complexes with apolipoprotein E ligands. *Biochem J* 43: 1037-1044.
- Fisher, C., Beglova, N., and Blacklow, S.C. 2006. Structure of an LDLR-RAP complex reveals a general mode for ligand recognition by lipoprotein receptors. *Mol Cell* 22: 277-283.
- Fisher, C.A., and Ryan, R.O. 1999. Lipid binding-induced conformational changes in the N-terminal domain of human apolipoprotein E. *J Lipid Res* 40: 93-99.
- Gupta, V., Narayanaswami, V., Budamagunta, M.S., Yamamoto, T., Voss, J.C., and Ryan, R.O. 2006. Lipid-induced extension of apolipoprotein E helix 4 correlates with low density lipoprotein receptor binding ability. *J Biol Chem* 281: 39294-39299.
- Herz, J., Goldstein, J.L., Strickland, D.K., Ho, Y.K., and Brown, M.S. 1991. 39-kDa protein modulates binding of ligands to low density lipoprotein receptor-related protein/alpha 2-macroglobulin receptor. *Journal of Biological Chemistry* 266: 21232-21238.
- Hoffman, R.M.B., Li, M.X., and Sykes, B.D. 2005. The Binding of W7, an Inhibitor of Striated Muscle Contraction, to Cardiac Troponin C. *Biochemistry* 44: 15750-15759.
- Huang, W., Dolmer, K., and Gettins, P.G. 1999. NMR solution structure of complement-like repeat CR8 from the low density lipoprotein receptor-related protein. *J Biol Chem* 274: 14130-14136.
- Hui, D.Y., Innerarity, T.L., and Mahley, R.W. 1984. Defective hepatic lipoprotein receptor binding of B-very low density lipoproteins from type 111 hyperlipoproteinemic patients: importance of apolipoprotein E. *J Biol Chem* 259.

- Hussain, M.M., Maxfield, F.R., Más-Oliva, J., Tabas, I., Ji, Z.S., Innerarity, T.L., and Mahley, R.W. 1991. Clearance of chylomicron remnants by the low density lipoprotein receptor-related protein/alpha 2-macroglobulin receptor. *J Biol Chem* 266: 13936-13940.
- Innerarity, T.L., Friedlander, E.J., Rall, S.C.J., Weisgraber, K.H., and Mahley, R.W. 1983. The Receptor Binding Domain of Human Apolipoprotein E. Binding Of Apolipoprotein E fragments. *J Biol Chem*. 258: 12341-12347.
- Jez, M., J., Ferrer, J., Bowman, M., E., Dixon R., A., and Noel J., P. 2000. Dissection of Malonyl-Coenzyme A Decarboxylation from Polyketide Formation in the Reaction Mechanism of a Plant Polyketide Synthase. *Biochemistry* 39: 890-902.
- Kiss, R.S., Weers, P.M., Narayanaswami, V., Cohen, J., Kay, C.M., and Ryan, R.O. 2003. Structure-guided protein engineering modulates helix bundle exchangeable apolipoprotein properties. *J Biol Chem* 278: 21952-21959.
- Kowal, R.C., Herz, J, Goldstein, J. L., Esser, V., and Brown, M. S. 1989. Low density receptor-related protein mediates uptake of cholesteryl esters derived from apolipoprotein E-enriched lipoproteins. *Proc. Natl. Acad. Sci. USA* 86: 5810-5814.
- Lalazar, A., and Mahley, R.W. 1989. Human apolipoprotein E. Receptor binding activity of truncated variants with carboxyl-terminal deletions. *J Biol Chem* 264: 8447-8450.
- Lalazar, A., Weisgraber, K.H., Rall, S.C.J., Gilad, H., Innerarity, T.L., Levanon, A.Z., Boyles, J.K., Amit, B., Gorecki, M., Mahley, R.W., et al. 1988. Site-specific Mutagenesis of human apolipoprotein E. Receptor binding activity of variants with single amino acids substitutions. *J Biol Chem*. 263: 3542-3545.
- Lund-Katz, S., Zaiou, M., Wehrli, S., Dhanasekaran, P., Baldwin, F., Weisgraber, K.H., and Phillips, M.C. 2000. Effects of lipid interaction on the lysine microenvironments in apolipoprotein E. *J Biol Chem* 275: 34459-34464.
- Mahley, R.W., Innerarity, T.L., Rall, S.C., and Weisgraber, K.H. 1984. Plasma lipoproteins: apolipoprotein structure and function. *J. Lipid Res*. 25: 1277-1294.
- Mims, M.P., Darnule, A.T., Tovar, R.W., Pownall, H.J., Sparrow, D.A., Sparrow, J.T., Via, D.P., and Smith, L.C. 1994. A nonexchangeable apolipoprotein E peptide that mediates binding to the low density lipoprotein receptor. *J Biol Chem* 269: 20539-20547.

- Mokuno, H., Yamada, N., Shimano, H., Ishibashi, S., Mori, N., Takahashi, K., Oka, T., Yoon, T. H., Takaku, F. 1991. The enhanced cellular uptake of very-low-density lipoprotein enriched in apolipoprotein E. *Biochim. Biophys. Acta* 1082: 63-70.
- Morrow, J.A., Arnold, K.S., Dong, J., Balesta, M.E., and Innerarity, T.L. 2000. Effect of Arginine 172 on the Binding of Apolipoprotein E to the Low Density Lipoprotein Receptor. *J Biol Chem* 275: 2576-2580.
- Neels, J.G., van den Berg, B.M.M., Lookene, A., Olivecrona, G., Pannekoek, H., and van Zonneveld, A.J. 1999. The second and fourth cluster of class A cysteine-rich repeats of the low density lipoprotein receptor-related protein share ligand binding properties. *J. Biol. Chem.* 274: 31305-31311.
- Nicholas, K.B., and Jr., N.H.B. 1997. GeneDoc: a tool for editing and annotating multiple sequence alignments.
- Peters-Libeu, C.A., Newhouse, Y., Hall, S.C., Witkowska, H.E., and Weisgraber, K.H. 2007. Apolipoprotein E.dipalmitoylphosphatidylcholine particles are ellipsoidal in solution. *J Lipid Res* 48: 1035-1044.
- Peters-Libeu, C.A., Newhouse, Y., Hatters, D.M., and Weisgraber, K.H. 2006. Model of biologically active apolipoprotein E bound to dipalmitoylphosphatidylcholine. *J Biol Chem* 281: 1073-1079.
- Pitas, R.E., Innerarity, T.L., and Mahley, R.W. 1980. Cell surface receptor binding of phospholipids protein complexes containing different ratios of receptor-active and inactive E apoprotein. *J Biol Chem* 255: 5454-5460.
- Prévost, M., and Raussens, V. 2004. Apolipoprotein E-low density lipoprotein receptor binding: study of protein-protein interaction in rationally selected docked complexes. *Proteins.* 55: 874-884.
- Rall, S.C.J., Weisgraber, K.H., Innerarity, T.L., and Mahley, R.W. 1982. Structural basis for receptor binding heterogeneity of apolipoprotein E from type III hyperlipoproteinemic subjects. *Proc Natl Acad Sci* 79: 4696-4700.
- Rudenko, G., and Deisenhofer, J. 2003. The low-density lipoprotein receptor: ligands, debates and lore. *Curr Opin Struct Biol* 13: 683-689.
- Rudenko, G., Henry, L., Henderson, K., Ichtchenko, K., Brown, M.S., Goldstein, J.L., and Deisenhofer, J. 2002. Structure of the LDL receptor extracellular domain at endosomal pH. *Science* 298: 2353-2358.

- Ruiz, J., Kouivskaia, D., Migliorini, M., Robinson, S., Saenko, E.L., Gorlatova, N., Li, D., Lawrence, D., Hyman, B.T., Weisgraber, K.H., et al. 2005. The apoE isoform binding properties of the VLDL receptor reveal marked differences from LRP and the LDL receptor. *J Lipid Res* 46: 1721-1731.
- Russell, D.W., Brown, M.S., and Goldstein, J.L. 1989. Different combinations of cysteine-rich repeats mediate binding of low density lipoprotein receptor to two different proteins. *J Biol Chem* 264: 21682-21688.
- Simmons, T., Newhouse, Y.M., Arnold, K.S., Innerarity, T.L., and Weisgraber, K.H. 1997. Human low density lipoprotein receptor fragment. Successful refolding of a functionally active ligand-binding domain produced in *Escherichia coli*. *J Biol Chem* 272: 25531-25536.
- Tacken, P.J., Teusink, B., Jong, M.C., Harats, D., Havekes, L.M., van Dijk, K.W., and Hofker, M.H. 2000. LDL receptor deficiency unmasks altered VLDL triglyceride metabolism in VLDL receptor transgenic and knockout mice. *J Lipid Res* 41: 2055-2062.
- Takahashi, S., Kawarabayasi, Y., Nakai, T., Sakai, J., and Yamamoto, T. 1992. Rabbit very low density lipoprotein receptor: a low density lipoprotein receptor-like protein with distinct ligand specificity. *Proc Natl Acad Sci* 89: 9252-9256.
- Verdaguer, N., Fita, I., Reithmayer, M., Moser, R., and Blaas, D. 2004. X-ray structure of a minor group human rhinovirus bound to a fragment of its cellular receptor protein. *Nat Struct Mol Biol* 11: 429-434.
- Weisgraber, K.L., Innerarity, T. L., Harder, K. J., Mahley, R. W., Milne, R. W., Marcel, Y. L., Sparrow, J. T. 1983. The Receptor Binding Domain Of Human Apolipoprotein E. *J. Biol. Chem* 258: 12348-12354.
- Willnow, T.E., Armstrong, S.A., Hammer, R.E., and Herz, J. 1995. Functional expression of low density lipoprotein receptor-related protein is controlled by receptor-associated protein in vivo. *Proc Natl Acad Sci* 92: 4537-4541.
- Wilson, C., Wardell, M.R., Weisgraber, K.H., Mahley, R.W., and Agard, D.A. 1991. Three-dimensional structure of the LDL receptor-binding domain of human apolipoprotein E. *Science* 252: 1817-1822.
- Zaiou, M., Arnold, K.S., Newhouse, Y.M., Innerarity, T.L., Weisgraber, K.H., Segall, M.L., Phillips, M.C., and Lund-Katz, S. 2000. Apolipoprotein E₃-low density lipoprotein receptor interaction. Influences of basic residue and

amphipathic alpha-helix organization in the ligand. *J Lipid Res* 41: 1087-1095.

This chapter is in part, a reprint of a submitted manuscript in review:
Miklos Decoding of lipoprotein – receptor interactions; Properties of ligand binding modules governing interactions with ApoE. Guttman, M., Prieto, J.H., Croy, J.E., Komives, E.A. (2009) *Submitted*. The dissertation author was the primary researcher and author of this manuscript.

Chapter Four
Structure of the Minimal Interface
Between ApoE and LRP

Introduction

Members of the Low Density-lipoprotein Receptor (LDLR) family are responsible for the uptake of a variety of other ligands, and are essential for cholesterol homeostasis (Herz and Strickland 2001; Blacklow 2007). Ligand interactions occur through binding events in ligand binding clusters of 2-11 Complement repeats (CRs). Each CR is composed of 40-50 amino acids with the overall fold stabilized by three disulfide bonds and a high affinity calcium binding site (Brown et al. 1997; Fass 1997). A number of NMR and crystallographic structures have now been solved for these repeats, and the structures show very little deviation in overall fold as recently reviewed (Rudenko and Deisenhofer 2003). Besides the six cysteines and the calcium coordinating residues, only few residues are required for proper folding (Abdul-Aziz et al. 2005). These domains are, therefore, able to achieve the same fold with high variation in their many surface exposed loops, which is thought to be the basis for specificity for various ligands (Blacklow 2007).

The LDL receptor-related protein, LRP1, is responsible for the clearance of at least 30 ligands (Herz and Strickland 2001). This very large protein contains three complete clusters of CRs each of which are larger than the cluster of CRs in LDLR. Several studies have shown that these clusters of CRs in LRP, termed sLRPs, can interact with many ligands *in vitro* (Neels et al. 1999; Croy et al. 2003). During maturation LRP is processed into two chains by furin cleavage (Willnow 1996). The sLRP containing extracellular α -chain remains non-covalently associated with the transmembrane β -chain. Like other members of

this receptor family LRP can bind and internalize Apolipoprotein E (ApoE)-containing β -migrating very low density lipoproteins (β -VLDLs) (Beisiegel et al. 1989; Kowal 1989).

Apolipoprotein E is found in several classes of lipoproteins and common variants are associated with type III hyperlipoproteinemia (Rall et al. 1982). As mentioned in previous chapters, ApoE(130-149) has been shown to be the critical receptor recognition site, but can bind isolated CRs with only low affinity (Chapter 3). The lipid free crystal structure of the N-terminal domain of ApoE revealed that this region forms a helix, with solvent exposed lysines (Wilson et al. 1991). NMR studies revealed that this region still maintains helical structure when bound to lipid (Raussens et al. 2003). Upon lipid association, two critical lysine residues undergo pKa perturbations and show difference susceptibilities for chemical modification (Lund-Katz et al. 2000).

The receptor associated protein (RAP) has been shown to be a folding chaperone for LRP, and it can also block binding of several ligands of LRP (Herz et al. 1991; Bu et al. 1995). RAP is composed of three domains which each form a three helix bundle that is capable of binding to sLRPs of LRP (Bu et al. 1995; Lee et al. 2007). Domain 3 (RAPD3), has been shown to have the highest affinity to CR pairs, followed by Domain 1 (RAPD1), and the second domain only exhibited very weak binding to CRs (Andersen et al. 2001). RAPD3 has also been shown to be able to interact with single CRs with affinities in the mid μ M range (Chapter 3).

There have been structural studies of CRs in complex with binding partners, including RAPD3 and D1, the rhinovirus capsid, and an internally inhibited form with LDL's β -propeller domain (Rudenko et al. 2002; Verdaguer et al. 2004; Fisher et al. 2006; Jensen et al. 2006). Each interaction occurs around the calcium binding site in the CRs. Basic residues from the ligand form contacts with a surface exposed aromatic residue along with acidic residues positioned around the calcium binding site. Computational and homology models have been proposed for the ApoE interaction with LA5 from LDLR (Prévost and Raussens 2004; Fisher et al. 2006), but as of yet no structural information has been obtained for the ApoE-CR interaction. To elucidate the structure of this interaction, we have used NMR titrations in combination with a fusion strategy to obtain specific structural information on the interface between ApoE(130-149) and CR17 of LRP.

Materials and Methods

Protein expression and purification. Cloning of CR17 (residues 2712-2754 of mature human LRP-1) in a modified pMMHb vector was described in chapter two. Residues 130-149 of ApoE were PCR amplified and ligated into the modified pMMHb with an extra tyrosine at the N terminus for quantitation purposes. The fusion protein, CR17-ApoE(130-149), was constructed by re-cloning CR17 without a stop codon, then inserting PCR amplified ApoE(130-149) with an extra 4x(glycine-serine) linker at the 3' BamH1 site to link the coding sequences. All mutants were made using either inverse PCR (Clackson et al. 1991) or

Quickchange (Stratagene) mutagenesis, and verified by DNA sequencing. Ubiquitin (Ub) fused RAPD1(19-112) and RAP(244-263) were cloned as described previously for RAPD3(218-323) and ApoE(130-149) in Chapter Three.

All Ub-fused ligands (various RAP constructs and ApoE(130-149)) were prepared as described previously in Chapter Three. ApoE(130-149) peptide was expressed in BL21-DE3s at 37°C for 12 hours as inclusion bodies. Inclusion bodies were purified over Ni-NTA in resolubilizing buffer (8M Urea, 50mM Tris (pH 8.0), 500mM NaCl). A gradient was run from resolubilizing buffer to thrombin cleavage buffer (50mM Tris, pH 8.0, 150mM NaCl, 2mM CaCl₂, total volume 100mL), and peptide was eluted by cleavage with 4µg/column active bovine thrombin at 25°C for 2 hours (30mL volume). A final HPLC purification by C18 reverse phase HPLC (Waters), in 0.1% trifluoroacetic acid (TFA) with a gradient of 10 to 50% acetonitrile, yielded around 300µg pure peptide per liter growth media. All expressed constructs were analyzed by MALDI-TOF mass spectrometry on a Voyager DE-STR (Applied Biosystems), in sinnapinic acid (Agilent). Protein was lyophilized from HPLC buffer and stored at -80°C.

ITC. Calcium binding was measured with a MicroCal VP-ITC calorimeter at 35°C. Dried protein was resuspended in Chelex (Biorad, Hercules, CA, USA)-treated buffer (20mM Hepes (pH 7.45), 150mM NaCl, 0.02% azide). Complement repeats were titrated with 10 fold molar excess of CaCl₂ in the same buffer. All data were analyzed in Origin 7.0 (OriginLab).

Tryptophan fluorescence measurements of intramolecular interaction. In order to determine whether the ApoE(130-149) was interacting with the fused

CR17, native tryptophan fluorescence was used to monitor effects of binding. CR17, CR17-ApoE(130-149), and CR17-ApoE(130-136) were resuspended into 20mM Hepes (pH 7.4), 150mM NaCl, 10mM CaCl₂, 0.02% azide. An equal aliquot of protein (10 μM) was resuspended with 10mM EDTA instead of CaCl₂ and treated with 10mM DTT at 55°C for 30 minutes to measure the intrinsic fluorescence of the completely unfolded protein as a control. Fluorescence emission spectra were collected on a Fluoromax-2 spectrofluorimeter (Spex) at 35°C using excitation at 293nm. All spectra were normalized to the appropriate buffer blank.

Analytical Ultracentrifugation. Equilibrium sedimentation experiments were performed on a Beckman Optima XL-1, at 37°C to determine the oligomeric state of CR17. All buffers were based on 40mM Hepes pH 7.4, 150mM NaCl, 20mM CaCl₂, with variations in salt, pH and the presence of additives such as Arginine and Glutamate. CR17 was centrifuged at 30, 40, 50 and 55 krpm. Buffer and protein constants were calculated with the program SEDNTERP, and data were fit using Ultraspin 2.0 (Dmitry Veprintsev, Ultraspin 2, MRC Centre for Protein Engineering, Cambridge).

NMR. All spectra were collected on a Bruker Avance III 600 MHz spectrometer equipped with a cryoprobe collected at 307°K. ¹⁵N,¹³C labeled CR17 was resuspended in 20mM D18 Hepes (pH 7.45), 50mM D7-Arginine and 50mM D5-Glutamic acid (Cambridge Isotope Labs), 50mM NaCl, 5mM CaCl₂, 10% D₂O and 0.02% sodium azide (final conc. 0.8mM). Backbone resonances were assigned with CBCA(CO)NH (Grzesiek and Bax 1992b), CBCANH

(Grzesiek and Bax 1992a), and HNCO (Kay et al. 1990b). Sidechain assignments were made with HCC(CO)NH (Clowes et al. 1993), 3D ^{15}N NOESY (150msec mixing time) (Talluri and Wagner 1996), 3D HCNH NOESY (150msec mixing time) (Kay et al. 1990a), 3D HCCH TOCSY (Bax et al. 1990), and 3D HCCH NOESY (150msec mixing time) (Zuiderweg et al. 1990) spectra as described previously (Lougheed et al. 2002). Spin systems for residues not visible in amide resolved experiments were assigned with the HCCH-TOCSY and connectivity established with NOESY spectra. The NOESY spectra were also used to unambiguously assign all of the aromatic resonances. Additional ^1H - ^{15}N HSQC and ^1H - ^{13}C HSQCs were collected for CR17 at 298°K to directly compare the chemical shifts to CR17-ApoE(130-149). A 3D ^{15}N -NOESY (100 msec mixing time) was collected on ^{15}N labeled CR17 (K5A) to confirm the changes observed in amide cross peak positions as compared to wild-type. CR17-ApoE(130-149) fusion (0.8mM) was assigned in the same manner as CR17 except all spectra were collected at 298°K and the sample was exchanged into 100% deuterated buffer prior to collection of 3D HCCH TOCSY, 3D HCCH NOESY and HCCH COSY spectra.

^{13}C , ^{15}N ApoE(130-149) peptide was dissolved in 20mM D-18-Hepes (Cambridge Isotope Labs) pH 7.45, 150mM NaCl, 2mM EDTA (D-12) (Cambridge Isotope Labs), 0.02% sodium azide at a final concentration of 0.5mM. The peptide resonances were assigned using ^1H - ^{15}N HSQC, CBCA(CO)NH, CBCANH, HNCO, HCC(CO)NH, and ^1H - ^{13}C HSQC experiments. Data were processed using Azara (Wayne Boucher and the Department of

Biochemistry, University of Cambridge, Cambridge, UK) and analyzed in Sparky (T. D. Goddard and D. G. Kneller, SPARKY 3, University of California, San Francisco).

For dynamics measurements, ^{15}N labeled samples were prepared at final concentrations of $\sim 0.6\text{mM}$ in the same buffer used for assignments at 298°K . Standard Bruker sequences were used for relaxation measurements with the following delay times: for T1 (0.001, 0.08, 0.14, 0.3, 0.5, 0.9, 1.5, 3.0 sec) and for T2 (14.4, 28.8, 43.2, 57.6, 72, 100.8, 129.6, 158.4, 201.6 msec). Duplicate ^1H - ^{15}N heteronuclear NOE experiments were collected in an interleaved manner with and without ^1H saturation with a recycle delay of 6 sec. Data were processed in NMR pipe (Delaglio et al. 1995) and analyzed in Sparky. Peak intensities for T1 and T2 were fit to a decaying exponential in Sparky, with errors taken from the uncertainty of the fit. NOE measurements were calculated by the ratio of peak heights, and error determined by the standard deviation between duplicate experiments. Relaxation data were analyzed using the model free approach (Lipari and Szabo 1982) assuming isotropic tumbling in the program Tensor2 (Martin Blackledge, Institut de Biologie Structurale, Grenoble, France). For amide exchange measurements, a 0.3mM sample of ^{15}N labeled CR17/CR17-ApoE was dried with buffer, resuspended in 100% D_2O , and rapidly scanned with a series of 15 minute HSQC experiments.

NMR titrations. CR17 was titrated with various ligands and monitored by ^1H , ^{15}N HSQC at 307°K . In order to minimize secondary effects in the titrations, identical aliquots of ^{15}N labeled CR17 constructs were resuspended in either a

solution of Ub-fused ligand or Ub, in 20mM Hepes (pH 7.45), 150mM NaCl, 10mM CaCl₂, and 0.02% azide in 10% D₂O. The pH was adjusted to 7.45, and the Ub/Ub-fused ligand samples mixed in various ratios to yield samples with varying concentrations of ligand but identical total protein concentration. To examine changes on ApoE(130-149) peptide a similar strategy was used in which ¹⁵N labeled 100μM ApoE(130-149) was resuspended with buffer alone or in a solution containing 1.8mM CR17, and subsequently mixed in different ratios. ¹H, ¹⁵N HSQCs as well as 2D ¹H, ¹³C HNCQ, and ¹H, ¹³C HSQC spectra were collected at 298°K. K_Ds were calculated from titrations as described previously in Chapter Three.

CR17 Structural Refinement. Peak lists from ¹⁵N-NOESY, HCNH-NOESY and HCCH NOESY, were used as inputs for ARIA2/CNS iterative assignment calculations (Rieping et al. 2007). 18 pseudo-calcium coordination restraints were added to specify the octahedral geometry around the calcium binding site (North and Blacklow 2000). After initial refinement without disulfide restraints showed that the expected disulfide pattern (C1-C3, C2-C5, C4-C6) was present in CR17, the 3 disulfide bonds were included as distance restraints, and later as covalent bonds in the final refinement. Dihedral angle restraints (44 total) were predicted from NH, H, H α , CO, C α , and C β resonance shifts using TALOS (Cornilescu et al. 1999). Slowly exchanging amides (W25, L26 and E39) from amide exchange experiments, and H-bonding donor acceptor pairs were identified from partially refined structures. Final calculations with calcium were

done in CNS 1.2 using the distance geometry simulated annealing (dgsa) protocol (Brunger 2007), with 6 direct distance restraints to the calcium ion as used previously (Jensen et al. 2006). The top 20 (of 100) calculated structures were selected based on minimum restraint violation and deviation from ideal stereochemistry. Structural and restraint statistics for these 20 lowest energy structures are listed in Table 4.1.

CR17-ApoE(130-149) Structural Refinement. Peak lists extracted from ^{15}N , HCN, and ^{13}C NOESY spectra were used for iterative assignments/structural calculations in ARIA2/CNS as before. Initial refinement showed that CR17 adopts the same overall fold as for the previous structure of CR17. Backbone dihedrals and secondary structure for CR17-ApoE(130-149) were predicted using TALOS and CSI (Wishart and Sykes 1994; Cornilescu et al. 1999). Several unambiguous restraints between CR17 and ApoE(130-149) obtained from the HCN NOESY and HCCH NOESY spectra were included as long range (1.8-6.0Å) restraints. Additional restraints for these calculations included 78 dihedral angle, 3 H-bonds, 18 pseudo-calcium coordination, and 3 disulfide bonds. To minimize ambiguity, assignments for H_2O and D_2O experiments were kept separate as minor deviations in resonance shifts between these samples were seen. Final calculations including the calcium ion were performed exactly as for CR17, and final statistics are listed in Table 4.1. Coordinates and NMR assignment data for both CR17 and CR17-ApoE(130-149) have been deposited to the PDB (2knx, 2kny), and BRMB (accession numbers 16482, 16483). Structure figures were made in PyMOL (DeLano 2002).

Results

Chemical shift perturbation of CR17 upon ligand binding. Titrations were first performed side by side with Ub-RAPD3 and Ub-RAPD1 to compare the interface between these two domains (Fig. 4.1). Both RAP domains caused a downfield shift in the H ϵ 1 resonance of W25, but this shift was much larger upon Ub-RAPD3 binding than upon Ub-RAPD1 binding. The amide cross peaks of L26, F12 and D32 showed similar changes in both titrations. Cross peaks for D38, C33, R24, W25, D30 showed large perturbations upon binding, but the shifts with Ub-RAPD1 were in different directions compared to the shifts caused by binding Ub-RAPD3. L46 and Y47 at the C-terminal end of CR17 were only perturbed by Ub-RAPD1, whereas V21 was only perturbed by Ub-RAPD3. Cross peaks for C14 and C20 are broadened in CR17, but upon Ub-RAPD1 binding, both became sharp peaks. In contrast, Ub-RAPD3 binding caused both of these cross peaks to disappear.

Chemical shift perturbations from RAP titrations were compared to those from Ub-ApoE(130-149) to assess any similarities in the interfaces. Just as with Ub-RAPD3 binding, the largest change observed was a strong downfield shift of W25 H ϵ 1 (Fig. 4.1). The changes in F12, L26, D32, E23 and R24 were also similar to those seen in RAP titrations. Similar to Ub-RAPD1 binding, strong peaks for C14 and C20 appeared upon titration with Ub-ApoE(130-149). D30 was one of the largest perturbations upon RAPD1 and RAPD3 binding, but this residue only showed a slight change upon Ub-ApoE(130-149) binding.

Because lysines 253 and 256 form critical contacts with LA4 in the structure of RAPD3 bound to LA34 (Fisher et al. 2006), and this sequence has homology with ApoE(130-149) we also expressed Ub-RAP(244-263) for NMR titration experiments (Fig. 4.1). This construct could also bind CR17 and produced perturbations very similar to those seen with ApoE(130-149). Subtle differences included a smaller change in the cross peaks for E23 and D28 and a slightly larger change in V21, D32 and D38. The same enhancement of peaks for C14 and C20 was also seen, just as with Ub-ApoE(130-149). Overall the perturbations from RAP(244-263) resembled those from ApoE(130-149) much more than those from RAPD3.

Affinity calculations from these titrations showed that both Ub-RAPD1 and Ub-RAPD3 had relatively high affinities for CR17 (96 +/- 12 μ M, 35 +/- 4 μ M respectively). The K_D calculated from the interaction with Ub-RAP(244-263) was significantly weaker (2000 +/- 450 μ M), and about two fold weaker than that measured for Ub-ApoE(130-149) (930 +/- 90 μ M).

Chemical shift perturbation of ApoE(130-149) upon CR17 binding. To examine changes within ApoE(130-149) upon binding CR17, ^{13}C , ^{15}N labeled ApoE(130-149) peptide was prepared with an additional Tyr at the N-terminus for quantification purposes. Comparisons of αC and αH chemical shifts to random coil values indicate that much of the peptide is helical, even in the unbound state (Wishart et al. 1991; Wishart and Sykes 1994). Cross peaks for T130, S139, H140, K143, R145, K146, and R147 were weak or invisible indicating intermediate exchange or multiple conformations. The addition of CR17 caused

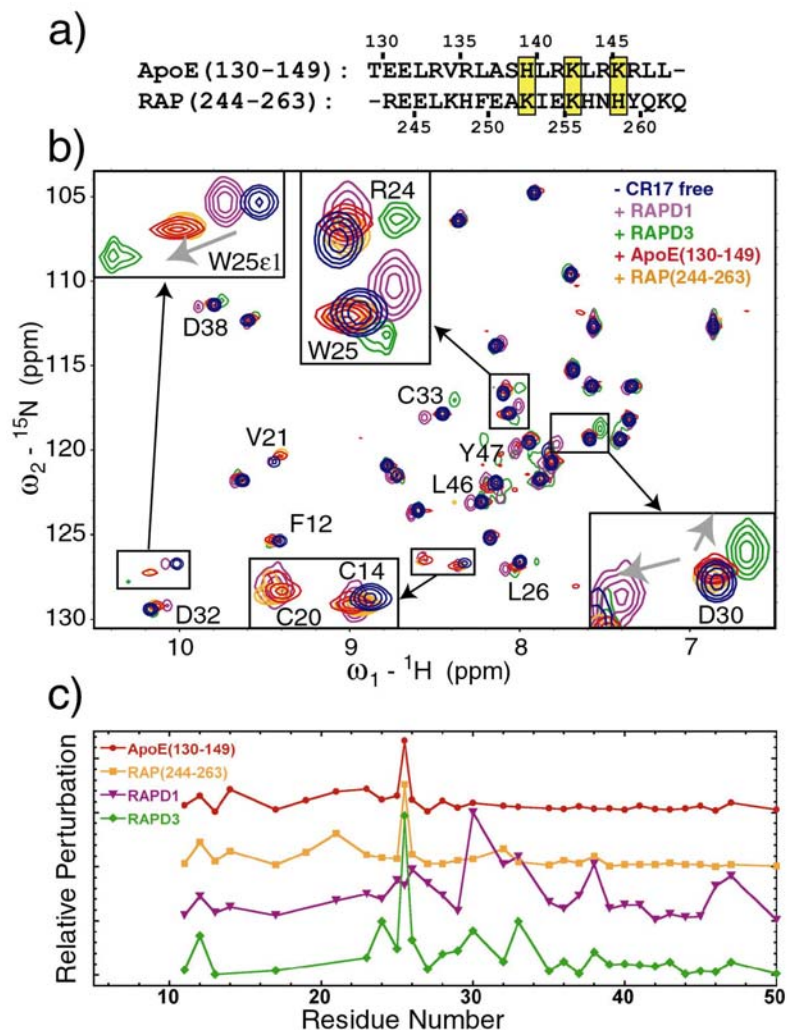


Figure 4.1: **a)** Alignment of ApoE(130-149) with RAP (144-163). **b)** ^1H - ^{15}N HSQC overlays of CR17 with Ub (blue), Ub-ApoE(130-149) (red), Ub-RAP(244-263) (orange), RAPD1 (purple), and RAPD3 (green). Residues undergoing strong changes are labeled and in some cases expanded. Grey arrows indicate direction of perturbations. **c)** Plot of total chemical shift for each visible cross peak in NMR perturbation experiments, with the same color scheme as in b). Values for the perturbation of W25 sidechain indole are shown at residue number 25.5.

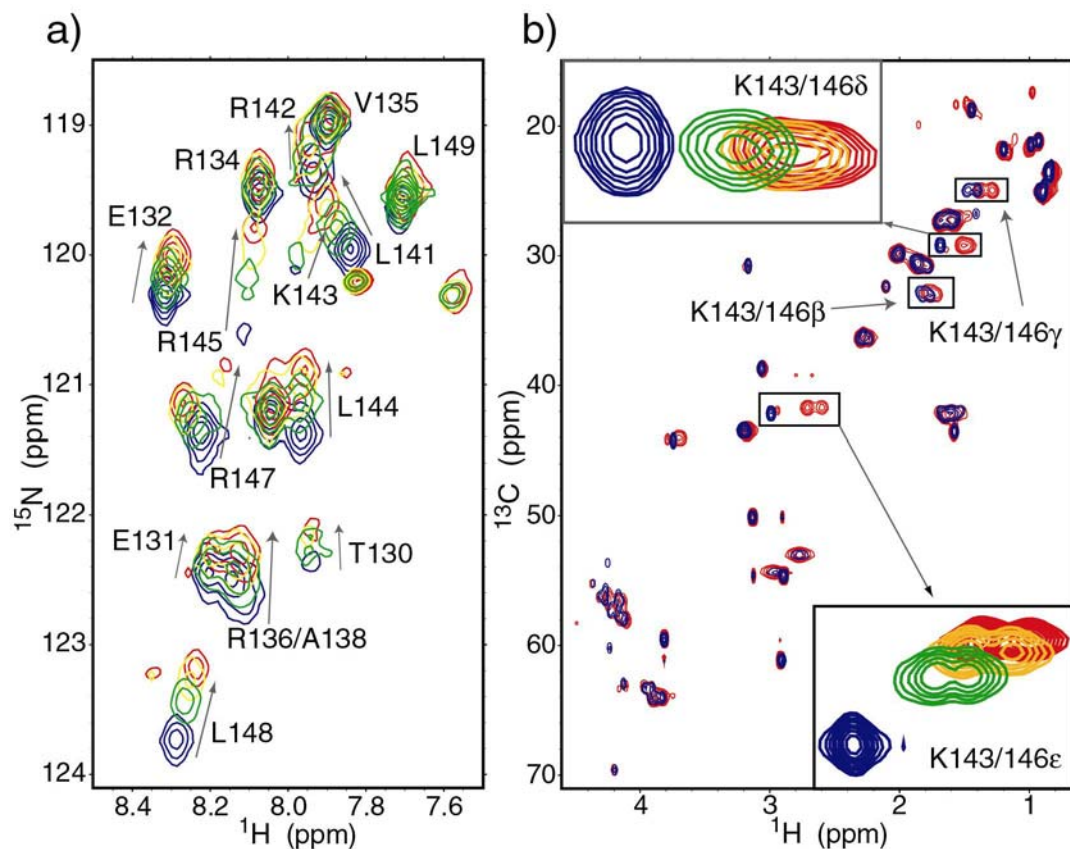


Figure 4.2: **a)** ^1H - ^{15}N HSQCs overlays of ApoE(130-149) peptide (blue), and with 0.6mM (green), 1.2mM (yellow) and 1.8mM CR17 (red). Lines indicate direction of shifts upon CR17 binding. **b)** ^1H - ^{13}C HSCQ overlay of the same samples from a).

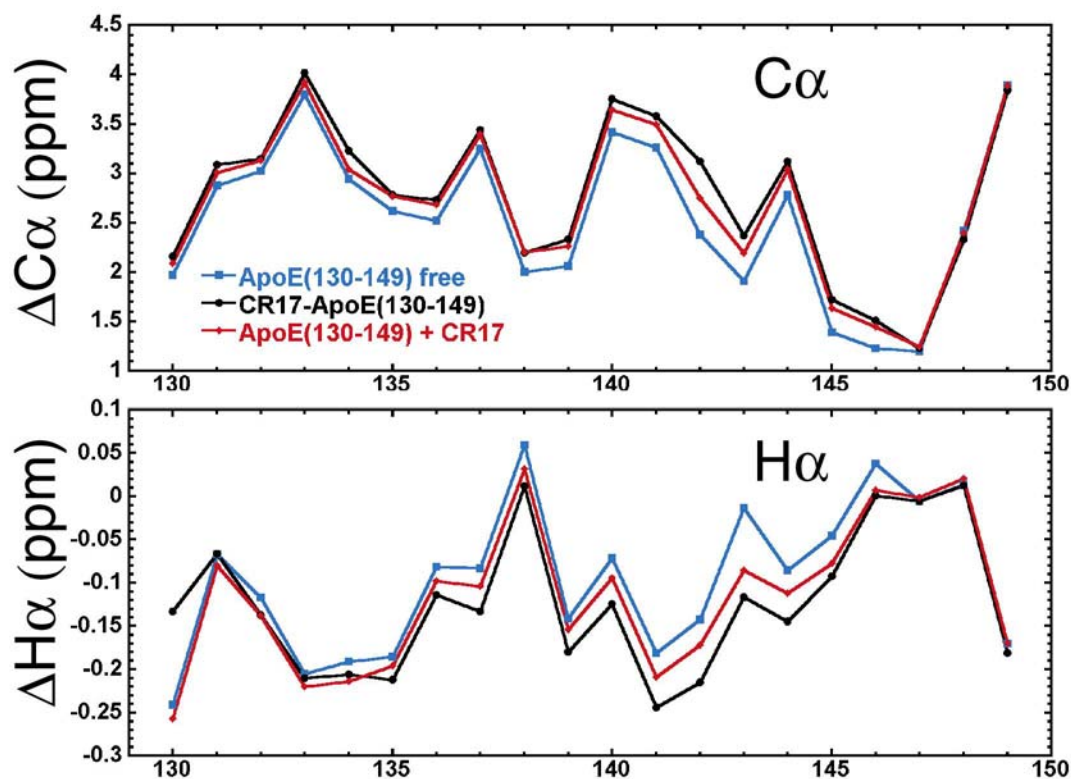


Figure 4.3: Plot of chemical shift index for ApoE(130-149) free (blue), upon addition of CR17 (red), and in the context of CR17-ApoE(130-149) (black) for αC , αH , N, and NH resonances.

an upfield shift in nearly all ^{15}N resonances consistent with higher helical content (Fig. 4.2). The αC and αH resonance shifts also indicated higher helicity especially within residues 138-146 (Fig. 4.3). These titrations followed by ^1H - ^{13}C HSQCs showed very large upfield shifts for β , γ , δ , and ϵ protons of K143 and K146 (Fig. 4.2). The changes in these two lysines were by far the largest in the ApoE(130-149) peptide. From the titration data, the affinity of the peptide for CR17 was calculated to be $780 \pm 180 \mu\text{M}$, very similar to the value obtained for Ub-ApoE(130-149) binding to CR17 ($930 \pm 90 \mu\text{M}$).

Structure of CR17. To understand perturbations on CR17 from the binding of various ligands we sought to solve the solution structure at physiological pH. Unlike CR16 and CR18 which were monomeric even at high concentrations, CR17 displayed significant self-association as assessed by analytical ultracentrifugation (AUC). Various buffer conditions were tested to alleviate self-association. Addition of 50mM arginine and 50mM glutamate minimized this effect and rendered a stable sample of CR17 for structural NMR studies, as seen for other systems (Golovanov et al. 2004). Addition of arginine and glutamate also slowed any visible aggregation of CR17 over longer periods.

^{15}N , ^{13}C and HCN NOESY experiments yielded a total of 971 distance restraints from iterative NOE assignments with ARIA2 (Rieping et al. 2007). Initial structures calculated without disulfide restraints showed that the expected disulfide-bonding pattern seen in all CR structures to date (C1-C3, C2-C4, C4-C6) was present in CR17. In addition 9 NOEs were observed in the ^{13}C NOESY

between sidechains of disulfide bonded cysteines ($C\alpha$ - $C\beta$ or $C\beta$ - $C\beta$), further confirming the disulfide bonds. Amide exchange experiments only showed weak protection for amides W25, L26, D32, and E39 and no protection for any other residues. Restraint statistics are listed in Table 4.1.

The 20 lowest energy structures of CR17 showed a high degree of flexibility for the six N- and four C-terminal residues (Fig. 4.4). The overall fold of CR17 with the anti-parallel beta sheet in the N-terminal half, and regions with helical turns in the C-terminal half, is nearly identical to previously solved CRs (Rudenko and Deisenhofer 2003), with the exception of the orientation of the N-terminal residues. Despite the absence of amide signals for all residues N-terminal to S11 (including the extra gly-ser at the N terminus resulting from the thrombin cleavage site), five unambiguous NOEs were observed in the ^{13}C NOESY between W25-K5 and W25-T6 revealing an interaction with this N-terminal region. Because of these restraints the N-terminal tail is bent back onto the surface of CR17 to form this interaction.

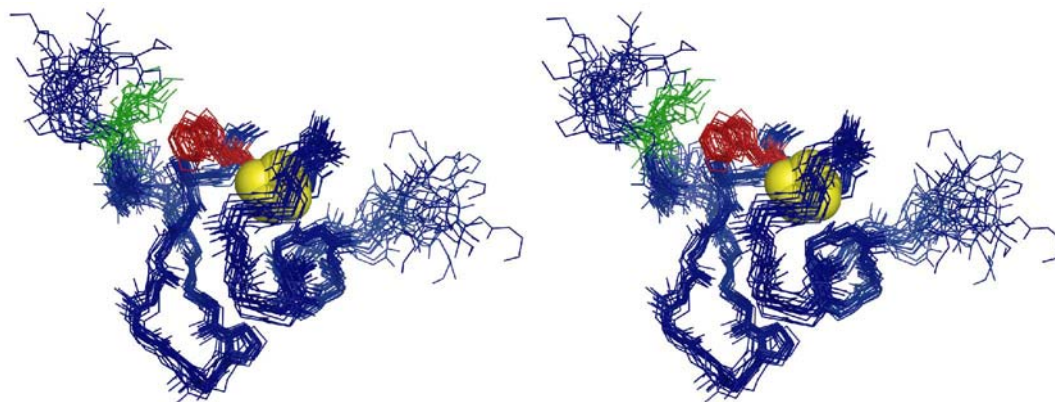


Figure 4.4: Stereo view of the backbone of the 20 lowest energy structures of CR17 shown in blue with sidechains of W25 (red) and K5 (green), with calcium ion as yellow spheres.

Table 4.1: Refinement statistics

NMR Constraints	CR17	CR17-ApoE(130-149)
Distance Constraints		
Total unambiguous NOEs	759	1138 (192) ⁽¹⁾
Intra-residue	169	217 (59) ⁽¹⁾
Sequential ($ i - j = 1$)	152	289 (40) ⁽¹⁾
Medium-range ($ i - j < 4$)	148	248 (36) ⁽¹⁾
Long-range ($ i - j > 5$)	200	384 (57) ⁽¹⁾
Intermolecular*		49
Ambiguous	212	876
Hydrogen bonds	3	3
Dihedral angle restraints	44	78
ϕ	22	39
ψ	22	39
Structural Statistics		
Violations (mean and s.d.)		
Distance constraints (Å)	0.0555 +/- 0.0031	0.0459 +/- 0.0038
Dihedral Angle Constraints (°)	0.7575 +/- 0.03415	0.5681 +/- 0.1294
Max distance constraint violation (Å)	0.4251 +/- 0.03415	0.433 +/- 0.03277
Max dihedral angle violation (°)	3.1276 +/- 1.291	3.441 +/- 1.132
Deviations from idealized geometry		
Bond lengths (Å)	0.0013 +/- 0.00009	0.0016 +/- 0.00001
Bond angles (°)	0.2613 +/- 0.0106	0.3325 +/- 0.0117
Impropers (°)	0.129 +/- 0.0122	0.177 +/- 0.0152
Average pairwise r.m.s. deviation (Å) (20 structures)		
All backbone atoms	0.92 +/- 0.18 ⁽²⁾	0.64 +/- 0.13 ⁽²⁾
All heavy atoms	1.13 +/- 0.19 ⁽²⁾	0.76 +/- 0.11 ⁽²⁾
All backbone atoms		0.83 +/- 0.15 ⁽³⁾
All heavy atoms		1.11 +/- 0.16 ⁽³⁾
Rmsd between structures (Å) ⁽⁴⁾		
All backbone atoms	1.29	
All heavy atoms	1.75	
Ramachandran Plot Statistics (%)		
Most favored regions	73.9 ⁽¹⁾	74.2 ⁽²⁾
Additionally allowed regions	25.3	24.9
Generously allowed regions	0.6	0.6
Disallowed regions	0.2	0.3

* Unambiguous restraint between ApoE(130-149) and CR17 (residues 1-50)

¹ Unambiguous NOEs for only the GS linker and ApoE(130-149) region.

² Statistics calculations were limited to residues (7-45)

³ Statistics calculations were limited to residues (7-45, 130-146)

⁴ Pairwise rmsd was calculated between the average structures of CR17 & CR17-ApoE, limited to residues (7-45)

Fusion construct of CR17-ApoE(130-149). Due to the weak affinity and fast kinetics of the interaction between CR17 and ApoE(130-149), obtaining specific contact information from intermolecular NOEs did not seem feasible. Therefore, a chimeric CR17-ApoE(130-149) fusion was constructed by appending the sequence for ApoE(130-149) at the C terminus of CR17 with an 8 residue gly-ser linker. The same expression and refolding protocol used for CR17 successfully yielded fusion protein that was able to bind calcium with similar binding affinity to that of isolated CR17 (Fig. 4.5).

Comparisons of the ^1H - ^{15}N HSQCs of CR17 and CR17-ApoE(130-149) under identical conditions showed that CR17 had the same overall fold, but with several cross peaks shifted in a manner consistent with ApoE(130-149) binding. W25 H ϵ 1 and the amides of W25, R24, and D30 shifted exactly as seen upon Ub-ApoE(130-149) binding to CR17 (Fig. 4.6). In addition, the sharp cross peaks for C20 and C14 that were observed upon Ub-ApoE(130-149) binding to CR17 were also observed in the fusion construct. Chemical shifts within the ApoE(130-149) region revealed an increase in helicity compared to free ApoE(130-149) peptide (Fig. 4.3). Amide crosspeaks for S139 and H140, which were invisible in the free peptide, were still weak but observable in the fusion construct. In the course of the preparation, a degradation product resulting from non-specific thrombin cleavage, was also isolated and identified to be CR17-ApoE(130-136). This proteolytic degradation product served as an important control because none of the chemical shift perturbations just mentioned for the full-length

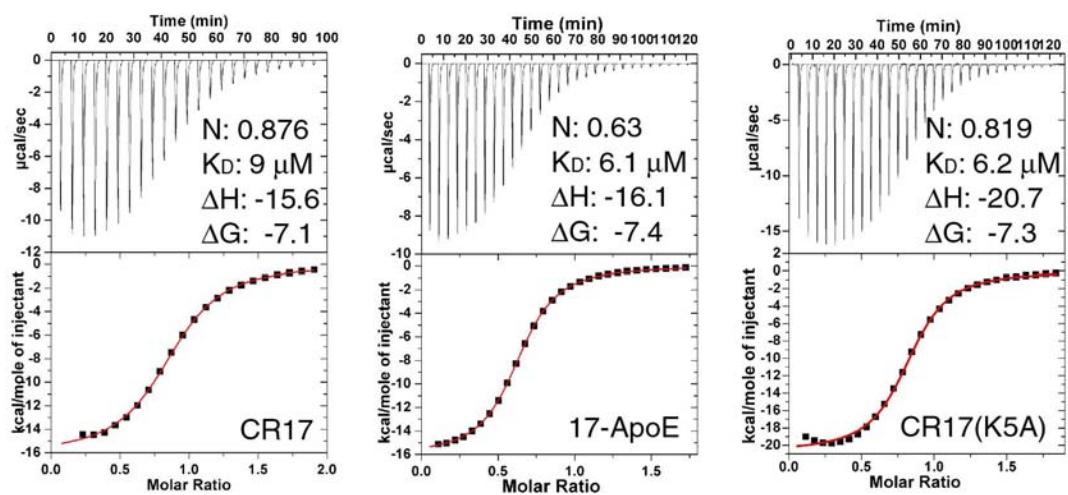


Figure 4.5: Isothermal titration calorimetry (binding isotherms) for CR17 and CR17-ApoE(130-149), and CR17(K5A). Thermodynamic parameters are listed under the binding isotherms.

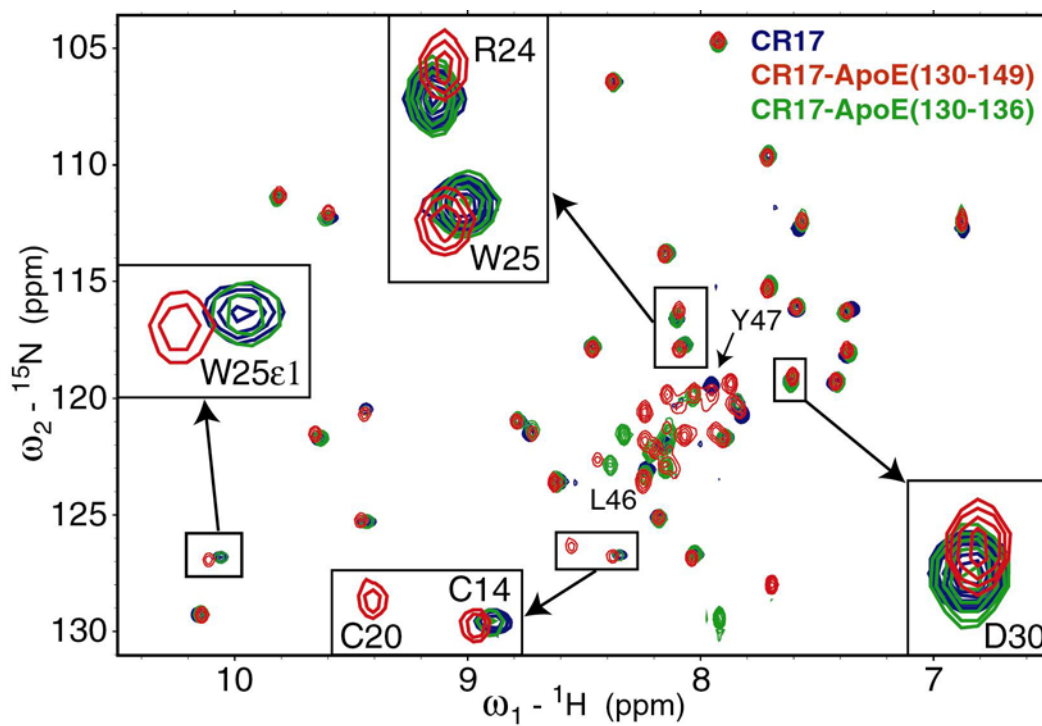


Figure 4.6: ^1H - ^{15}N HSQC overlays of CR17 (blue), CR17-ApoE(130-136) (green), and CR17-ApoE(130-149) (red). Large changes are labeled and expanded.

construct were observed for the truncated construct. The perturbations seen in L46 and Y47 in the fusion construct were not solely the result of the linker at the C-terminus, as the same degree of perturbations was not evident in the truncated CR17-ApoE(130-136) (Fig. 4.6).

To further examine changes seen in W25, native tryptophan fluorescence emission spectra were recorded of CR17, CR17-ApoE(130-149) and CR17-ApoE(130-136) (Fig. 4.7). The emission of W25 in CR17 and the truncated fusion construct looked identical, but a significant blue-shift was seen for W25 in the full length fusion construct. This difference was lost upon treatment with EDTA and DTT to unfold CR17. We were concerned about the possibility of the ApoE(130-149) region on one molecule of the fusion construct interacting with CR17 on another molecule to give intermolecular NOEs. Changes in fluorescence signals were not concentration dependent (from 1 μ M to 100 μ M) indicating that the interaction is intra-molecular. Size exclusion chromatography also indicated that CR17-ApoE(130-149) is monomeric in solution.

Both RAPD1 and RAPD3 were titrated into CR17-ApoE(130-149) to see whether the binding site would be blocked by the tethered ApoE(130-149). Perturbations were visible in HSQCs similar to those seen with free CR17 (Fig. 4.8). In both titrations changes were also seen within the ApoE(130-149) region of the fusion protein. The K_D for the RAP domains decreased more than 2-fold due to competition with the tethered ApoE(130-149) (from 35 +/- 4 to 75 +/- 30 μ M RAPD3, and from 96 +/-12 to 238 +/- 13 μ M RAPD1). Ub-ApoE(130-149) was also titrated into the fusion construct but only very slight perturbations were

observed, and the K_D for this ApoE(130-149) added in trans to the tethered construct was calculated to be ~5mM.

Structure of the CR17-ApoE(130-149) fusion. The CR17-ApoE(130-149) fusion construct was used for NMR structural determination under buffer conditions previously used for CR17. The number of NOE restraints within CR17 in the fusion construct was considerably higher than for the isolated CR17, as many broadened peaks became well resolved. R24 and H18 in particular had resonances that were poorly resolved and yielded few restraints (7 and 2 respectively) in CR17, but resonances of these residues were well resolved in the CR17-ApoE(130-149) fusion and yielded more restraints (20 and 9, respectively). Thus the precision of CR17 is higher with an overall RMSD of 0.64 +/- 0.13Å in the fusion as compared to 0.92 +/- 0.18Å in the isolated CR (Table 4.1, Fig. 4.9).

The overall fold of CR17 was similar in the presence and absence of the ApoE(130-149) fusion as indicated by the RMSD between the average structures for residues 7-45 was only 1.29Å (backbone) and 1.61Å (heavy atoms). The largest differences in CR17 were at the loop around C7 and at the C-terminal region (Fig. 4.10). The difference around C7 is likely because the interaction between W25 and K5 in free CR17 is not observed in the fusion construct, most likely because the ApoE(130-149) replaces this interaction. The change at the C-terminal end is likely due to the presence of the linker tethering the ApoE(130-149).

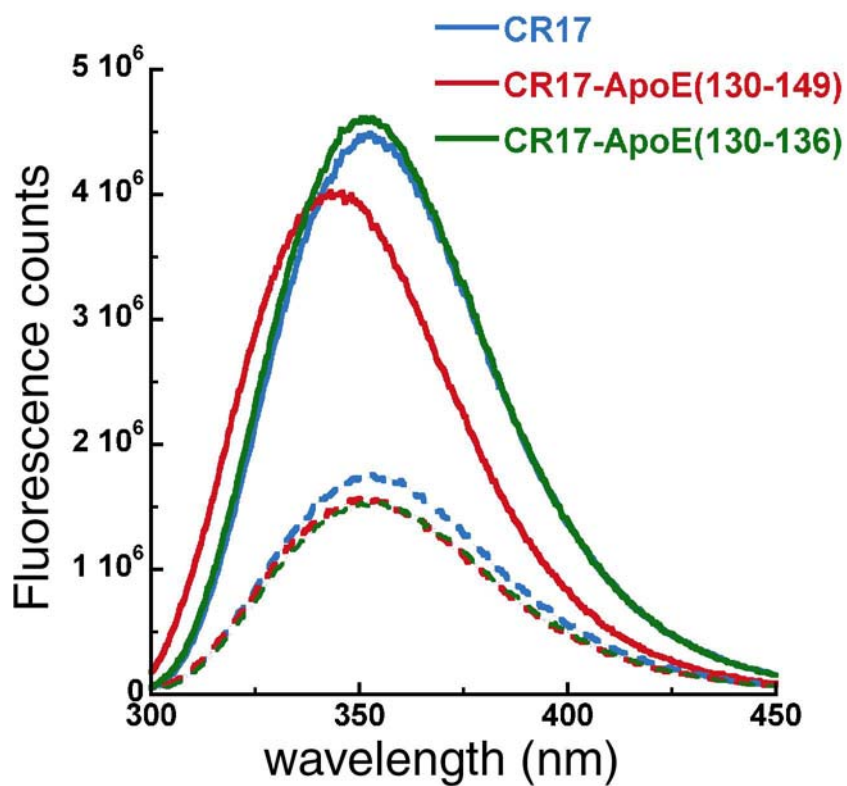


Figure 4.7: Tryptophan fluorescence emission spectra of CR17 (blue), CR17-ApoE(130-136) (green) and CR17-ApoE(130-149) (red) in with calcium (solid lines), and after treatment with DTT and EDTA (dashed lines).

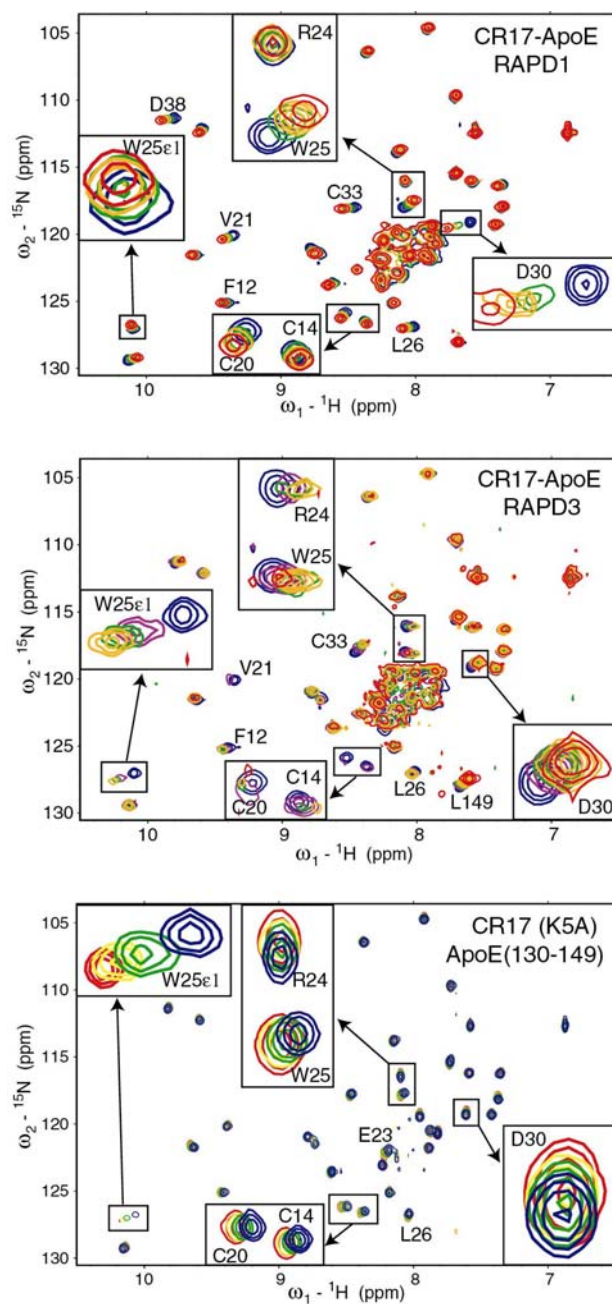


Figure 4.8: NMR titrations of CR17-ApoE(130-149) with Ub-RAPD1, CR17-ApoE(130-149) with Ub-RAPD3, and CR17(K5A) with Ub-ApoE(130-149). Titration points are zero ligand (blue), increasing ligand (purple, green, orange), and final ligand concentration (red).

We were able to assign all backbone and side chain resonances of the ApoE(130-149) region in the fusion protein. Secondary structure prediction using the chemical shift index showed helical propensity for residues 130-144 (Wishart and Sykes 1994). Dihedral restraints obtained from TALOS also indicated helical conformation for these same residues (Cornilescu et al. 1999). Unambiguous i to $(i+3)$ and $(i+4)$ NOEs were observed in residues E131, E132, R134, V135, L137, A138, S139, and H140 also identifying the region as forming a helix.

Analysis of ^{13}C -NOESY and HCN-NOESY spectra identified several NOEs between CR17 and ApoE(130-149) in the fusion construct. After initial refinement, a total of 49 unambiguous restraints were identified locking down this interface. The final lowest energy structures showed very little deviation for the ApoE region ($1.01 \pm 0.22\text{\AA}$ backbone, $1.48 \pm 0.27\text{\AA}$ heavy atom within residues 130-146 of ApoE). Even with a well defined structure, many of the restraints for the ApoE region remained ambiguous, likely due to resonance overlap of many Arg and Leu sidechains within this region (Fig 4.1). To ensure that this ambiguity was not affecting the final result, structural calculations were performed without the ambiguous restraints and yielded an average structure with 0.55\AA backbone and 0.72\AA heavy atom RMSD to the average structure calculated with the ambiguous restraints. As expected, excluding the ambiguous restraints led to slightly higher deviations within the ensemble (RMSDs of 1.02\AA vs. 0.83\AA backbone and 1.36\AA vs. 1.11\AA heavy atom for the 20 structures).

W25 of CR17, K143 of ApoE and to a lesser degree K146 of ApoE(130-149) are directly involved in forming the interface. The ApoE forms an alpha helix

up to residue S139 and turns nearly 90 degrees along the surface of CR17. The side chain of a lysine (K143) packs against the aromatic sidechain (W25) and points towards the acidic residues around the calcium ion (Fig. 4.9). The N-terminal part of the helix runs along the side of CR17. A138 and V135 face directly towards CR17 packing against the side chain of R24 and also C27. E131 and E132 are positioned on one side of the ApoE helix possibly forming an ionic interaction with R24 on CR17. On the other side of the helix, R134 appears to be making an ionic interaction with E23 and a hydrophobic interaction with L46. Some of the minimized structures showed the imidazole of H140 forming a contact with S10. These interactions position the ApoE(130-149) helix in a unique rotational configuration (with respect to the long helical axis) along the surface of CR17. Comparisons of ^{13}C HSQC spectra of free CR17, free ApoE(130-149) and CR17-ApoE(130-149) confirm that changes occur within the sidechain aromatic resonances of W25 and E23 along with K143 and K146 of ApoE.(Fig. 4.11).

Mutational analysis of the binding interface. To test the importance of lysines 143 and 146 in CR17-ApoE(130-149), mutations K143A and K143A/K146A (KKAA) were also prepared and screened by comparing of the ^1H - ^{15}N HSQC spectra. The chemical shift of the W25 H ϵ 1 cross peak had a smaller perturbation in the K143A mutant as compared to the wild type fusion, and the double mutant, KKAA, resulted in no difference in chemical shifts compared to those observed in unbound CR17 (Fig. 4.11).

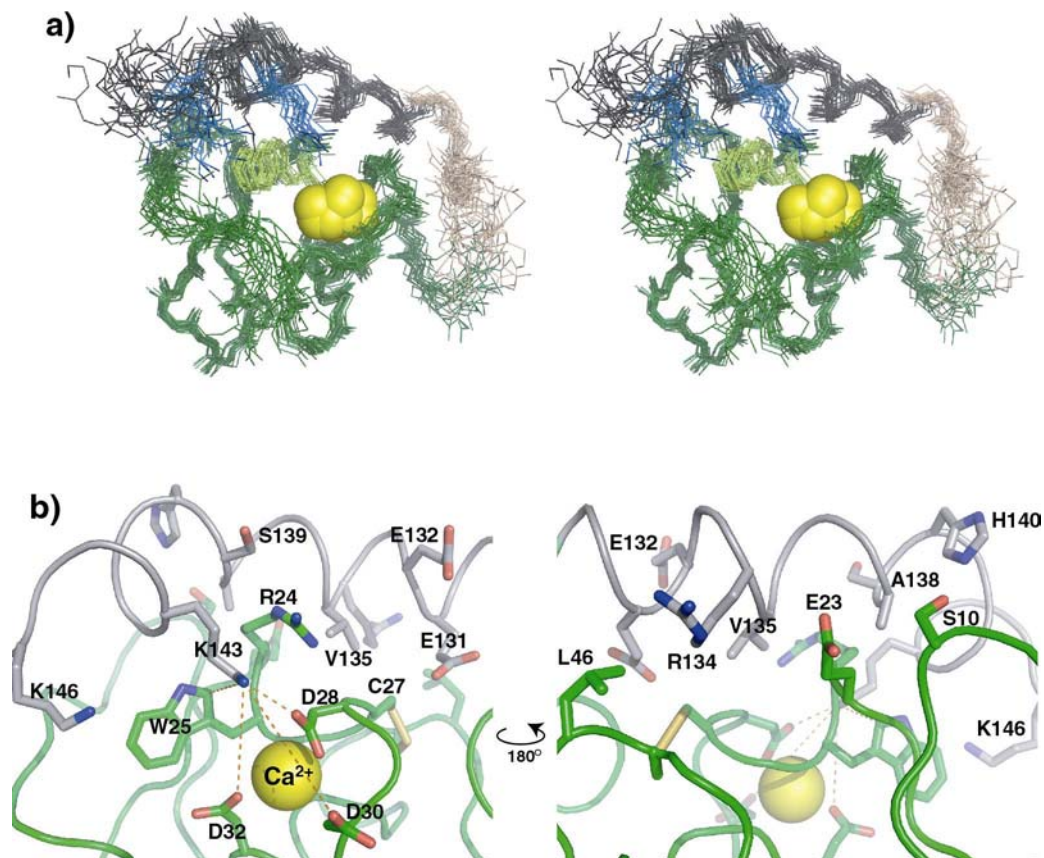


Figure 4.9: **a)** Stereo view of the backbone of the 20 lowest energy structures of CR17-ApoE(130-149). Colors are CR17 (blue), gly-ser linker (orange), and ApoE(130-149) (purple), calcium (yellow spheres), W25 sidechain (red), K143 and K146 sidechains (green). **b)** Interface of ApoE(130-149) (grey) and CR17 (green). Contacts for K143 to (W25, D28, D32, and D30) are shown as dashed lines.

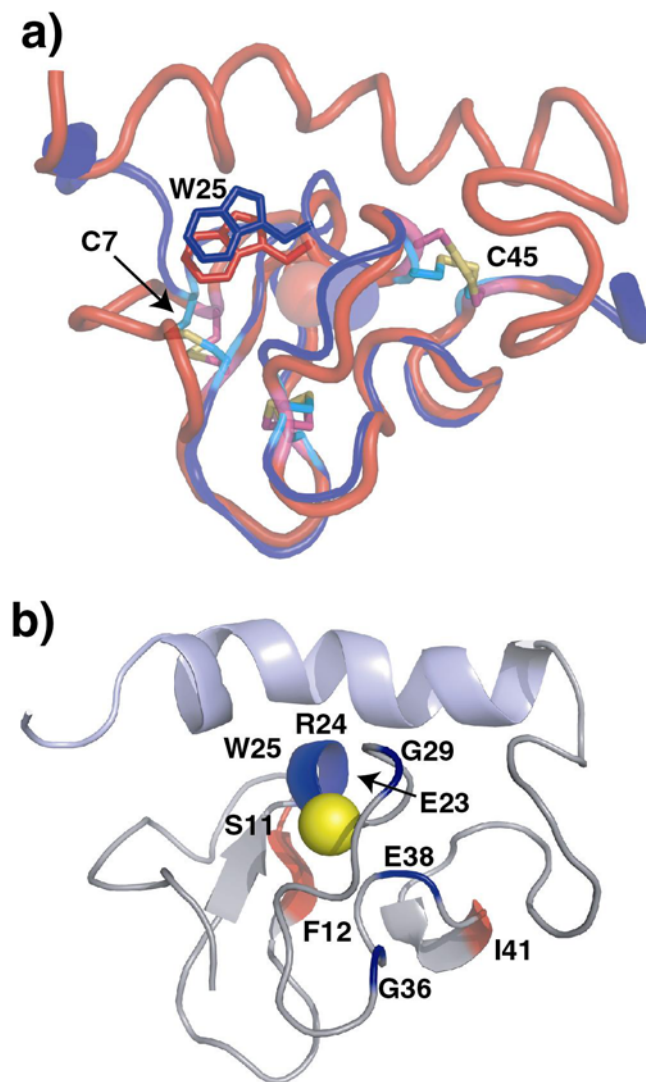
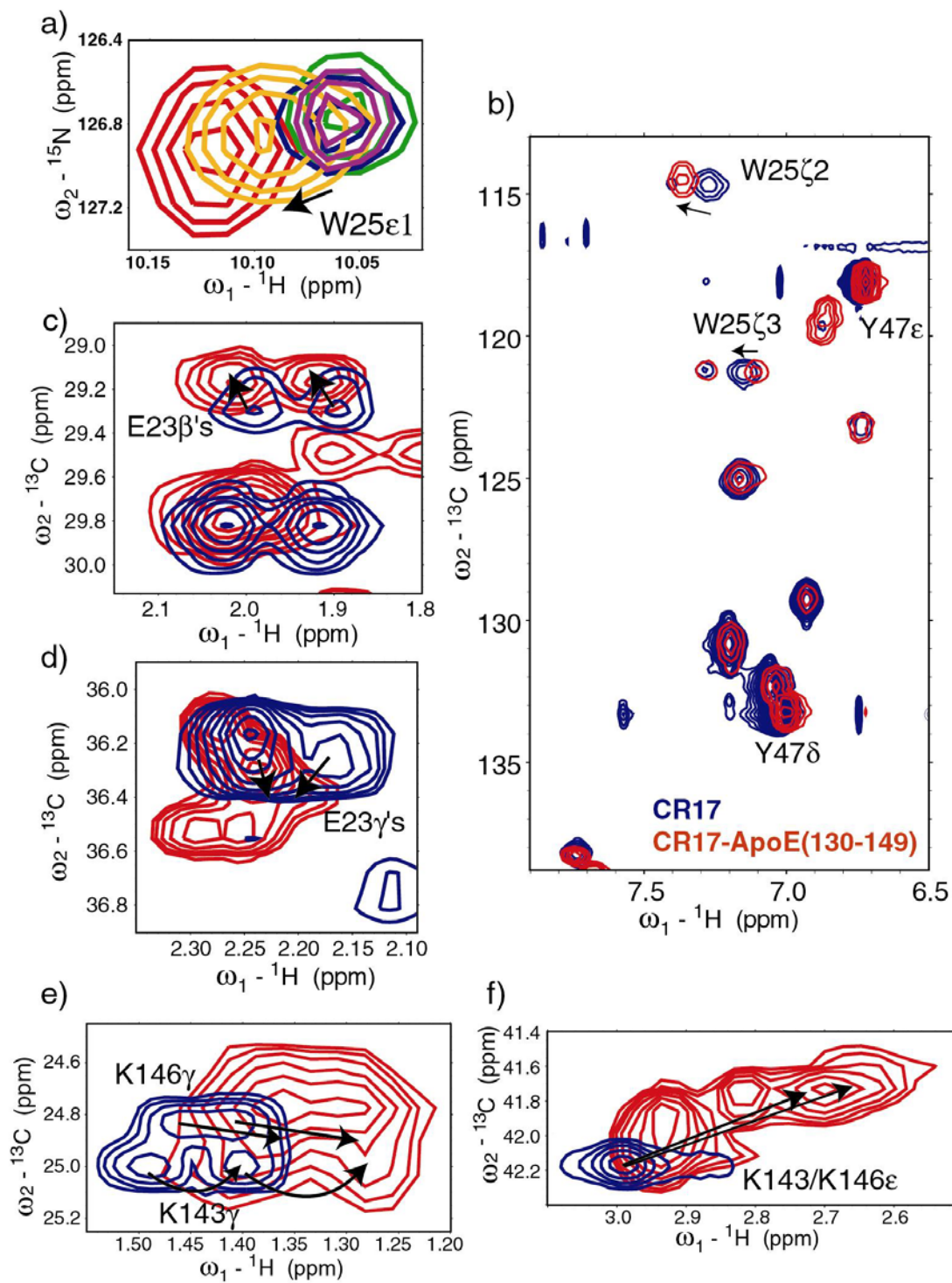


Figure 4.10: a) Structural alignment of the average structures of CR17 (blue) and CR17-ApoE(130-149) (red). The cysteines are shown as sticks along with the sidechain of W25. b) Cartoon representation of CR17-ApoE(130-149) showing residues that become more ordered (blue) and more disordered (red).

Figure 4.11: **a)** Overlay of HSQCs showing W25 ϵ 1 cross peak of CR17 (blue), CR17-ApoE(130-136) (green), CR17-ApoE(130-149) (red), CR17-ApoE(130-149)(K143A) (orange), and CR17-ApoE(130-149)(K143/146A) (purple). ^{13}C HSQC overlays for CR17 (blue) and CR17-ApoE(130-149) (red) showing aromatic region **(b)** E23 β **(c)** and E23 γ **(d)**. K143/146 γ **(e)** and K143/146 ϵ **(f)** are also shown for ApoE(Y+130-149) (blue) and CR17-ApoE(130-149) (red). Arrows indicate change in resonance shifts.



Dynamics of CR17 and CR17-ApoE(130-149). The majority of the cross peaks for CR17 are broader than we have observed for other CRs. Even in the context of the triple repeat CR16-18, CR17 had broader linewidths than CR16 or CR18 (unpublished observations). In addition, although all of the amide cross peaks are observed for CR16 and for CR18, cross peaks for residues E3, G4, K5, T6, C7, G8, S10, G16, H18, K31, and A34 in CR17 were not observed. ^1H - ^{15}N heteronuclear NOE (hNOE) values for visible amides were high, except at the C-terminal region (residues 47-50), indicating a well-structured domain.

^{15}N relaxation measurements were performed on both CR17 and CR17-ApoE(130-149) to examine any differences in the intrinsic dynamics of CR17 upon ligand binding. Comparisons of R1 and R2 relaxation rates between CR17 and CR17-ApoE(130-149) indicated that, as expected, the fusion construct tumbles as a larger protein (Fig. 4.12). Several weak (C14, C20, V19, and V21) or absent (T6, K5, E4 and G3) amide cross peaks in CR17 became stronger both upon binding ApoE(130-149) as well as in the CR17-ApoE(130-149) fusion construct. hNOE measurements indicated that residues E23, R24, W25, G29, G36, and D38 become more ordered when bound to ApoE(130-149). Interestingly F12 and I41 showed the opposite effect. Comparisons of hNOE values between free ApoE(130-149) peptide and the ApoE region of CR17-ApoE(130-149) showed much higher hNOEs in the fusion construct, but not quite as high as amides within CR17 (Fig. 4.12). Order parameters obtained from model free fitting of both CR17 and CR17-ApoE(130-149) indicated that residues

23-25 were indeed becoming more ordered in the fusion protein and residues 11-13 actually become more disordered upon binding ApoE(130-149).

We hypothesized that the interaction between the N-terminal region and W25 in CR17 was disrupted in the CR17-ApoE(130-149), presumably because the ApoE region was binding to W25, causing intrinsic dynamic changes in CR17. To test whether the disruption of this interaction in CR17 would have similar effects, we mutated Lys5, which interacts with W25, to an alanine. This mutant CR17(K5A), maintained a similar affinity for calcium (Fig. 4.5). The HSQC spectrum of this mutant had more uniform peak shapes with well resolved peaks for C20, C14, V21, and V19 (Fig. 4.8). Ub-ApoE(130-149) still bound CR17(K5A) causing identical perturbations as seen in wild-type, with a slightly weaker K_D (1,360 +/- 100 μ M vs. 930 +/- 90 μ M).

The hNOE values for this mutant showed that C27, D36, D38, W25, and to a lesser degree R24 showed higher hNOE values compared to wild type CR17. The effects were similar to those seen upon ApoE(130-149) binding to the wild type CR17 (Fig. 4.12). However E23 still had a lower hNOE like apo wild-type CR17. Residues F12 and S13 had lower hNOE values indicating less order in this region compared to apo wild type CR17. These results suggest that the K5-W25 interaction is partly responsible for the chemical exchange-broadening observed in apo CR17, and that this causes the wild type apo CR17 to be dynamic. In fact, the disruption of the K5-W25 interaction partly elicits the dynamic changes in CR17 seen upon ApoE(130-149) binding.

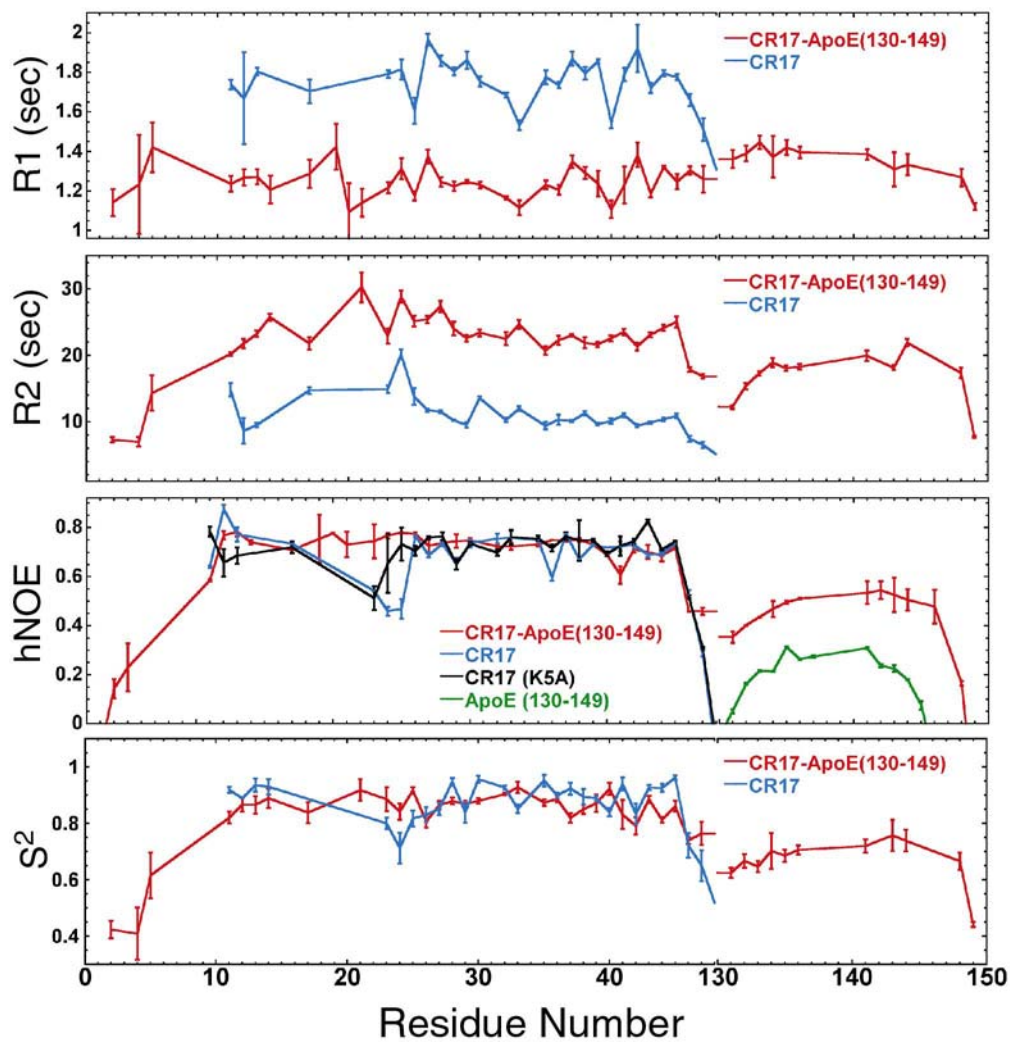


Figure 4.12: R1, R2, hNOE, and S² measurements for CR17 (blue), CR17-ApoE(130-149) (red), CR17(K5A) (black), and ApoE(Y130-149) (green). Order parameters (S²) were calculated from model free fitting of the ¹⁵N relaxation data.

Discussion

Complement repeats in the LDL receptor family are responsible for mediating most ligand interactions. Structures have also been predicted for the interaction with ApoE but so far the interface has remained elusive to atomic-level structural characterization. We have previously observed specific, albeit weak, binding of the receptor binding portion of ApoE (residues 130-149) to several CRs from LDLR and LRP, with CR17 of LRP showing a relatively high affinity. We have now solved the NMR solution structures of free CR17 and CR17 fused to ApoE(130-149), to examine the structural interface along with dynamic changes that result from this binding event.

A novel interface between CR17 and its N-terminal tail. The structure of free CR17 shows very little deviation from previously studied CRs. The calcium binding, disulfide bonding pattern and the overall fold (Greek Ω) match that described for several previously solved CR structures (Daly 1995; Fass 1997; Huang et al. 1999; Dolmer 2000; Simonovic 2001). Linewidth comparisons to other CRs previously studied indicate that CR17 exhibits chemical exchange broadening. In addition, even structured amides were completely exchanged after only 30 minutes, similar to what was seen for the second CR of LDLR (Daly et al. 1995). The rotational correlation time calculated from R2/R1 ratios was also higher than expected for a compact protein of ~5kDa (Beglova et al. 2001), but could be due to unstructured termini (residues 1-4 and 47-50) creating a larger hydrodynamic radius. Despite these effects 971 NOEs were obtained that

resulted in a well-determined structure of the protein with a backbone RMSD of 0.92 +/- 0.18Å (Table 4.1).

Although the structure of CR17 is highly similar to other CR structures, the position of the N-terminal tail, which would be the linker to CR16 in the context of the full receptor, is unique. Many unambiguous NOEs indicated an intramolecular interaction between K5 and W25. The mutation of K5 to Ala, designed to weaken this interaction, led to global changes in the HSQC spectrum, with more uniform line widths within CR17. Therefore this interaction was likely occurring on an intermediate timescale causing line broadening. It is possible that this interaction has functional relevance, orienting multiple CRs in the context of the full receptor. A lysine at this position (K5) is not very common (3/31 in LRP and 1/7 in LDLR), but the linker between the 2nd and 3rd CRs in LDLR has a conserved lysine (K86) at this position. In the full LDLR crystal structure at endosomal pH (Rudenko et al. 2002) no interaction was seen involving this lysine, none the less it may be interesting to test whether removal of this lysine affects receptor function.

A fusion of CR17 and ApoE(130-149) to examine the interface. Since the interaction between Ub-ApoE(130-149) and CR17 was relatively weak, and likely short lived, we engineered a fusion construct. CR17-ApoE(130-149) could still be correctly refolded as assessed by calcium binding and showed an intra-molecular interaction between ApoE and CR17 by comparison of the native Trp fluorescence and HSQC spectrum for CR17 alone and fused to ApoE(130-149). Although the tethering of ApoE(130-149) limits the binding mode, the gly-ser linker along with the C-terminal tail of CR17 should provide 30Å of

conformational freedom, and should allow the ApoE helix to access 180 degrees in its orientation along CR17. Importantly, although differences in chemical shift perturbations were observed for each of the different ligands studied here, the fused ApoE(130-149) caused the same chemical shift perturbations of the binding residues in CR17 as did Ubq-ApoE(130-149) added to CR17 in trans. This fusion construct allowed for specific NOEs to be obtained revealing the structure of the interface, and was also used to examine dynamics of the ApoE(130-149) bound form of CR17.

Regions in CR17 show both increased and decreased backbone dynamics upon ApoE(130-149) binding. To our knowledge this is the first examination of dynamic changes occurring within CRs upon ligand binding. Dynamics measurements showed that ApoE(130-149) binding rigidifies the loop around W25, while the region around F12 becomes less ordered. Most residues in CR17 for which a decrease in dynamics is observed upon binding ApoE(130-149) are located at the binding site (Fig. 4.10). The interaction may also be decreasing the dynamics of the calcium cage, which could explain the changes seen in hNOE values for E38, G29 and G36. Residues showing more disorder (S11 and F12) upon binding are on the opposite face of the molecule. I41 also shows decreased hNOE values upon binding, but this could result from the change at the C-terminal end due to the Gly-Ser linker in the fusion construct.

Several chemical shift perturbations in CR17 upon ApoE(130-149) are not near the binding interface, and thus are reporting indirect effects. F12 is

perturbed both upon Ub-ApoE(130-149) binding and in the fusion construct, but is located at the opposite face of CR17. Only a very slight structural change is observed for this region upon ApoE(130-149) binding, thus some perturbations may be reporting intrinsic dynamics changes as seen for F12. This illustrates the importance of considering indirect effects when predicting interfaces based on amide perturbations alone. These indirect effects could also explain the changes seen in V21, V19, C14 and C20 as they are all perturbed but are not near the binding interface. Unfortunately these residues were poorly resolved in the free CR17 and were not observable in our dynamics experiments.

A conserved motif for CR-interface formation. The structure of ApoE(130-149) fused to CR17 shows the ApoE(130-149) helix binding along the side of CR17, then forming a sharp bend around H140, with the C-terminal portion of ApoE, packing against W25 and making electrostatic interactions with the acidic residues around the calcium ion. This part of the interface has been seen in all other structures of CR-ligand interactions (Jensen et al. 2006; Blacklow 2007). This aspect of the interface had also had been predicted for the mode of ApoE binding to LA5 of LDLR from comparison to the RAPD3 co-structure (Fisher et al. 2006) and from rationally docked structures of ApoE to LA5 (Prévost and Raussens 2004). Both studies favored K146 of ApoE to form the critical contacts with the acidic cluster surrounding the calcium ion. From NMR perturbations it was clear that both K146 and K143 were heavily involved in the interface, and both showed NOEs to the aromatic sidechain of W25. K146 is facing the

interface and making contacts with W25, but in contrast to the predictions, it is K143 that is making contacts with both W25 and the acidic cluster around the calcium binding site.

Mapping of changes between free and bound CR17 revealed that the largest changes were directly at the ApoE binding interface (Fig. 4.13). The interaction of K143 and K146 with W25 is in agreement with chemical shift perturbations and intrinsic tryptophan fluorescence experiments indicating that the surface exposed aromatic sidechain of W25 is critically involved in interface. Mutation of these two interacting lysines to alanines in Ub-ApoE(130-149) was previously shown to decrease the binding affinity 5 fold (Chapter 3). Comparison between ApoE(130-149) peptide and CR17-ApoE(130-149) reveal the same large upfield shifts for the side chain resonances of K143 and K146 that were seen in titrations with CR17 (Fig 4.11). In addition to the $\epsilon 1$ resonance shift of W25 large deviations are also seen at positions $\zeta 2$ and $\zeta 3$ of W25 in the fusion protein (Fig. 4.11).

ApoE(130-149) binds with a bend in its helix. In agreement with previous structural studies, ApoE(130-149) is highly helical (Wilson et al. 1991; Raussens et al. 2002; Raussens et al. 2003). Upon binding CR17 an increase in helicity was visible, particularly in the C-terminal half, indicating that binding stabilizes this helical conformation. In the bound state, this region of ApoE has a bend in the helix at residues S139-H140. This could directly result from the binding interface with CR17 as K143 stretches to interact with the acidic residues around

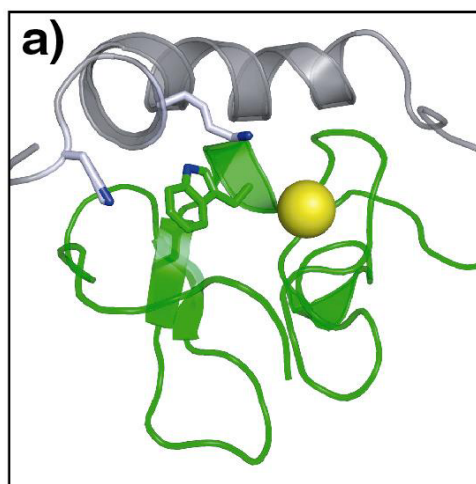
the calcium site in CR17. Both S139 and H140 had very weak amide cross peaks in both CR17-ApoE(130-149) and free ApoE(130-149) peptide, so in solution this portion of the helix may already be sampling bent states prior to binding. Earlier studies resolved H140 and S139 and saw no break in the helical structure, possibly because TFE and lipid binding stabilized this helix of ApoE (Raussens et al. 2002; Raussens et al. 2003).

The structure of ApoE(130-149) bound to CR17 allows some speculation as to why the lipid-free ApoE binds more weakly. In fact, the structure is consistent with binding to a lipid-bound form of ApoE since all of the leucines in this helical region are facing away from the CR17 interface and so could be interacting with lipid. Although most of the ApoE residues involved in the CR17 interface are already surface exposed in lipid free ApoE (Wilson et al. 1991), some may become more accessible in the lipid-bound form of ApoE. For example, it has been reported that upon lipid binding the sidechains of K143 and K146 are also more accessible (Lund-Katz et al. 2000). NMR studies on ApoE showed a helix for this region when complexed with DPC micelles, resulting in a curvature further exposing K143 and K146 (Raussens et al. 2003) which could enhance binding as both of these lysines protrude away from the helix in the bound form, to make contacts with CR17. In addition, some of the structures we determined showed H140 bending back to interact with CR17. It is possible that upon lipid association, the helices unwind (Fisher and Ryan 1999) and now have the freedom to access this bent conformation.

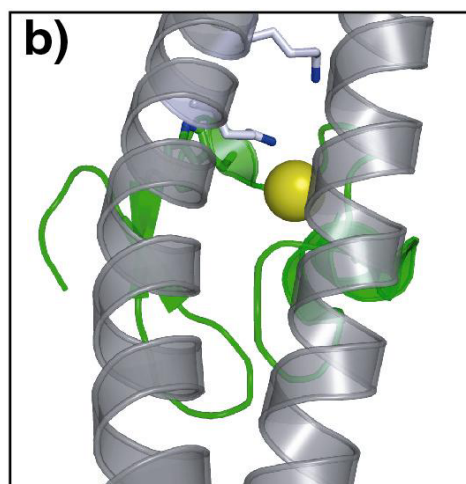
The CR17 ApoE(130-149) interaction is still transient. The ApoE region of the fusion construct shows lower hNOEs than expected for a compact protein. ApoE residues C-terminal to K146 are unstructured as seen from lower hNOE values as well as the deviations in the structural ensemble. Given the weak binding affinity, it is likely that even in the fusion, the binding is still transient with fast binding kinetics. Strong evidence that the interaction is still transient is that the ApoE(130-149)-tethered to CR17 did not effectively compete for binding with RAPD3. In fact, RAPD3 only bound 2-fold more weakly to the tethered construct. Based on the structures of RAPD3-LA34 (Fisher et al. 2006) and of our CR17-ApoE(130-149) it would be impossible for both to bind simultaneously.

Novel features within the CR17-ApoE interface. Several aspects of the ApoE(130-149) interaction appear distinct from previously reported CR interactions. Unlike the interfaces of LA34 with RAPD3 (Fisher et al. 2006) and the haddock model of CR56 bound to RAPD1 (Jensen et al. 2006), the ApoE helix contacts CR17 on the side rather than directly at the calcium binding site (Fig. 4.13). Instead of a continuous α -helix, this bound form of ApoE(130-149) has a turn at residues 139-140 which directs the downstream region to the acidic cluster around the calcium ion. N-terminal to this turn, ApoE is positioned so that it makes favorable electrostatic interactions on both helical faces. E131 and E132 are positioned near R24, and R134 on the other side is positioned near E23 (Fig. 4.9). H140 faces into the helical bundle in lipid-free ApoE and was seen to embed in the lipid surface in NMR studies of ApoE. In our structural ensemble

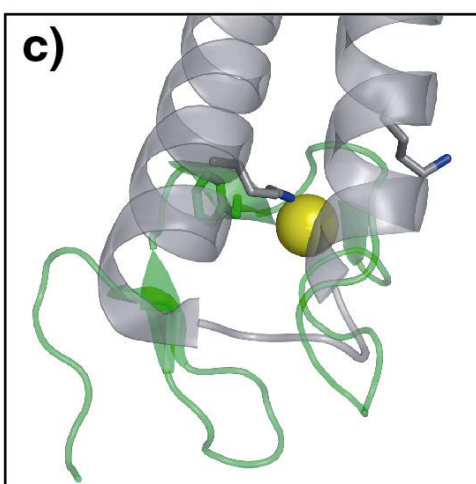
Figure 4.13: Difference in orientation among CR-ligand interfaces **a)** CR17-ApoE(130-149), **b)** LA4-RAPD3 (pdb 2FCW), **c)** LA4-RAPD3 (pdb 2FCW), **d)** CR5-RAPD1 (pdb 2FYL). Each interface is aligned relative to CR17-ApoE(130-149) with CR in green and ligand in grey. Critical Trp/Phe and Lys residues at the interfaces are shown as sticks, and calcium ions are shown as yellow spheres. **e)** Mapping of chemical shift perturbations from fusion of ApoE(130-149) (grey) on the surface CR17. Residues on CR17 are colored based on degree of perturbations; strong (red), medium (pink), weak (orange), no shift (yellow) and no data (blue). V21 is at the center of CR17, and therefore not visible in this representation.



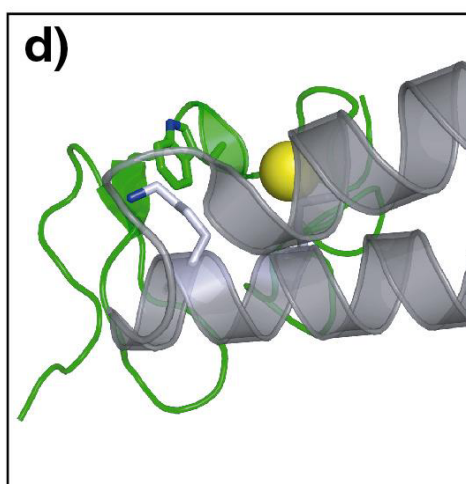
CR17-ApoE(130-149)



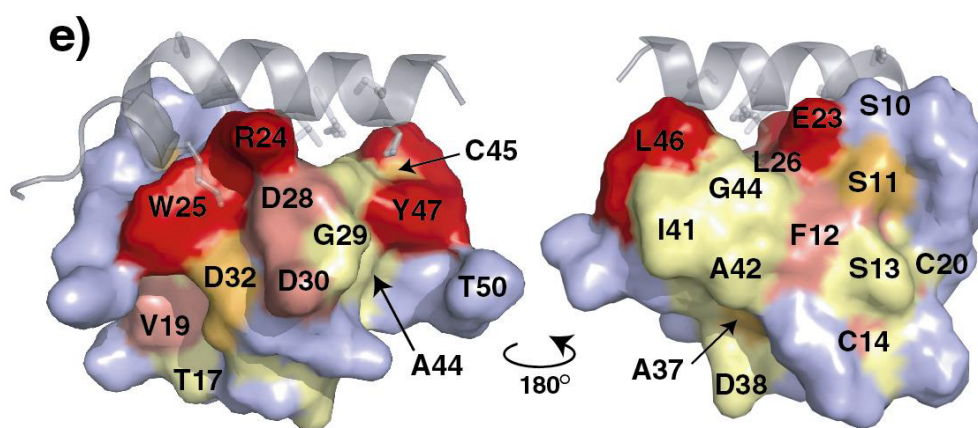
LA4-RAPD3



LA3-RAPD3



CR5-RAPD1



H140 has some conformational heterogeneity, potentially forming contacts with S10, although no NOEs were observed for the aromatic resonances of H140 to confirm this contact. Residues at these positions (E23, and S10) are not at the interface with RAPD3 in LA3 or LA4, as they both face away from the calcium binding site.

One surprising aspect of the CR17-ApoE(130-149) structure was the large distance (7Å) between the amine of K143 and the carboxylate of D30. This aspartate has been proven to be essential for high affinity RAP binding (Andersen et al. 2000), and is less than 3Å apart from the binding lysine in both LA3 and LA4 bound to RAPD3. We have previously shown that mutation of D30A in CR17 decreases the affinity for Ub-ApoE(130-149) nearly 10 fold (Chapter 3). Therefore we speculate that the presence of D30 is creating a more electronegative environment next to the indole ring of W25, tightening the interaction with the interacting lysine.

NMR chemical shift perturbation experiments that were performed with CR3 of LRP interacting with the receptor binding domain of alpha 2 macroglobulin (α 2M-RBD) (Dolmer 2000) have many similarities to our observations of CR17 binding to ApoE(130-149) and RAP. These include the large downfield shift in the indole of W23 (W25 in CR17), and the direction of the shifts of cross peaks for F11, I19, E21, K24 and D30 (corresponding to F12, V21, E23, L26, and D32 in CR17) are the same as observed for CR17 binding ApoE(130-149). Much like ApoE, α 2M also has two critical lysine residues required for receptor binding (Nielsen et al. 1996). In light of these similarities it is

likely that α 2M binds CR3 with a similar interface, in which lysine 1370 or 1374 interacts with W23 of CR3 along with the acidic residues around the calcium ion.

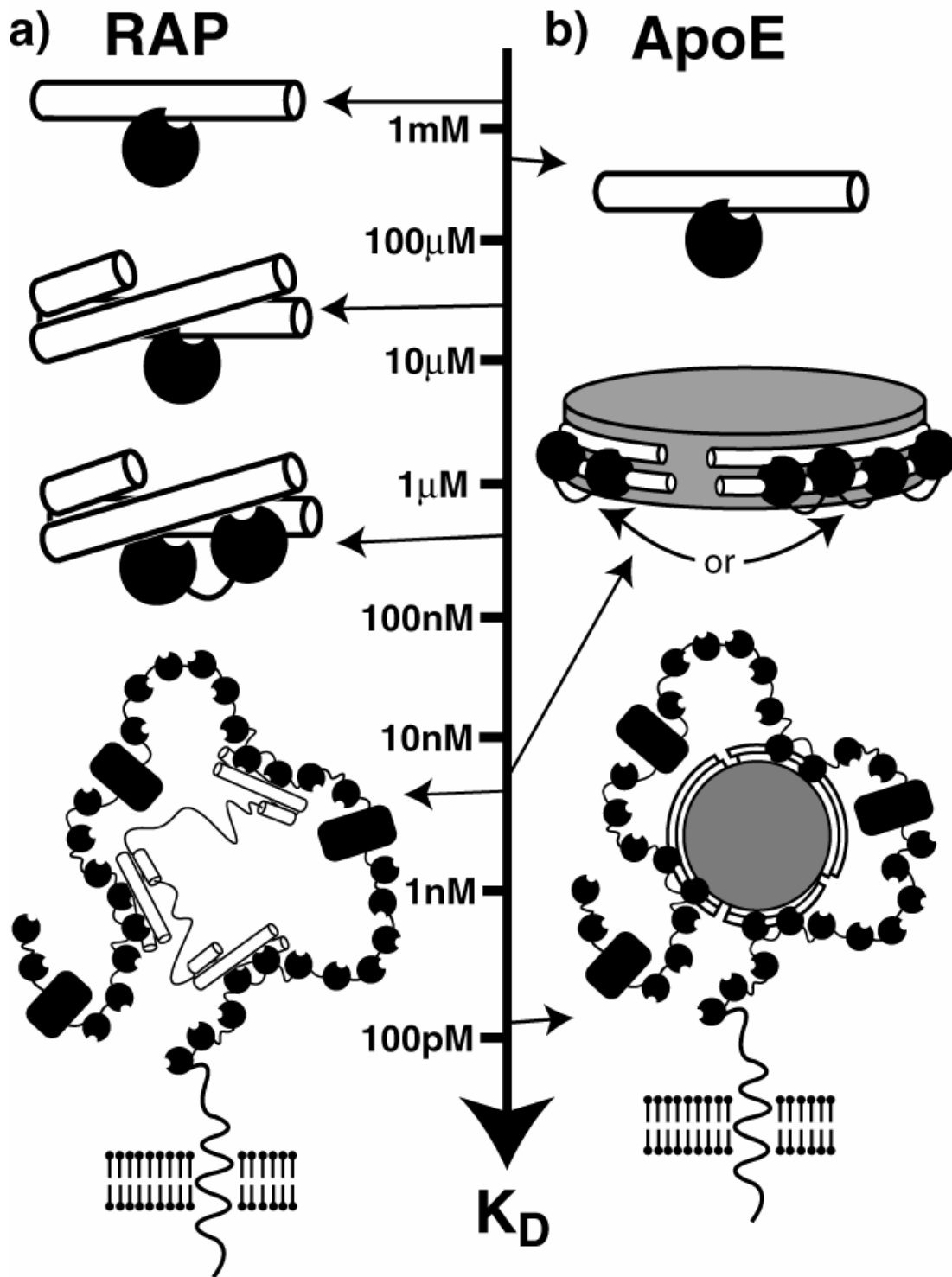
The structure represents a minimal binding interface for ApoE-LDLRs.

Since ApoE(130-149) segment only represents a portion of the lipid-bound ApoE molecule required for full receptor binding affinity, it is interesting to compare the relative affinities as more of the binding interface is assembled (Fig. 4.14). RAP(244-263), just like ApoE(130-149), could bind CRs with low mM affinity. However, the full helix bundle of RAPD3 bound a single CR with a K_D in the mid μ M range. Lipid association may reorganize the ApoE helices to form a high affinity receptor site similar in conformation to the helix bundle in RAPD3 (Fisher et al. 2006). Binding of a pair of CRs to RAPD3 then increases the affinity into the high nM range (Andersen et al. 2001). Although we still don't know if a single molecule of lipid bound ApoE can bind multiple CRs, studies in which only one active ApoE was present per micelle showed a receptor affinity of 2.6nM (Pitas et al. 1980). As depicted in Figure 4.14, the interaction involves at least two CRs (Fisher et al. 2004), but may achieve even higher affinity with more than two.

It is likely that *in vivo*, several of these interactions occur simultaneously to achieve very high affinity interactions. RAP has three domains that can each interact with a pair of CRs, which further increases the affinity to the low nM range (Williams et al. 1992). Similarly, several copies of ApoE on the surface of lipoprotein particles could engage the receptor and generate very high affinity

binding (Innerarity et al. 1979; Ruiz et al. 2005). A 26 fold increase in receptor affinity was observed when multiple copies of ApoE were present on the surface of lipoprotein particles, which is similar to the roughly 15 fold increase of RAPD3 vs. full RAP binding to LRP (200nM vs. 4-14nM) (Andersen et al. 2001; Williams et al. 1992). Thus the mechanisms by which these ligands build specificity and binding affinity for the receptor may be similar.

Figure 4.14: Small interactions assemble to create high affinity ligand-receptor interactions. **a)** CRs from LRP (black circles) can interact with a single helix (top), a helical bundle of RAP, or all three helical bundles of RAP (bottom). **b)** CRs can similarly interact with a single helix of ApoE (top), a molecule of lipid associated ApoE, or lipoproteins containing multiple copies of ApoE (bottom). Figure not draw to scale, and for simplicity the EGF and β -propeller domains of LRP have been represented as single black rectangles.



References

- Abdul-Aziz, D., Fisher, C., Beglova, N., and Blacklow, S.C. 2005. Folding and binding integrity of variants of a prototype ligand-binding module from the LDL receptor possessing multiple alanine substitutions. *Biochem J* 44: 5075-5085.
- Andersen, O.M., Christensen, L.L., Christensen, P.A., Sørensen, E.S., Jacobsen, C., Moestrup, S.K., Etzerodt, M., and Thøgersen, H.C. 2000. Identification of the minimal functional unit in the low density lipoprotein receptor-related protein for binding the receptor-associated protein (RAP). A conserved acidic residue in the complement-type repeats is important for recognition of RAP. *J Biol Chem* 275: 21017-21024.
- Andersen, O.M., Schwarz, F.P., Eisenstein, E., Jacobsen, C., Moestrup, S.K., Etzerodt, M., and Thøgersen, H.C. 2001. Dominant thermodynamic role of the third independent receptor binding site in the receptor-associated protein RAP. *Biochem J* 40: 15408-15417.
- Bax, A., Clore, G.M., and Gronenborn, A.M. 1990. Proton-proton correlation via isotropic mixing of carbon-13 magnetization, a new three-dimensional approach for assigning proton and carbon-13 spectra of carbon-13-enriched proteins. *J Magn Reson* 88: 425-431.
- Beglova, N., North, C.L., and Blacklow, S.C. 2001. Backbone dynamics of a module pair from the ligand-binding domain of the LDL receptor. *Biochemistry* 40: 2808-2815.
- Beisiegel, U., Weber, W., Ihrke, G., Herz, J., and Stanley, K.K. 1989. The LDL-receptor-related protein, LRP, is an apolipoprotein E-binding protein. *Nature* 341: 162-164.
- Blacklow, S.C. 2007. Versatility in ligand recognition by LDL receptor family proteins: advances and frontiers. *Curr Opin Struct Biol* 17: 419-426.
- Brown, M.S., Herz, J., and Goldstein, J.L. 1997. LDL-receptor structure: Calcium cages, acid baths and recycling receptors. *Nature* 388: 629-630.
- Brunger, A.T. 2007. Version 1.2 of the Crystallography and NMR System. *Nature Protocols* 2: 2728-2733.
- Bu, G.J., Geuze, H.J., Strous, G.J., and Schwartz, A.L. 1995. 39 kDa receptor-associated protein is an ER resident protein and molecular chaperone for LDL receptor-related protein. *EMBO J* 14: 2269-2280.

- Clackson, T., Detlef, G., and Jones, P. 1991. PCR, a Practical Approach. (eds. M. McPherson, P. Quirke, and G. Taylor), pp. 202. IRL Press, Oxford.
- Clowes, R.T., Boucher, W., Hardman, C.H., Domaille, P.J., and Laue, E.D. 1993. A 4D HCC(CO)NNH experiment for the correlation of aliphatic side-chain and backbone resonances in $^{13}\text{C}/^{15}\text{N}$ -labelled proteins. *J Biomol NMR* 3: 349–354.
- Cornilescu, G., Delaglio, F., and Bax, A. 1999. Protein backbone angle restraints from searching a database for chemical shift and sequence homology. *Journal of Biomolecular NMR* 13: 298-302.
- Croy, J.E., Shin, W.D., Knauer, M.F., Knauer, D.J., and Komives, E.A. 2003. All three LDL receptor homology regions of the LDL receptor-related protein (LRP) bind multiple ligands. *Biochemistry* 42: 13049-13057.
- Daly, N.L., Djordjevic, J.T., Kroon, P.A., and Smith, R. 1995. Three-dimensional structure of the second cysteine-rich repeat from the human low-density lipoprotein receptor. *Biochemistry* 34: 14474-14481.
- Daly, N.L., Scanlon, M. J., Djordjevic, J. T., Kroon, P.A., and Smith, R. 1995. Three-dimensional structure of a cysteine-rich repeat from the low-density lipoprotein receptor. *Proc. Natl. Acad. Sci. USA* 92: 6334-6338.
- Delaglio, F., Grzesiek, S., Vuister, G., Zhu, G., Pfeifer, J., and Bax, A. 1995. NMRPipe: a multidimensional spectral processing system based on UNIX pipes. *J. Biomol. NMR* 6: 277-293.
- DeLano, W.L. 2002. DeLano Scientific, San Carlos, CA, USA.
- Dolmer, K., Huang, W., and Gettins, P. G. 2000. NMR solution structure of complement-like repeat CR3 from the low density lipoprotein receptor-related protein. Evidence for specific binding to the receptor binding domain of human alpha(2)-macroglobulin. *J Biol Chem* 275: 3264-3269.
- Fass, D., Blacklow, S., Kim, P. S., and Berger, J. M. 1997. Molecular basis of familial hypercholesterolaemia from structure of LDL receptor module. *Nature* 388: 691-693.
- Fisher, C., Abdul-Aziz, D., and Blacklow, S.C. 2004. A two-module region of the low-density lipoprotein receptor sufficient for formation of complexes with apolipoprotein E ligands. *Biochem J* 43: 1037-1044.

- Fisher, C., Beglova, N., and Blacklow, S.C. 2006. Structure of an LDLR-RAP complex reveals a general mode for ligand recognition by lipoprotein receptors. *Mol Cell* 22: 277-283.
- Fisher, C.A., and Ryan, R.O. 1999. Lipid binding-induced conformational changes in the N-terminal domain of human apolipoprotein E. *J Lipid Res* 40: 93-99.
- Golovanov, A.P., Hautbergue, G.M., Wilson, S.A., and L.Y., L. 2004. A simple method for improving protein solubility and long-term stability. *J Am Chem Soc*. 126: 8933-8939.
- Grzesiek, S., and Bax, A. 1992a. Correlating backbone amide and side chain resonances in larger proteins by multiple relayed triple resonance NMR. *J Am Chem Soc* 114: 6291-6293.
- Grzesiek, S., and Bax, A. 1992b. An Efficient Experiment For Sequential Backbone Assignment of Medium-Sized Isotopically Enriched Proteins. *J Magn Reson* 99: 201-207.
- Herz, J., Goldstein, J.L., Strickland, D.K., Ho, Y.K., and Brown, M.S. 1991. 39-kDa protein modulates binding of ligands to low density lipoprotein receptor-related protein/alpha 2-macroglobulin receptor. *Journal of Biological Chemistry* 266: 21232-21238.
- Herz, J., and Strickland, D.K. 2001. LRP: A multifunctional scavenger and signaling receptor. *J. Clin. Invest.* 108: 779-784.
- Huang, W., Dolmer, K., and Gettins, P.G. 1999. NMR solution structure of complement-like repeat CR8 from the low density lipoprotein receptor-related protein. *J Biol Chem* 274: 14130-14136.
- Innerarity, T.L., Pitas, R.E., and Mahley, R.W. 1979. Binding of arginine-rich (E) apoprotein after recombination with phospholipid vesicles to the low density lipoprotein receptors of fibroblasts. *J Biol Chem* 254: 4186-4190.
- Jensen, G.A., Andersen, O.M., Bonvin, A.M., Bjerrum-Bohr, I., Etzerodt, M., Thøgersen, H.C., O'Shea, C., Poulsen, F.M., and Kragelund, B.B. 2006. Binding site structure of one LRP-RAP complex: implications for a common ligand-receptor binding motif. *J Mol Biol* 362: 700-716.
- Kay, L.E., Clore, G.M., Bax, A., and Gronenborn, A.M. 1990a. Four-dimensional heteronuclear triple-resonance NMR spectroscopy of interleukin-1 beta in solution. *Science* 249: 411-414.

- Kay, L.E., Ikura, M., Tschudin, R., and Bax, A. 1990b. Three-dimensional triple-resonance NMR spectroscopy of isotopically enriched proteins. *J Magn Reson* 89: 496-514.
- Kowal, R.C., Herz, J, Goldstein, J. L., Esser, V., and Brown, M. S. 1989. Low density receptor-related protein mediates uptake of cholesteryl esters derived from apolipoprotein E-enriched lipoproteins. *Proc. Natl. Acad. Sci. USA* 86: 5810-5814.
- Lee, D., Walsh, J.D., Migliorini, M., P., Y., Cai, T., Schwieters, C.D., Krueger, S., Strickland, D.K., and Wang, Y.X. 2007. The structure of receptor-associated protein (RAP). *Protein Sci* 16: 1628-1640.
- Lipari, G., and Szabo, A. 1982. Model-free approach to the interpretation of nuclear magnetic resonance relaxation in macromolecules. 1. Theory and range of validity. *Journal of the American Chemistry Society* 104: 4546-4559.
- Lougheed, J.C., Domaille, P.J., and Handel, T.M. 2002. Solution structure and dynamics of melanoma inhibitory activity protein. *Journal of biomolecular NMR* 22: 211-223.
- Lund-Katz, S., Zaiou, M., Wehrli, S., Dhanasekaran, P., Baldwin, F., Weisgraber, K.H., and Phillips, M.C. 2000. Effects of lipid interaction on the lysine microenvironments in apolipoprotein E. *J Biol Chem* 275: 34459-34464.
- Neels, J.G., van den Berg, B.M.M., Lookene, A., Olivecrona, G., Pannekoek, H., and van Zonneveld, A.J. 1999. The second and fourth cluster of class A cysteine-rich repeats of the low density lipoprotein receptor-related protein share ligand binding properties. *J. Biol. Chem.* 274: 31305-31311.
- Nielsen, K.L., Holtet, T.L., Etzerodt, M., Moestrup, S.K., Gliemann, J., Sottrup-Jensen, L., and Thogersen, H.C. 1996. Identification of residues in alpha-macroglobulins important for binding to the alpha2-macroglobulin receptor/Low density lipoprotein receptor-related protein. *J Biol Chem* 271: 12909-12912.
- North, C.L., and Blacklow, S.C. 2000. Solution structure of the sixth LDL-A module of the LDL receptor. *Biochem J* 39: 2564-2571.
- Pitas, R.E., Innerarity, T.L., and Mahley, R.W. 1980. Cell surface receptor binding of phospholipids protein complexes containing different ratios of receptor-active and inactive E apoprotein. *J Biol Chem* 255: 5454-5460.

- Prévost, M., and Raussens, V. 2004. Apolipoprotein E-low density lipoprotein receptor binding: study of protein-protein interaction in rationally selected docked complexes. *Proteins*. 55: 874-884.
- Rall, S.C.J., Weisgraber, K.H., Innerarity, T.L., and Mahley, R.W. 1982. Structural basis for receptor binding heterogeneity of apolipoprotein E from type III hyperlipoproteinemic subjects. *Proc Natl Acad Sci* 79: 4696-4700.
- Raussens, V., Slupsky, C.M., Ryan, R.O., and Sykes, B.D. 2002. NMR structure and dynamics of a receptor-active apolipoprotein E peptide. *J Biol Chem* 277: 29172-29180.
- Raussens, V., Slupsky, C.M., Sykes, B.D., and Ryan, R.O. 2003. Lipid-bound structure of an apolipoprotein E-derived peptide. *J Biol Chem* 278: 25998-26006.
- Rieping, W., Habeck, M., Bardiaux, B., Bernard, A., Malliavin, T., E., and Nilges, M. 2007. ARIA2: automated NOE assignment and data integration in NMR structure calculation. *Bioinformatics* 23: 381-382.
- Rudenko, G., and Deisenhofer, J. 2003. The low-density lipoprotein receptor: ligands, debates and lore. *Curr Opin Struct Biol* 13: 683-689.
- Rudenko, G., Henry, L., Henderson, K., Ichtchenko, K., Brown, M.S., Goldstein, J.L., and Deisenhofer, J. 2002. Structure of the LDL receptor extracellular domain at endosomal pH. *Science* 298: 2353-2358.
- Ruiz, J., Kouliavskaja, D., Migliorini, M., Robinson, S., Saenko, E.L., Gorlatova, N., Li, D., Lawrence, D., Hyman, B.T., Weisgraber, K.H., et al. 2005. The apoE isoform binding properties of the VLDL receptor reveal marked differences from LRP and the LDL receptor. *J Lipid Res* 46: 1721-1731.
- Simonovic, M., Dolmer, K., Huang, W., Strickland, D. K., Volz, K., Gettins, P. G. W. 2001. Calcium Coordination and pH dependence of the calcium affinity of ligand-binding repeat CR7 from the LRP. Comparison with related domains from the LRP and the LDL receptor. *Biochemistry* 40: 15127-15134.
- Talluri, S., and Wagner, G. 1996. An Optimized 3D NOESY-HSQC. *J Magn Reson* 112: 200-205.
- Verdaguer, N., Fita, I., Reithmayer, M., Moser, R., and Blaas, D. 2004. X-ray structure of a minor group human rhinovirus bound to a fragment of its cellular receptor protein. *Nat Struct Mol Biol* 11: 429-434.

- Williams, S.E., Ashcom, J.D., Argraves, W.S., and Strickland, D.K. 1992. A novel mechanism for controlling the activity of alpha 2-macroglobulin receptor/low density lipoprotein receptor-related protein. Multiple regulatory sites for 39-kDa receptor-associated protein. *J Biol Chem* 267: 9035-9040.
- Willnow, T.E., and Moehring, J. M., Inocencio, N. M., Moehring, T. J., and Herz, J. 1996. The low-density-lipoprotein receptor-related protein (LRP) is processed by furin in vivo and in vitro. *Biochem. J.* 313: 71-76.
- Wilson, C., Wardell, M.R., Weisgraber, K.H., Mahley, R.W., and Agard, D.A. 1991. Three-dimensional structure of the LDL receptor-binding domain of human apolipoprotein E. *Science* 252: 1817-1822.
- Wishart, D.S., and Sykes, B.D. 1994. The ¹³C Chemical-Shift Index: A Simple Method for the Identification of Protein Secondary Structure Using ¹³C Chemical-Shift Data. *J Biomol NMR* 4: 171-180.
- Wishart, D.S., Sykes, B.D., and Richards, F.M. 1991. Relationship between Nuclear Magnetic Resonance Chemical Shift and Protein Secondary Structure. *J Mol Biol* 222: 311-333.
- Zuiderweg, E.R.P., McIntosh, L.P., Dahlquist, F.W., and Fesik, S.W. 1990. Three-dimensional carbon-13-resolved proton NOE spectroscopy of uniformly carbon-13-labeled proteins for the NMR assignment and structure determination of larger molecules. *J Magn Reson* 86: 210-216.

This chapter is in part, a reprint of a submitted manuscript in preparation title: How the ApoE Receptor Binding Sequence binds LRP; Structure of the minimal interface between ApoE and LRP. Guttman, M., Prieto, J.H., Croy, J.E., Ostrem, J., Komives, E.A. (2009) *manuscript in preparation*. The dissertation author was the primary researcher and author of this manuscript.

Chapter 5

Interactions of the NPXY microdomains of the LDL Receptor-Related Protein (LRP-1)

Introduction

The LDL receptor-related protein 1 (LRP1) is an integral membrane protein that carries out the internalization of a large number of proteins, protein complexes and lipoproteins including very low-density lipoproteins, chylomicron remnants, activated α_2 macroglobulin, and the amyloid precursor protein (Herz et al. 1988; Strickland and Ranganathan 2003). LRP1 plays a role in lipid transport, the uptake of protease-inhibitor complexes and has been implicated in Alzheimer's disease (Herz and Strickland 2001).

LRP1 is composed of an entirely extracellular α -chain of 3924 amino acids that is non-covalently linked to a β -chain of 601 amino acids that contains an extracellular region, a single transmembrane region, and a highly conserved cytoplasmic region composed of 100 amino acids including four tyrosine residues. Two of these, Tyr 4473 and Tyr 4507, are present in the context of Asn-Pro-X-Tyr (NPXY) motifs. The NPXY motif was first identified in the LDL receptor where it is essential for clathrin-mediated internalization (Bansal and Gierasch 1991). The CED-6/GULP protein involved in receptor trafficking has also been shown to bind LRP1 and the membrane-distal NPXY₄₅₀₇ motif was implicated in binding (Su et al. 2002). The NPXY₄₅₀₇ motif in LRP1 has been implicated in binding other PTB domain-containing intracellular signaling proteins such as ShcA, Fe65 and Disabled (Dab1) (Trommsdorff et al. 1998; Trommsdorff et al. 1999; Barnes et al. 2001). Yeast two hybrid analysis of the LRP1-CT found a number of proteins including several with PTB domains (Gotthardt et al. 2000). This study also found that LRP1-CT interacted with a homolog of PIP 4, 5 kinase

hinting of a broader role for LRP1, perhaps in assembling signaling complexes. Indeed, other members of the LRP family also play important roles as mediators of signal transduction (Kikuchi et al. 2007).

LRP1 is tyrosine phosphorylated in v-Src transformed mouse fibroblasts, and Tyr 4507, one of two NPXY tyrosines, was identified as the principle v-Src phosphorylation site in LRP1 (Barnes et al. 2001). Others have found that LRP1 is tyrosine phosphorylated in response to platelet-derived growth factor (Boucher et al. 2002). The ShcA PTB domain is known to bind to phosphorylated tyrosine residues present in the context of NPXY motifs, and has been shown to bind phosphorylated LRP1 (van der Geer et al. 1996; Barnes et al. 2001). We recently showed that phosphorylation of the two NPXY motifs in LRP1-CT is sequential. Phosphorylation of the membrane-distal NPXY₄₅₀₇ motif microdomain causes exposure of the membrane-proximal NPXY₄₄₇₃ motif microdomain which is then subsequently phosphorylated (Betts et al. 2008). In addition, tyrosine phosphorylation at NPXY₄₄₇₃ prevented binding of Snx17 and enhanced binding of Shp2, which has two SH2 domains that can each bind an NPXY motif (Betts et al. 2008). These observations led us to investigate whether other proteins might interact with the NPXY-containing microdomains of LRP1-CT and whether their binding might depend on tyrosine phosphorylation. Since experiments in which LRP1 is isolated from cells could not reveal which NPXY motif microdomain was the site of binding nor the phosphorylation dependence, we decided to prepare each NPXY motif microdomain separately in both

phosphorylated and unphosphorylated forms to discover specific protein-protein interactions that were occurring at each site.

Materials and Methods

Immobilization of LRP1-CT microdomains. The microdomains containing Tyr 4507 (Cys-amino aminohexanoic acid-TNFTNPVY₄₅₀₇ATLY) and Tyr 4473 (Cys-amino aminohexanoic acid-VEIGNPTY₄₄₇₃KMYEGGE) in both phosphorylated and unphosphorylated forms were synthesized and purified from AnaSpec, San Jose, CA. The peptides were immobilized using Sulfolink coupling gel according to the manufacturer's directions (Pierce, Rockford, IL). Due to poor solubility of the unphosphorylated peptides all immobilization reactions were carried out in 3.5M Guanidine HCl, TBS pH 8.0. The amount of peptide immobilized was quantified by UV absorbance. Efficiency of immobilization was found to be 1.5-2.5mg peptide per milliliter of beads.

To verify that peptides were correctly immobilized and accessible, 10 μ L of peptide beads were added to a 25 μ g/mL chymotrypsin solution in TBS pH 7.4 and agitated at room temperature for 2 hours. Resulting peptides were mixed 1:1 with alpha-cyano-cinnamic acid (Agilent). Analysis by MALDI-TOF on an Applied Biosystems DE-STR yielded m/z 1063.5 for NPXY₄₅₀₇ [(F)TNPVYATLY], 1143.4 for NPXpY₄₅₀₇ [(F)TNPVpYATLY], 813.3 for NPXY₄₄₇₃ [(Y)KMYGEEG], but not for NPXpY₄₄₇₃, since chymotrypsin did not cleave after phosphor-tyrosine. This showed that peptides were susceptible to proteases, thus exposed on the bead surface.

As a further control for specificity of binding, the immobilized NPXpY₄₅₀₇ microdomain (20 μ L of beads) was treated with 10U shrimp alkaline phosphatase (SAP) (Promega) at 37°C for 12 hours in TBS pH 9.0, 1mM MgCl₂. Non-phosphorylated NPXY₄₅₀₇ as well as NC beads were also treated with SAP the same way to rule out any other effects the phosphatase treatment may have on the beads.

Cell culture. Control and v-Src-transformed 14.30 and 14.30S3 mouse fibroblasts, and HEK293 cells were grown in Dulbecco's modified Eagle's medium containing 4 mM L-glutamine, 25 mM glucose and 10% calf serum at 37°C in 10% CO₂ until confluent and then starved for 12 hours in serum free medium. MEF cells were obtained from ATCC (Manassas, VA) and grown in Dulbecco's modified Eagle's medium containing 4 mM L-glutamine, 25 mM glucose and 10% fetal bovine serum at 37°C in 10% CO₂. The 11H4 hybridoma was obtained from ATTC (Manassas, VA) and grown in Iscoves-modified Dulbecco's medium containing 25 mM L-glutamine and 10% FBS at 37°C in 10% CO₂.

Preparation of rat brain lysates. Brains of 3 month old Long Evans rats were resuspended in PLC lysis buffer (50 mM Hepes pH 7.5, 150 mM NaCl, 10% glycerol, 1% Triton X100, 1.5 mM MgCl₂, 1 mM EGTA, 100 mM NaF, 10 mM Sodium Pyrophosphate, 500 μ M Sodium Vanadate, 1 mM PMSF, 2 mM DTT, with protease inhibitor cocktail (P8340, Sigma-Aldrich) (1 brain in 10 ml) by

Dounce homogenization. Lysates were cleared by high-speed centrifugation and incubated batch-wise with immobilized peptides (20 μ L) at 4°C on a rocker for 2 hrs. The beads were washed four times with PLC-lysis buffer, and bound proteins were analyzed by SDS-PAGE.

In-gel digestion. The proteins that bound to the NPXpY₄₅₀₇ microdomain were separated by 1-D SDS-PAGE using 10% Bis-Tris NuPAGE gels (Invitrogen). Gels were stained overnight with Gel Code Blue (Pierce) according to manufacturer's suggested protocol. Bands unique to the NPXpY₄₅₀₇ -bound sample were excised, washed twice with 200 μ L of 50% acetonitrile (ACN) and 50% 5 mM DTT / 25 mM NH₄HCO₃ (pH 7.4), reduced in 100mM DTT for 30 minutes at 50°C, washed again, and subsequently alkylated with 100mM iodoacetamide. The gel pieces were dehydrated in pure ACN, rehydrated by addition of 20 μ L of ice-cold 10 ng/ μ L trypsin (Promega) in 25 mM NH₄HCO₃ (pH 7.4), incubated on ice for 30 min and the remaining trypsin solution was removed and replaced with fresh 25 mM NH₄HCO₃ (pH 7.4). The digestion was allowed to continue at 37°C overnight. The peptide mixture was then acidified with 2 μ L of 2% trifluoroacetic acid (TFA) (Fluka) and 2 μ L of acetonitrile, vortexed for 30 min, and the supernatant extracted. Finally, 20 μ L of 20% acetonitrile/ 0.1% TFA was added followed by vortexing to extract the remaining peptides and combined with the previous fraction. The combined extractions were concentrated in a speedvac prior to mass spectrometry.

In solution digestion. Rat brain lysates (3 mls) were cleared by high-speed centrifugation and incubated batch-wise with immobilized peptides (35 μ L) at 4°C on a rocker for 2 hrs. After washing as before, the beads were washed twice with TBS 2mM EDTA, pH 8.0, then resuspended in the same buffer with 0.5% Rapigest[®] (Waters), and boiled for 10 min to elute bound proteins. The mixture was treated with 3mM TCEP (Sigma) for 30 min, then 6mM iodoacetamide (Sigma) for 30 min, and finally quenched with another 3mM TCEP. Freshly dissolved proteomics grade trypsin (10 μ g, Roche), was added to each sample, and digestion was carried out overnight at 37°C. The digestion was stopped with the addition of 100mM HCl, and incubated at 37°C for 1 hr to breakdown the Rapigest[®]. Samples were then centrifuged for 30 min at 4°C to remove beads and insoluble degraded lipid. Resulting peptides were extracted via C18 solid phase extraction (Varian, A57203) according to manufacturer's suggested protocol, and concentrated by speedvac prior to MS analysis.

Mass spectrometry. Digested samples were analyzed by electrospray ionization using a QSTAR-Elite hybrid mass spectrometer (Applied Biosystems) interfaced to a capillary column (180 μ m ID, 365 μ mOD) packed with C18 and capped with 0.2 mm filters on either end connected via 4 cm 25 ID (365 μ m OD) capillary to the nanospray source. The spray needle was a pulled capillary 180~15 tip packed with C18. One dimensional chromatography was used for the samples from in-gel digests, whereas 2-dimensional "MUDPIT" chromatography was used for the in solution digests. For 2D chromatography, a strong cation

exchange column was inserted in between the autosampler and injector valve. To accomplish the 2D chromatographic separation, the TEMPO LC high flow rate Channel 1 (10 μ l/min) was used to load and separate on the SCX column with buffers A: 2.5%ACN, 0.2 % TFA 0.005%TFA; and Channel 1 B: 500mM ammonium acetate, 5%ACN, 0.2 % TFA. To separate on the C18 reverse phase, the low flow rate Channel 2 (400 nl/min flow) with buffer A: 2.5%ACN, 0.2 %FA 0.005%TFA and Channel 2 B: 100%ACN, 0.2 %FA 0.005%TFA was used. MUDPIT runs were carried out as described previously (Wolters et al. 2001) with an 8 step ion exchange elution. Each was then separated on a 35-min linear gradient from 5 to 40% buffer B at a flow rate of 400 nL/min. LCMSMS data were acquired in a data-dependent fashion by selecting the 4 most intense peaks with charge state 2-4 that exceeded 10 counts with exclusion of former target ions set to "always" and the mass tolerance for exclusion set to 100 ppm. TOF MS were acquired at m/z 400-1600 Da for 1 sec with 20 time bins to sum. MSMS spectra were acquired from m/z 65 – 2000 Da using "enhance all" and 20 time bins to sum, Dynamic Background Subtract, Automatic Collision Energy, and Automatic MS/MS Accumulation with the Fragment Intensity Multiplier set to 4 and Maximum Accumulation set to 2 sec before exiting the scan.

Database search. Data were analyzed by Analyst 2.0 (Applied Biosystems) and subjected to two different database search protocols. First, spectra were searched with Protein Pilot using the paragon algorithm (Shilov et al. 2007) against both the rat database alone (*Rattus norvegicus*, ncbi

07/06/2006, ftp://ftp.ncbi.nih.gov/genomes/R_norvegicus/protein/) as well as the non-redundant swissprot database (swissprot 10/29/2008, ftp://ftp.ncbi.nih.gov/blast/db/FASTA/). Search parameters included fixed carboxymethyl modification of cysteines and included common forms of variable modifications. Only protein hits with at least 2 strong unique peptide matches (>95) were kept. Any hits in the negative control were subtracted from the other samples. The spectra were also searched using Mascot 2.2.1 (Matrix Science) with Mascot Daemon 2.2 (Matrix Science) data import filter parameters set as follows: default precursor charge state 2-4; precursor and MSMS data centroiding using 50% height and 0.05 amu merge distances. MSMS peaks with intensity less than 1% of the base peak were discarded, as were MSMS spectra with less than 22 peaks remaining. Data were searched against the Swissprot database obtained at ftp://ftp.ncbi.nlm.nih.gov/blast/db/FASTA/ containing 237,168 sequences. The search identified tryptic peptides with up to 2 missed cleavages and used mass tolerances of 100 ppm (MS) and 0.10 Da (MSMS), with variable modifications as follows: deamidation (NQ), oxidation (M), pyro-Glu (N-term E). The search results indicated that individual ion scores > 42 indicate identity or extensive homology ($P < 0.05$). Numbers of peptides reported are for non-redundant peptides. MASCOT and Protein Pilot both identified the same proteins, so the data from Protein Pilot are presented. The data is available in the PRIDE database (Martens et al. 2005) (www.ebi.ac.uk/pride) under accession numbers 9944-9949. The data was converted using PRIDE Converter (Barsnes et al. 2009) (<http://code.google.com/p/pride-converter>).

Common contaminants including keratin, trypsin, and tubulin were omitted from the final table. Results for each microdomain were compared to the results without immobilized peptide and only those proteins that were not observed in the negative control were considered “real”. This criteria resulted in 14/39 “real” hits for the NPXpY₄₅₀₇ microdomain, 31/80 “real” hits for the NPXY₄₅₀₇ microdomain, 3/23 “real” hits for the NPXpY₄₄₇₃ microdomain, and no “real” hits for the NPXY₄₄₇₃ microdomain. All protein-protein interaction data has been submitted to the DIP database (<http://dip.doe-mbi.ucla.edu>) and assigned IMEx identifier IM-11705.

Antisera, immunoprecipitation, and immunoblotting. A polyclonal anti-Shp-2 serum was raised against a GST fusion protein containing both SH2 domains. The same technique was used to generate polyclonal anti-Grb2, anti-ShcA, and anti-CSK. a polyclonal anti-LRP1 serum was raised against a GST-fusion protein containing the cytoplasmic domain. Anti-phosphotyrosine monoclonal antibody 4G10, polyclonal anti-p85 PI3K serum, anti-HA (12CA5) and anti-Fe65 (3H6) were purchased from Upstate (Charlottesville, VA). Anti-PLC γ and anti-GAPDH (14C10) were purchased from Cell Signaling Technologies (Danvers, MA). Anti-Crkl (SC-31694) was purchased from Santa Cruz Biotechnology, Inc. (Santa Cruz, CA). Anti-Src monoclonal antibody 327 was a gift from Dr. T. Hunter (La Jolla, CA). Anti-14-3-3 (57-0700), anti-Ubiquitin (13-1600) and anti-CamK2B (13-9800) were purchased from Zymed (Carlsbad, CA). Anti-GST antibody (27457701) was from GE Healthcare.

Immunoprecipitation and immunoblotting were carried out exactly as described previously (Barnes et al. 2001), with the exception of Ubiquitin blots which were autoclaved for 20 minutes after transfer for increased sensitivity (Mimnaugh EG 1999).

Recombinant protein expression and purification. GST tagged SH2 domains from human Grb2 (58-159), PLC γ -1 (“N” 544-659 & “C” 663-759), and PI3K (“N” 314-446 & “C” 614-724) and full length 14-3-3 γ (genbank ID 21464100) were cloned into pGEX2T (GE Healthcare) using BamH1 and EcoR1 restriction sites. BL21-DE3 cells were grown to OD₆₀₀ 0.5 at 37°C and protein expression induced with 0.3mM IPTG at 18°C overnight. Cells were harvested by centrifugation, resuspended in 50mM Tris pH 8.0, 500mM NaCl, 1mM DTT, and 1mM PMSF (Sigma) and lysed by sonication. After clearing debris by centrifugation at 12krpm for 40 min, cell extract was loaded over Glutathione-sepharose (GE Biosciences) according to manufacturer’s instructions. Eluted protein was buffer exchanged and concentrated over Y10K centricon (Millipore). 14-3-3 γ was also cloned into pET15 with an N-terminal His tag, and purified by Nickel affinity chromatography followed by gel filtration. Recombinant purified His tagged CSK was a gift from Patricia Jennings. His-tagged CamKII β was purchased from Sigma. Purified calmodulin was purchased from Millipore. SH2 domains of Shp-2 and HA tagged Snx17 were expressed and purified as previously described (Betts et al. 2008). For recombinant pulldown reactions 10 μ L of NPXY beads were incubated in a 100nM solution of protein in the same

PLC-lysis buffer used for previous pulldowns except for CamKII β which contained 50nM CamKII β and 200nM Calmodulin. Reactions were washed and blotted as described for samples of rat brain lysates.

Results

LRP1 co-immunoprecipitates with tyrosine phosphorylated proteins in v-Src transformed fibroblasts. Several groups have shown that LRP1 can become phosphorylated on Tyr in the distal NPXY₄₅₀₇ motif by activated protein-tyrosine kinases (Barnes et al. 2001, Barnes, 2003 #17; Loukinova et al. 2002). Association of LRP1-CT with “signaling” proteins such as Shp2 and Src has also been demonstrated (Barnes et al. 2001). These observations led us to hypothesize that other proteins may also bind to LRP1 in a phosphorylation dependent manner.

To find out whether LRP1 is involved in multiple phosphotyrosine-dependent protein-protein interactions, LRP1 was isolated by immunoprecipitation from control and v-Src transformed fibroblasts and the immunoprecipitate was analyzed by anti-P.Tyr immunoblotting. The results show LRP1 is associated with several P.Tyr-containing proteins in v-Src transformed cells (Fig. 5.1A). A significant increase in these interactions was observed when cells were treated with protein tyrosine phosphatase inhibitors orthovanadate and hydrogen peroxide (Fig. 5.1A).

Because tyrosine phosphorylation sites can act as docking sites for other proteins we asked whether any of the proteins that coimmunoprecipitate with

LRP1 require Tyr 4507 phosphorylation for binding. The NPXpY₄₅₀₇ microdomain was prepared and immobilized on agarose beads (TNFTNPV(pY₄₅₀₇)ATLY). This immobilized microdomain was first used to probe for binding proteins v-Src transformed fibroblasts (Fig. 5.1B). The results again showed a number of tyrosine-phosphorylated proteins were specifically binding to the microdomain.

LRP1(NPXY)-interacting proteins in the brain. Because LRP1 is highly expressed in the mammalian brain, we sought to find out whether these interactions were only found in v-Src transformed fibroblasts, or whether they were also present in brain tissue. Figure 5.2 shows that a similarly large number of proteins were found to bind specifically to the phosphorylated microdomain when rat brain lysates were probed. The bands corresponding to proteins binding specifically to the NPXpY₄₅₀₇ microdomain were excised and the proteins were identified by LC-MSMS sequencing (Table 5.1). A large number of signaling proteins were found to bind specifically to this microdomain in its phosphorylated form.

To better characterize the phosphorylation dependence of the NPXY microdomains, the four microdomains were prepared and analyzed simultaneously; the NPXY₄₄₇₃ microdomain, NPXpY₄₄₇₃ microdomain, NPXY₄₅₀₇ microdomain, and NPXpY₄₅₀₇ microdomain. Anti-P.Tyr blotting of the bound proteins showed a smear of tyrosine phosphorylated proteins binding to the phosphorylated NPXY₄₅₀₇ and NPXY₄₄₇₃, but not to the unphosphorylated forms

(Fig. 5.3A). To detect all proteins interacting with these peptides the bound proteins were analyzed by silver staining (Fig. 5.3B). It was evident that while the NPXY₄₄₇₃ microdomain did not seem to have many specifically bound proteins, the NPXY₄₅₀₇ microdomain had a large number of specific interactions.

To ensure the differences observed between NPXpY₄₅₀₇ and NPXY₄₅₀₇ were not the result of anything other than phosphorylation, NPXpY₄₅₀₇ beads were treated with shrimp alkaline phosphatase. The resulting silver stained gels showed that removal of the phosphate from NPXY₄₅₀₇ yields a binding profile identical to unphosphorylated NPXY₄₅₀₇ (Fig. 5.4).

Proteins bound to each NPXY motif were eluted and analyzed by in solution trypsin digest followed by 2D LC-MSMS. Proteins with at least two strong (>95 confidence) unique peptide hits are listed in Tables 5.2-5.4. The phosphorylated membrane distal NPXY₄₅₀₇ microdomain showed dozens of strong protein interactions (Table 5.2) whereas the phosphorylated membrane proximal NPXY₄₄₇₃ microdomain had very few (Table 5.3). Besides Grb-2 and Shc-3, both of which were also found in the NPXpY₄₅₀₇ sample, the only protein identified as interacting specifically with NPXpY₄₄₇₃ was peptidyl-prolyl cis-trans isomerase A (Table 5.3). The unphosphorylated NPXY₄₅₀₇ microdomain also bound many more proteins (Table 5.4) than the unphosphorylated NPXY₄₄₇₃, which had no protein hits that were not also found in the negative control. A few of the proteins that were observed in the in gel digest analysis of the phosphorylated NPXY₄₅₀₇ interacted more strongly with the unphosphorylated NPXY₄₅₀₇ microdomain. The most likely explanation of these results is that some

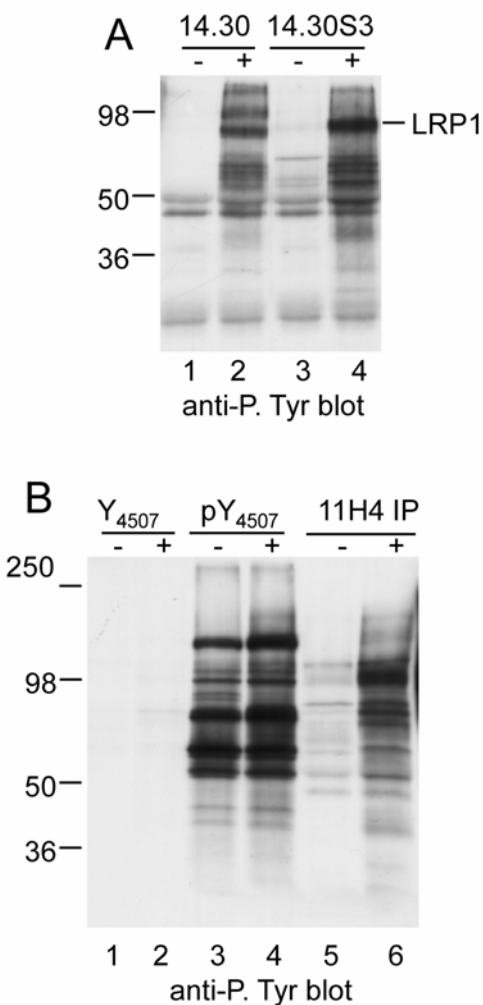


Figure 5.1: A) LRP1 was isolated by immunoprecipitation from control (-) or vanadate/hydrogen peroxide treated (+) 14.30 and v-Src transformed (14.30S3) mouse fibroblasts. Immunoprecipitates were analyzed by anti-P.Tyr immunoblotting. B) Lysates from control or vanadate/hydrogen peroxide treated fibroblasts were incubated with agarose beads containing phosphorylated or unphosphorylated NPXY₄₅₀₇ microdomains. Bound proteins were analyzed by anti-P.Tyr immunoblotting. Anti-LRP1 immunoprecipitates were analyzed in parallel.

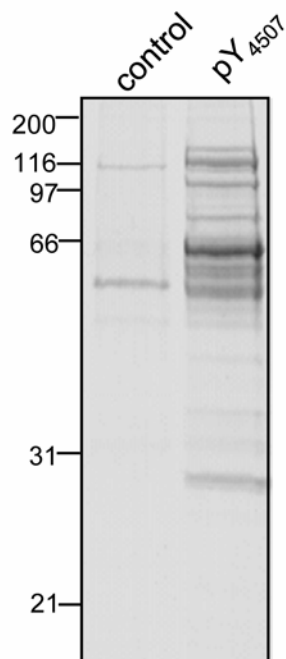


Figure 5.2: Rat brain extracts were incubated with either unreacted agarose beads or the phosphorylated NPXY₄₅₀₇ microdomain linked to agarose beads. Bound proteins were analyzed by Gelcode blue staining. Individual protein bands were isolated and identified by mass spectrometry and data-base searching.

dephosphorylation of the microdomain occurred during the experiment prior to in gel digestion.

Western blotting confirmation of binding interactions. To confirm the binding of several of the identified proteins to the microdomains of LRP1, bound proteins were resolved by SDS-PAGE, transferred to PVDF membranes and analyzed by immunoblotting. This experiment confirmed that PI3-kinase, Shp-2, PLC- γ , Src, CSK, Shc-3, and Grb-2, present in lysates of rat brains are able to bind to the NPXpY₄₅₀₇ microdomain (Fig. 5.5). As expected from the mass spectrometry data, Shc-3 and Grb2 were found to interact with the NPXpY₄₄₇₃ microdomain also. GAPDH and 14-3-3 γ can bind to the non phosphorylated NPXY₄₅₀₇. In agreement with our mass spectrometry data, CamKII seems to bind preferentially to unphosphorylated NPXY₄₅₀₇ microdomain with a weaker signal in the NPXpY₄₅₀₇ microdomain lane.

A few expected binding interactions were not observed in our mass spectrometry experiments, and these were also probed by Western blotting. Fe65 had previously been reported to interact with LRP at the NPXY motifs (Pietrzik et al. 2004), but was not identified in our study. Blotting of the NPXY-bound proteins for Fe65 revealed that indeed, it could bind to both the phosphorylated and unphosphorylated NPXY₄₅₀₇ microdomains. We and others had previously shown that Sorting nexin 17 (Snx17) bound LRP1-CT and that this binding depended on the presence of the NPXY₄₄₇₃ motif (van Kerkhof et al. 2005; Betts et al. 2008). Figure 5.6 shows that recombinant HA tagged Snx17

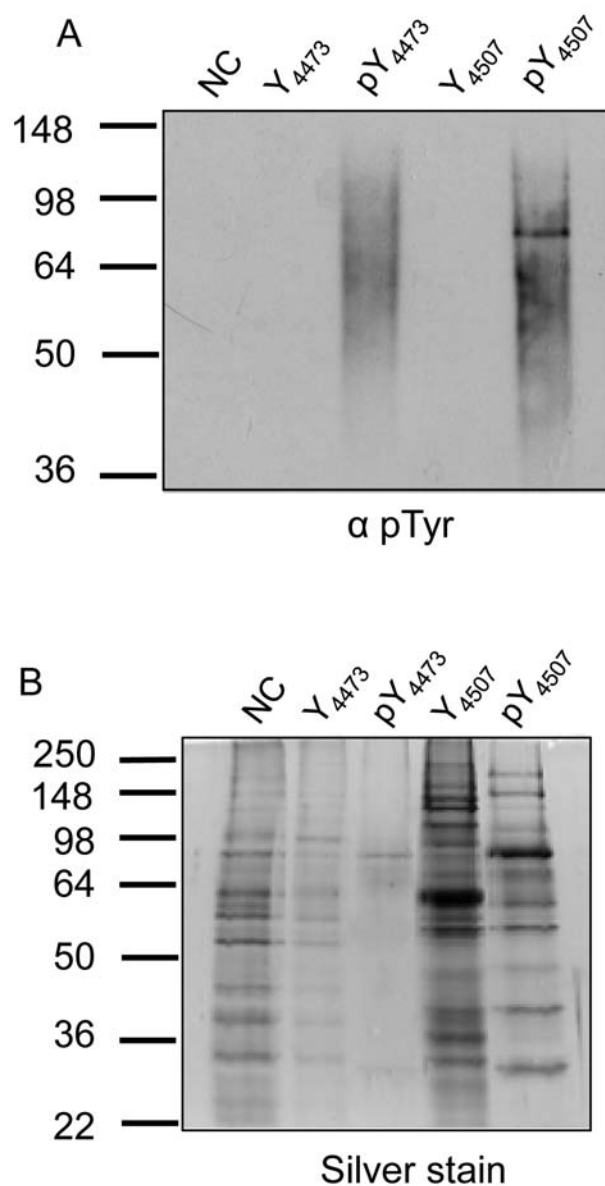


Figure 5.3: Rat brain extracts were incubated with the each microdomain linked to agarose beads. The sequences were: NC uncoupled beads, Y₄₄₇₃ VEIGNPTYKMYEGGE, pY₄₄₇₃ VEIGNPTpYKMYEGGE, Y₄₅₀₇ TNFTNPVYATLY, and pY₄₅₀₇ TNFTNPVpYATLY. Bound proteins were analyzed by (A) anti-phosphotyrosine blotting or (B) silver staining.

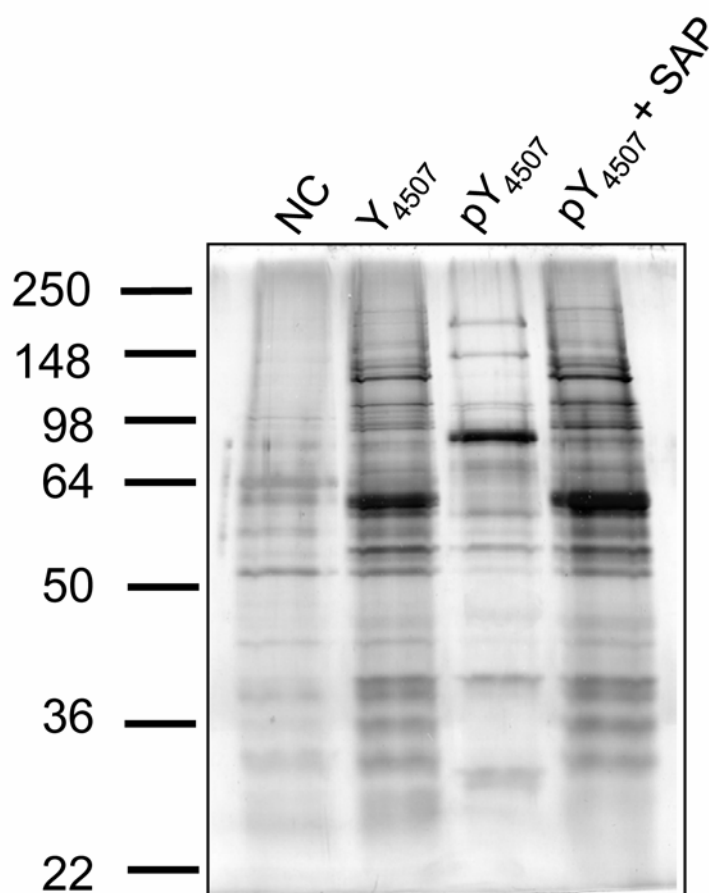


Figure 5.4: To ascertain whether the differences between the phosphorylated and unphosphorylated NPXY₄₅₀₇ microdomains was due purely to the tyrosine phosphorylation, NPXpY₄₅₀₇ and NPXY₄₅₀₇ beads were treated extensively with Shrimp alkaline phosphatase, and subsequently used to probe rat brain lysates, along with untreated pY₄₅₀₇. Samples were visualized by silver staining.

binds both the unphosphorylated NPXY₄₄₇₃ and the unphosphorylated NPXY₄₅₀₇ motif. These results recapitulate our previous finding in v-Src transformed fibroblasts in which phosphorylation inhibited Snx17 binding, but add an additional finding that Snx17 binds to both of the NPXY motifs in LRP1-CT. It is not too surprising that Snx17 and FE65 were not observed in the proteomics analysis as we have observed low abundance of these proteins in our rodent lysates (Betts et al. 2008).

Assessment of which proteins bind directly to LRP1-CT. Given the large number of proteins that were observed to bind to the NPXY₄₅₀₇ microdomain, it was possible that most of the interactions were indirect and that the proteins were bound in some sort of large signaling complex. To test for direct interactions, recombinant proteins were prepared and probed for binding to the NPXY microdomains. These experiments revealed that 14-3-3 γ reproducibly interacts with only the NPXY₄₅₀₇ microdomain in either a GST tagged or a His-tagged construct (Fig. 5.6). All SH2 domains from PLC γ , Grb-2, PI3K, Shp-2, and full length CSK were also tested either with a GST or His₈-Ubiquitin tag. These experiments revealed that certain SH2 domains can bind both phosphorylated NPXY₄₄₇₃ and NPXY₄₅₀₇ motifs, and others only bind avidly to NPXpY₄₅₀₇ (Fig. 5.6). Recombinant CamKII β was able to bind to both phosphorylated and non-phosphorylated NPXY₄₅₀₇.

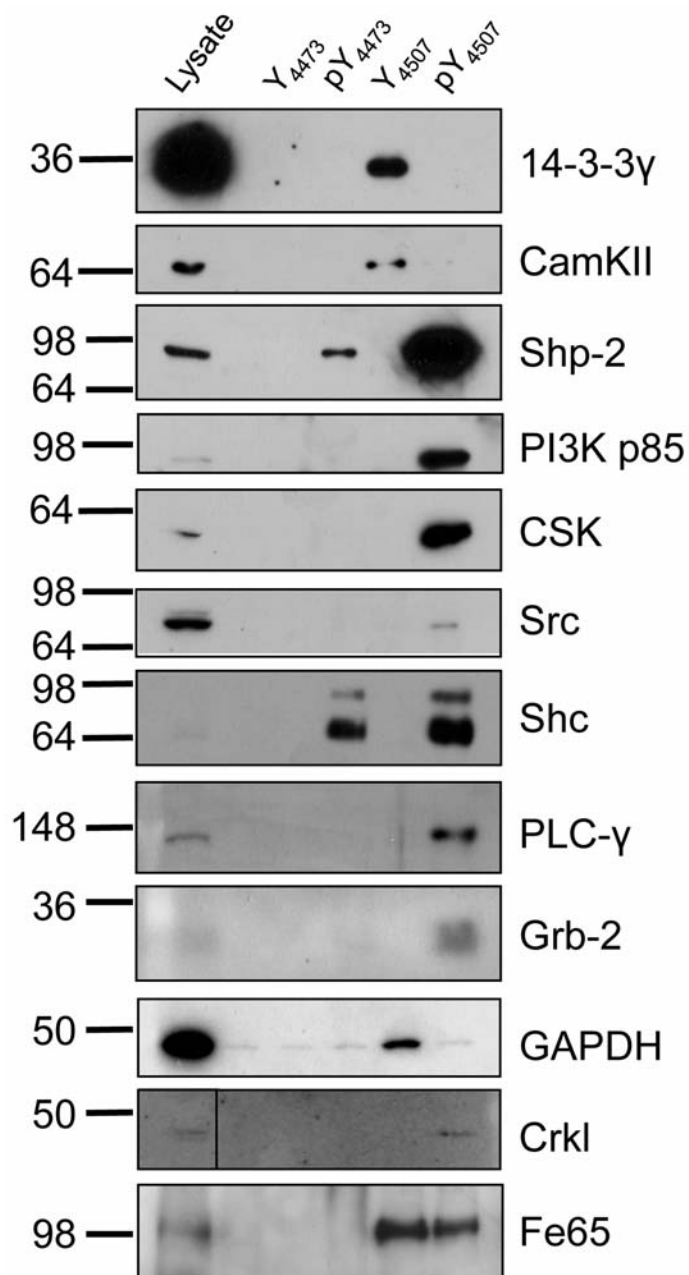


Figure 5.5: Rat brain extracts were incubated with each immobilized peptide. Bound proteins were analyzed by immunoblotting with antisera raised against 14-3-3 γ , CamKII, Shp-2, PI3K p85, CSK, Src, N-Shc, PLC γ , Grb-2, GAPDH, Crkl, and Fe65.

One of the most abundant proteins that bound to the NPXpY₄₅₀₇ motif microdomain was identified as Shp-2. Since previous studies have shown that Shp-2 can interact with both phosphorylated NPXY₄₄₇₃ and NPXY₄₅₀₇ of LRP (Betts et al. 2008), we used recombinant SH2(N) or SH2(C) domains of Shp-2 fused to ubiquitin to test for direct binding to each NPXY motif. Consistent with our previous results, the NPXpY₄₅₀₇ is the high-affinity binding site (Fig. 5.6). Only on much longer exposures could a band for SH2(C) be detected in the NPXpY₄₄₇₃ lane (data not shown).

Discussion

The LRP1-CT NPXY₄₅₀₇ microdomain may be a signaling “hub”. The LRP1 cytoplasmic domain has been implicated by association in cell signaling. We originally identified LRP1 as a Shc-binding protein (Barnes et al. 2001), and later it was also shown to bind several PTB domain-containing proteins including disabled (Dab1) (Trommsdorff et al. 1999), and by yeast-two-hybrid studies JIP-1 and -2, CAPON, and a PIP4 kinase homolog among others (Gotthardt et al. 2000). In addition, it interacts with the PDGF receptor- δ (Newton et al. 2005), is phosphorylated in response to PDGFR ligand binding (Boucher et al. 2002), and is at least sometimes localized to lipid rafts (Wu and Gonias 2005). It also binds Shp2 only in the phosphorylated form, and Snx17 only in the unphosphorylated form (Betts et al. 2008). These results were the impetus for the studies presented here, in which the two NPXY microdomains and their phosphorylated

counterparts were separately analyzed for protein binding interactions in rodent brain lysates.

The only way to separately isolate such microdomains and to obtain them in pure form (either phosphorylated or unphosphorylated) is to prepare them synthetically. Previous work has shown that this approach is effective for identifying proteins that bind to NPXY motifs and in particular to probe the dependence of binding on tyrosine phosphorylation (Wilhelmsen et al. 2004; Smith et al. 2006). This approach led to the identification of a variety of proteins that bind specifically to the phosphorylated or unphosphorylated NPXY microdomains of LRP1-CT. In some cases the binding depended strongly on phosphorylation state, as previously seen with peptide array studies with NPXY motifs (Smith et al. 2006). Based on our findings the NPXY₄₄₇₃ has very few detectable binding partners, while the NPXY₄₅₀₇ had many direct interactions both in the phosphorylated and unphosphorylated states. It should be noted that the NPXpY₄₄₇₃ microdomain serves as an important specificity control. The proteins observed to bind to the NPXpY₄₅₀₇ microdomain must be recognizing more than just the NPXpY sequence, or they would have also been observed to bind to the NPXpY₄₄₇₃ microdomain. Of all the signaling proteins that bound to the distal NPXpY₄₅₀₇ microdomain, only Shc3 and Grb2 bound also to the NPXpY₄₄₇₃ microdomain.

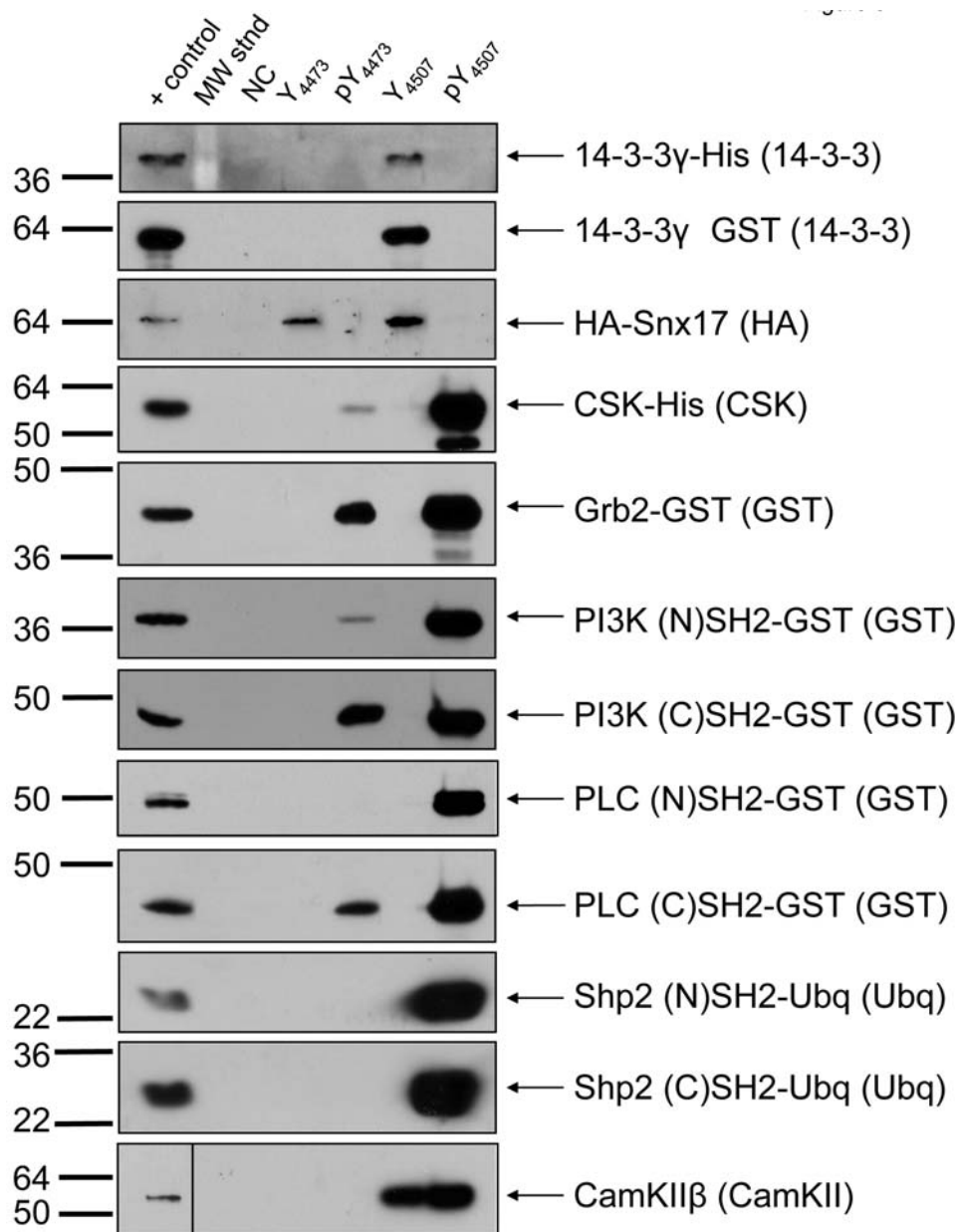


Figure 5.6: Purified recombinant proteins were incubated with each immobilized peptide. Bound proteins were analyzed by immunoblotting with anti-HA (Snx17), anti-GST (SH2's from Grb2, PLC γ , PI3K p85), anti-14-3-3 γ , anti-Ubiquitin (Shp2 SH2s), anti-CSK, and anti CamKII β .

Many of the signaling proteins bound to the phosphorylated form of the LRP1 NPXY₄₅₀₇ microdomain including PLC γ , PI 3-kinase, Shp-1, Shp-2, Src, Fyn, ShcC and CrkL, are proteins that are recruited to the plasma membrane and are tyrosine phosphorylated in response to extracellular signals (Anderson et al. 1990; Kazlauskas et al. 1992; Twamley et al. 1992; Keilhack et al. 1998; Kozlowski et al. 1998; Ronnstrand et al. 1999; Sakkab et al. 2000; Liu and Meakin 2002). Aside from Shp-2, these are all previously unreported interactions, and identification of these proteins as potential LRP1 binding proteins further substantiates the model in which LRP1 functions as a signaling receptor. The finding that CamKII binds both NPXY₄₅₀₇ and NPXpY₄₅₀₇ microdomains gives yet more support for the role of LRP1 in signaling. Meaningful co-localization experiments will require introduction of mutant forms of the LRP1-CT at endogenous levels under controlled phosphorylation conditions. These are quite challenging experiments and were outside the scope of the current project.

Several independent studies have found that the adaptor protein ShcA binds to tyrosine phosphorylated LRP1. In the current study we have identified Shc-3 (ShcC) as an LRP1 binding protein in rat brain lysates. ShcC is a Shc family member that is specifically expressed in the brain (O'Bryan et al. 1996; Liu and Meakin 2002; Ponti et al. 2005). It is well established that all Shc family members contain an amino-terminal PTB domain that binds to phosphorylated NPXY motifs. In the case of LRP1 it seems that both NPXY motifs in their phosphorylated forms can interact with ShcC.

Shp-2 is a protein-tyrosine phosphatase that contains two SH2 domains followed by a phosphatase domain. We have found that Shp-2 strongly binds to the NPXpY₄₅₀₇ motif and have confirmed that it also binds the phosphorylated LRP1 cytoplasmic domain (Betts et al. 2008). This is consistent with the fact that the amino-terminal SH2 domain of Shp-2 binds to phosphorylated tyrosine residues followed by non-polar residues at +1, +3 and +5 (Lee et al. 1994). This consensus is matched exactly by the sequence carboxy-terminal to NPXY₄₅₀₇, but not in NPXY₄₄₇₃ which has a much weaker apparent affinity for Shp2. The result that phosphorylated NPXY₄₄₇₃ can bind Shp-2 with weaker affinity agrees with previous results (Betts et al. 2008). The observation that Shp2 bound so strongly to the immobilized NPXpY₄₅₀₇ microdomain is most likely due to the fact that Shp2 has two SH2 domains, which can simultaneously engage the multiple copies of the microdomain that are available when it is immobilized. This phenomenon could also be occurring for the other proteins with multiple binding sites.

Both LRP1-CT NPXY microdomains may be involved in receptor sorting.

The unphosphorylated NPXY₄₅₀₇ microdomain specifically bound AP-2 adaptors and clathrin as well as many “house-keeping” and metabolic proteins (Table 5.3). These interactions were specific for the unphosphorylated microdomain and were not observed with the phosphorylated microdomain. These results show how phosphorylation is likely to affect receptor internalization and sorting. Indeed, such an effect has been previously observed in cells in which stimulation of

PDGFR causes changes in LRP1 phosphorylation and subsequent internalization of both proteins (Takayama et al. 2005).

In the course of this study nothing was found specifically interacting with NPXY₄₄₇₃ which was surprising. The peptide was clearly immobilized based on UV follow up of the immobilization and chymotryptic digestion of the beads. Since Snx17 was previously shown to interact with this region of the LRP1-CT (van Kerkhof et al. 2005; Betts et al. 2008), recombinant Snx17 was tested for binding with all four of the microdomains. In these experiments, specific binding to both NPXY₄₄₇₃ and NXPY₄₅₀₇ was observed. It is possible that in previous studies the NPXY₄₅₀₇ region was in a phosphorylated form thus unable to interact with Snx17, as we reported previously and observed again here (Betts et al. 2008). At the very least this demonstrates that NPXY₄₄₇₃ could have specific interactions in the brain, just below our detection limit in this study.

Connection between LRP1 and APP. Several lines of evidence have implicated LRP1 in the development of Alzheimer's disease. APP, the amyloid precursor protein, binds directly to LRP1 (Kounnas et al. 1995). In addition, it has been shown that A β constituent of amyloid plaques, can bind to α_2 M and ApoE; both of which are also ligands for LRP1 (Kang et al. 2000). Genetic evidence shows increased presence of certain alleles of LRP1, α_2 M and ApoE in Alzheimer's disease patients (Corder et al. 1993; Kang et al. 1997; Blacker et al. 1998). Thus it is generally thought that LRP1's involvement in Alzheimer's disease is related to its ability to interact directly or indirectly with APP or A β .

The proteins newly identified to bind to LRP1-CT microdomains in this study are peculiarly interesting when combined with recent findings that residues 4504-4510 of LRP affect APP processing and A β generation (Pietrzik et al. 2002; Yoon et al. 2005). Therefore these interactions at the NPXY₄₅₀₇ site could play a role in A β generation and thus the onset of Alzheimer's disease. Recent RNAi experiments provide a functional link between Shc and APP processing (Xie et al. 2007). It has also been shown that APP can become phosphorylated on Y682 which can then interact with ShcA and ShcC. (Tarr et al. 2002) although it was later found that phosphorylation of APP was not the underlying cause of its processing (Minopoli et al. 2007). The same study also showed that APP processing is affected by several tyrosine kinases including Src, and that the effects are dependent on the presence of LRP (Minopoli et al. 2007). Fluorescence lifetime imaging microscopy showed that APP and LRP are co-localized regardless of tyrosine phosphorylation of LRP (Peltan et al. 2006). Thus, LRP's affect on APP trafficking is probably best explained by LRP recruiting these signaling molecules to APP.

The specific interaction of NXPY₄₅₀₇ with 14-3-3 proteins provides another link between LRP1 and APP in the light of recent evidence that APP interacts with 14-3-3 γ (Sumioka et al. 2005). Fe65 is another adaptor protein that has been shown to interact with both APP and LRP, and modulate A β generation (Pietrzik et al. 2004). Fe65 from rat brains interacted only at the NPXY₄₅₀₇ in both phosphorylation states. This is in clear agreement that only the distal NPXY motif

was shown to have effects on APP trafficking and A β generation (Pietrzik et al. 2002).

The results described here identify several kinases that can bind to LRP1 including; CamKII, Src, Fyn, and CSK. Interestingly, CaM kinase II (Yamamoto et al. 2002; Sengupta et al. 2006) and Src family kinases (Lee et al. 1998; Williamson et al. 2002; Lee et al. 2004) have been implicated previously in Tau phosphorylation. These observations suggest that LRP1 could also be involved in linking APP and A β to Tau hyperphosphorylation, although this conjecture will need to be studied in much more detail.

Table 5.1: LRP1 NPXpY₄₅₀₇ interacting proteins identified by in-gel digest/LC-MSMS

Protein (Peps (>95)) Accession number	Sequence Coverage	# unique of
Shp-2 gi 84028250	41%	27
PLC-gamma 1 gi 6981370	15%	20
Son of sevenless homolog 1 gi 162287023	14%	16
pyrroline-5-carboxylate reductase family 2 gi 58865992	51%	17
growth factor receptor bound protein 2 (GRB2) gi 77539774	58%	13
CAM kinase II beta subunit gi 108796657	27%	12
Shc-3 (neuronal Shc) gi 48474721	23%	11
Tnf receptor-associated factor 3 gi 157823541	21%	11
PI3-kinase, regulatory subunit, (p85 alpha) gi 6981358	16%	9
v-crk sarcoma virus CT10 oncogene homolog gi 56605658	25%	7
megakaryocyte-associated tyrosine kinase gi 11177904	20%	7
PI3-kinase p110 subunit alpha (isoform 1-3) gi 109466432, gi 109466430, gi 109466434	8%	7*
casein kinase 1, delta gi 158631200	20%	7
LanC lantibiotic synthetase component C-like 2 gi 62079109	18%	6
Shp-1 gi 16758788	12%	5
inositol polyphosphate-5-phosphatase D gi 9506813	5%	5
casein kinase 1, alpha 1 gi 16758950	18%	5
2,4-dienoyl CoA reductase 1, mitochondrial gi 17105350	23%	5
pyrroline-5-carboxylate reductase 1 gi 157786894	33%	5
PREDICTED: similar to RIKEN cDNA 2810457I06 (Cbl-interacting protein p70) gi 109484556, gi 109483356	6%	4*
CAM kinase II, alpha gi 6978593	15%	4
c-src tyrosine kinase gi 71795633	12%	4
Rous sarcoma oncogene (Src) gi 14010835	5%	3

Table 5.1 continued:

CAM kinase II, gamma gi 19424316	23%	3
high mobility group box 1, (many isoforms) gi 6981026, gi 157820087, gi 109512438 ...	8%	3
Shc-2 gi 157820915	7%	3
similar to son of sevenless homolog 2 gi 109479476, gi 157820915*	4%	3
family with sequence similarity 120B gi 157818809	4%	3
fyn proto-oncogene gi 6978863	5%	3
RAS p21 protein activator 1 gi 6981460	2%	2
CAM kinase II, delta gi 6978595	12%	2
PI3-kinase, catalytic, beta polypeptide gi 16758236	2%	2
non-catalytic region of tyrosine kinase adaptor protein 2 gi 157817418	6%	2
v-crk sarcoma virus CT10 oncogene homolog gi 9506515	4%	1***
zeta-chain (TCR) associated protein kinase gi 58865580	2%	1***
Tyrosine-protein kinase SYK gi 3219819	2%	1***
Serine/threonine-protein kinase DCLK1 gi 20137987	2%	1***
AP-2 complex subunit mu-1-A gi 18034787	2%	1***
hydroxysteroid (17-beta) dehydrogenase 10 gi 13994225	5%	1***
protein kinase N3 gi 114145515	1%	1***
14-3-3 protein zeta/delta gi 62990183	5%	1***
profilin 2 gi 13540707	9%	1***
glycogen synthase kinase 3 beta gi 14091770	3%	1***
adaptor protein complex AP-1, beta 1 subunit gi 8392872	1.5%	1***
Ankyrin repeat and sterile alpha motif domain-containing protein 1B (AIDA-1) gi 182627625	1%	1***
PREDICTED: similar to Tripartite motif protein 7 gi 109490605	2%	1***

* Peptides can't unambiguously assign an isoform, so all possibilities are listed.

*** 1 strong peptide match, data available through PRIDE (accession 9944).

Table 5.2: LRP1 NPXpY₄₅₀₇ interacting proteins identified from solution digest/2DLC-MSMS

Protein (14/39 hits kept) (Peps (>95)) Accession number	Sequence Coverage	# unique of
Shp-2 gi 84028249	33%	15
Shc-3 gi 48474721	21%	7
growth factor receptor bound protein 2 gi 51702260	35%	5
Membrane-associated guanylate kinase inverted 1 gi 123782179	5%	4
CAM kinase II, alpha gi 125285	9%	3
CAM kinase II gamma or beta subunit gi 19424316, gi 108796657, gi 108796659, gi 108796663	3%	2*
c-src tyrosine kinase gi 417209	7%	2
Shp-1 gi 34922906	5%	2
v-crk sarcoma virus CT10 oncogene homolog gi 1169094	10%	2
PI3-kinase, regulatory subunit, (p85 alpha) gi 3914252	3%	2
glutaryl-Coenzyme A dehydrogenase gi 2492632	18%	3
glutamine synthetase 1 gi 55976526	10%	2
pyrroline-5-carboxylate reductase family 2 gi 60390248	18%	4

* Peptides can't unambiguously assign one isoform, so all possibilities are listed.

** Only 1 strong peptide match, data available through PRIDE (accession 9944).

Table 5.3: LRP1 NPXpY₄₄₇₃ interacting proteins from solution digests identified by mass spectrometry with protein pilot

Protein (3/23 hits kept) (Peps (>95)) Accession number	Sequence Coverage	# unique of
Shc-3 gi 48474721	16%	6
growth factor receptor bound protein 2 gi 82236546	12%	2
Peptidyl-prolyl cis-trans isomerase A gi 118107	17%	2

Table 5.4: LRP1 NPXY₄₅₀₇ interacting proteins from solution digests identified by mass spectrometry with protein pilot

Protein (Peps (>95)) Accession number	Sequence Coverage	# unique of
SEC23 homolog A gi 157786714	24%	13
clathrin, heavy polypeptide gi 9506497	10%	11
brain glycogen phosphorylase gi 158187544	21%	10
similar to SEC24 related gene family, member C gi 109502099, gi 109502097, gi 109502091, gi 109502093, gi 109502089, gi 109502095	14%	10
adaptor-related protein complex 2, beta 1 subunit gi 18034787	11%	9
adaptor-related protein complex 2, mu 1 subunit gi 16758938	29%	10
glutamine synthetase 1 gi 142349612	27%	7
pyrroline-5-carboxylate reductase family 2 gi 58865992	32%	8
glutaryl-Coenzyme A dehydrogenase gi 157820807	33%	7
hydroxysteroid (17-beta) dehydrogenase 10 gi 13994225	46%	7
CAM kinase II, alpha gi 6978593	23%	7
CAM kinase II beta subunit gi 108796657, gi 108796659, gi 108796663	9%	4*
14-3-3 protein epsilon gi 13928824	13%	3
14-3-3 protein gamma gi 9507245	10%	3
14-3-3 protein theta gi 6981712	29%	5
14-3-3 protein zeta gi 62990183	20%	4
granulin gi 8393493	6%	2
Membrane-associated guanylate kinase inverted 1 gi 71795664	11%	9
Solute carrier family 25 member 4 gi 32189355	15%	4
Solute carrier family 25 member 12 gi 34854800	9%	2
Solute carrier family 25 member 22 gi 62078785	12%	2
Solute carrier family 25 member 5 gi 32189350	8%	2

Table 5.4 continued:

3-hydroxyacyl-CoA dehydrogenase type-2 gi 7387724	33%	5
USO1 homolog, vesicle docking protein gi 9507177	8%	5
similar glyceraldehyde-3-phosphate dehydrogenase gi 109504062; gi 109503241	11%	2*
gephyrin gi 88853561	6%	3
phosphofructokinase, platelet gi 57977273	4%	7
phosphofructokinase, muscle gi 13929002	3%	2
sideroflexin 3 gi 12621120	14%	2
Ankyrin repeat and sterile alpha motif domain-containing protein 1B (AIDA-1) gi 182627625	3%	2
adaptor protein complex AP-2, alpha 1 subunit gi 157823677	6%	3
adaptor protein complex AP-2, alpha 2 subunit gi 162138932	2%	2

* Peptides can't unambiguously assign an isoform, so all possibilities are listed.

References

- Anderson, D., Koch, C.A., Grey, L., Ellis, C., Moran, M.F., and Pawson, T. 1990. Binding of SH2 domains of phospholipase C α 1, GAP, and Src to activated growth factor receptors. *Science* 250: 979-982.
- Bansal, A., and Gierasch, L.M. 1991. The NPXY internalization signal of the LDL receptor adopts a reverse-turn conformation. *Cell* 67: 1195-1201.
- Barnes, H., Larsen, B., Tyers, M., and van der Geer, P. 2001. Tyrosine-phosphorylated low density lipoprotein receptor-related protein 1 (LRP1) associates with the adaptor protein SHC in SRC-transformed cells. *J Biol Chem*. 276: 19119-19125.
- Barsnes, H., Vizcaíno, J.A., Eidhammer, I., and Martens, L. 2009. PRIDE Converter: making proteomics data-sharing easy. *Nat Biotechnol*. 27: 598-599.
- Betts, G.N., van der Geer, P., and Komives, E.A. 2008. Structural and functional consequences of tyrosine phosphorylation in the LRP1 cytoplasmic domain. *J Biol Chem* 283: 15656-15664.
- Blacker, D., Wilcox, M.A., Laird, N.M., Rodes, L., Horvath, S.M., Go, R.C., Perry, R., Watson, B.J., Bassett, S.S., McInnis, M.G., et al. 1998. Alpha-2 macroglobulin is genetically associated with Alzheimer disease. *Nat. Genet*. 19: 357-360.
- Boucher, P., Liu, P., Gotthardt, M., Hiesberger, T., Anderson, R.G., and Herz, J. 2002. Platelet-derived growth factor mediates tyrosine phosphorylation of the cytoplasmic domain of the low Density lipoprotein receptor-related protein in caveolae. *J Biol Chem*. 277: 15507-15513.
- Corder, E.H., Saunders, A.M., Strittmatter, W.J., Schmechel, D., Gaskell, P.C., Small, G.W., Roses, A.D., Haines, J.L., and Pericak-Vance, M. 1993. Gene doses of apolipoprotein E type 4 allele and the risk of Alzheimer's disease in late onset families. *Science* 261: 921-923.
- Gotthardt, M., Trommsdorff, M., Nevitt, M.F., Shelton, J., Richardson, J.A., Stockinger, W., Nimpf, J., and Herz, J. 2000. Interactions of the low density lipoprotein receptor gene family with cytosolic adaptor and scaffold proteins suggest diverse biological functions in cellular communication and signal transduction. *J Biol Chem*. 275: 25616-25624.
- Herz, J., Hamann, U., Rogne, S., Myklebost, O., Gausepohl, H., and Stanley, K.K. 1988. LRP and senile plaques in Alzheimer's disease: colocalization

with apolipoprotein E and with activated astrocytes. *EMBO J.* 7: 4119-4127.

Herz, J., and Strickland, D.K. 2001. LRP: A multifunctional scavenger and signaling receptor. *J. Clin. Invest.* 108: 779-784.

Kang, D.E., Pietrzik, C.U., Baum, L., Chevallier, N., Merriam, D.E., Kounnas, M.Z., Wagner, S.L., Troncoso, J.C., Kawas, C.H., Katzman, R., et al. 2000. Modulation of amyloid beta-protein clearance and Alzheimer's disease susceptibility by the LDL receptor-related protein pathway. *J. Clin. Invest.* 106: 1159-1166.

Kang, D.E., Saitoh, T., Chen, X., Xia, Y., Masliah, E., Hansen, L.A., Thomas, R.G., Thal, L.J., and Katzman, R. 1997. Genetic association of the low-density lipoprotein receptor-related protein gene (LRP), an apolipoprotein E receptor, with late-onset Alzheimer's disease. *Neurology* 49: 56-61.

Kazlauskas, A., Kashishian, A., Cooper, J.A., and Valius, M. 1992. GTPase-activating protein and phosphatidylinositol 3-kinase bind to distinct regions of the platelet-derived growth factor receptor β subunit. *Mol. Cell. Biol.* 12: 2534-2544.

Keilhack, H., Tenev, T., Nyakatura, E., Godovac-Zimmermann, J., Nielsen, L., Seedorf, K., and Bohmer, F.D. 1998. Phosphotyrosine 1173 mediates binding of the protein-tyrosine phosphatase SHP-1 to the epidermal growth factor receptor and attenuation of receptor signaling. *J Biol Chem* 273: 24839-24846.

Kikuchi, A., Yamamoto, H., and Kishida, S. 2007. Multiplicity of the interactions of Wnt proteins and their receptors. *Cell Signal.* 19: 659-671.

Kounnas, M.Z., Moir, R.D., Rebeck, G.W., Bush, A.I., Argraves, W.S., Tanzi, R.E., Hyman, B.T., and Strickland, D.K. 1995. LDL receptor-related protein, a multifunctional ApoE receptor, binds secreted beta-amyloid precursor protein and mediates its degradation. *Cell* 82: 331-340.

Kozlowski, M., Larose, L., Lee, F., Le, D.M., Rottapel, R., and Siminovitch, K.A. 1998. SHP-1 binds and negatively modulates the c-Kit receptor by interaction with tyrosine 569 in the c-Kit juxtamembrane domain. *Mol Cell Biol* 18: 2089-2099.

Lee, C.H., Kominos, D., Jacques, S., Margolis, B., Schlessinger, J., Shoelson, S.E., and Kuriyan, J. 1994. Crystal structures of peptide complexes of the amino-terminal SH2 domain of the Syp tyrosine phosphatase. *Structure.* 2: 423-438. .

- Lee, G., Newman, S.T., Gard, D.L., Band, H., and Panchamoorthy, G. 1998. Tau interacts with src-family non-receptor tyrosine kinases. *J Cell Sci* 111 (Pt 21): 3167-3177.
- Lee, G., Thangavel, R., Sharma, V.M., Litersky, J.M., Bhaskar, K., Fang, S.M., Do, L.H., Andreadis, A., Van Hoesen, G., and Ksiezak-Reding, H. 2004. Phosphorylation of tau by fyn: implications for Alzheimer's disease. *J Neurosci* 24: 2304-2312.
- Liu, H.Y., and Meakin, S.O. 2002. ShcB and ShcC activation by the Trk family of receptor tyrosine kinases. *J Biol Chem* 277: 26046-26056.
- Loukinova, E., Ranganathan, S., Kuznetsov, S., Gorlatova, N., Migliorini, M.M., Loukinov, D., Ulery, P.G., Mikhailenko, I., Lawrence, D.A., and Strickland, D.K. 2002. Platelet-derived growth factor (PDGF)-induced tyrosine phosphorylation of the low density lipoprotein receptor-related protein (LRP). Evidence for integrated co-receptor function between LRP and the PDGF. *J Biol Chem*. 277: 15499-15506.
- Martens, L., Hermjakob, H., Jones, P., Adamski, M., Taylor, C., States, D., Gevaert, K., Vandekerckhove, J., and Apweiler, R. 2005. PRIDE: the proteomics identifications database. *Proteomics* 5: 3537-3545.
- Mimnaugh EG, B.P., Neckers L. 1999. The measurement of ubiquitin and ubiquitinated proteins. *Electrophoresis* 20: 418-428.
- Minopoli, G., Passaro, F., Aloia, L., Carlomagno, F., Melillo, R.M., Santoro, M., Forzati, F., Zambrano, N., and Russo, T. 2007. Receptor- and Non-Receptor Tyrosine Kinases Induce Processing of the Amyloid Precursor Protein: Role of the Low-Density Lipoprotein Receptor-Related Protein. *Neurodegenerative Diseases* 4: 94-100.
- Newton, C.S., Loukinova, E., Mikhailenko, I., Ranganathan, S., Gao, Y., Haudenschild, C., and Strickland, D.K. 2005. Platelet-derived growth factor receptor-beta (PDGFR-beta) activation promotes its association with the low density lipoprotein receptor-related protein (LRP). Evidence for co-receptor function. *J Biol Chem*. 280: 27872-27878.
- O'Bryan, J.P., Songyang, Z., Cantley, L., Der, C.J., and Pawson, T. 1996. A mammalian adaptor protein with conserved Src homology 2 and phosphotyrosine-binding domains is related to Shc and is specifically expressed in the brain. *Proc Natl Acad Sci U S A* 93: 2729-2734.

- Peltan, I.D., Thomas, A.V., Mikhailenko, I., Strickland, D.K., Hyman, B.T., and von Arnim, C.A.F. 2006. Fluorescence lifetime imaging microscopy (FLIM) detects stimulus-dependent phosphorylation of the low density lipoprotein receptor-related protein (LRP) in primary neurons. *Biochemical and Biophysical Research Communications* 349: 24-30.
- Pietrzik, C.U., Busse, T., BMerriam, D.E., Weggen, S., and Koo, E.H. 2002. The cytoplasmic domain of the LDL receptor-related protein regulates multiple steps in APP processing. *EMBO J.* 21: 5691-5700.
- Pietrzik, C.U., Yoon, I.S., Jaeger, S., Busse, T., Weggen, S., and Koo, E.H. 2004. FE65 constitutes the functional link between the low-density lipoprotein receptor-related protein and the amyloid precursor protein. *J Neurosci.*: 4259-4265.
- Ponti, G., Conti, L., Cataudella, T., Zuccato, C., Magrassi, L., Rossi, F., Bonfanti, L., and Cattaneo, E. 2005. Comparative expression profiles of ShcB and ShcC phosphotyrosine adapter molecules in the adult brain. *Neuroscience* 133: 105-115.
- Ronnstrand, L., Arvidsson, A.K., Kallin, A., Rorsman, C., Hellman, U., Engstrom, U., Wernstedt, C., and Heldin, C.H. 1999. SHP-2 binds to Tyr763 and Tyr1009 in the PDGF beta-receptor and mediates PDGF-induced activation of the Ras/MAP kinase pathway and chemotaxis. *Oncogene* 18: 3696-3702.
- Sakkab, D., Lewitzky, M., Posern, G., Schaeper, U., Sachs, M., Birchmeier, W., and Feller, S.M. 2000. Signaling of hepatocyte growth factor/scatter factor (HGF) to the small GTPase Rap1 via the large docking protein Gab1 and the adapter protein CRKL. *J Biol Chem* 275: 10772-10778.
- Sengupta, A., Grundke-Iqbal, I., and Iqbal, K. 2006. Regulation of phosphorylation of tau by protein kinases in rat brain. *Neurochem Res* 31: 1473-1480.
- Shilov, I.V., Seymour, S.L., Patel, A.A., Loboda, A., Tang, W.H., Keating, S.P., Hunter, C.L., Nuwaysir, L.M., and Schaeffer, D.A. 2007. The Paragon Algorithm, a Next Generation Search Engine That Uses Sequence Temperature Values and Feature Probabilities to Identify Peptides from Tandem Mass Spectra. *Mol Cell Proteomics* 6: 1638-1655.
- Smith, M.J., Hardy, W.R., Murphy, J.M., Jones, N., and Pawson, T. 2006. Screening for PTB domain binding partners and ligand specificity using proteome-derived NPXY peptide arrays. *Mol Cell Biol.* 26: 8461-8474.

- Strickland, D.A., and Ranganathan, S. 2003. Diverse role of LDL receptor-related protein in the clearance of proteases and in signalling. *J. Thromb. Haemost.* 1: 1663-1670.
- Su, H.P., Nakada-Tsukui, K., Tosello-Tramont, A.C., Li, Y., Bu, G., Henson, P.M., and Ravichandran, K.S. 2002. Interaction of CED-6/GULP, an adapter protein involved in engulfment of apoptotic cells with CED-1 and CD91/low density lipoprotein receptor-related protein (LRP). *J Biol Chem.* 277: 11772-11779.
- Sumioka, A., Nagaishi, S., Yoshida, T., Lin, A., Miura, M., and Suzuki, T. 2005. Role of 14-3-3 γ in FE65-dependent Gene Transactivation Mediated by the Amyloid β -Protein Precursor Cytoplasmic Fragment. *J. Biol. Chem.* 280: 42364-42374.
- Takayama, Y., May, P., Anderson, R.G., and Herz, J. 2005. Low density lipoprotein receptor-related protein 1 (LRP1) controls endocytosis and c-CBL-mediated ubiquitination of the platelet-derived growth factor receptor beta (PDGFR beta). *J Biol Chem.* 280: 18504-18510. .
- Tarr, P.E., Roncarati, R., Pelicci, G., Pelicci, P.G., and D'Adamio, L. 2002. Tyrosine Phosphorylation of the beta -Amyloid Precursor Protein Cytoplasmic Tail Promotes Interaction with Shc. *J. Biol. Chem.* 277: 16798-16804.
- Trommsdorff, M., Borg, J.P., Margolis, B., and Herz, J. 1998. Interactions of cytosolic adaptor proteins with neuronal apolipoprotein E receptors and the amyloid precursor protein. *J. Biol. Chem.* 273: 1031-1039.
- Trommsdorff, M., Gotthardt, M., Hiesberger, T., Shelton, J., Stockinger, W., Nimpf, J., Hammer, R.E., Richardson, J.A., and Herz, J. 1999. Reeler/Disabled-like disruption of neuronal migration in knockout mice lacking the VLDL receptor and ApoE receptor 2. *Cell.* 97: 689-701.
- Twamley, G.M., Kypta, R.M., Hall, B., and Courtneidge, S.A. 1992. Association of Fyn with the activated platelet-derived growth factor receptor: requirements for binding and phosphorylation. *Oncogene* 7: 1893-1901.
- van der Geer, P., Wiley, S., Gish, G.D., Lai, V.K., Stephens, R., White, M.F., Kaplan, D., and Pawson, T. 1996. Identification of residues that control specific binding of the Shc phosphotyrosine-binding domain to phosphotyrosine sites. *Proc Natl Acad Sci U S A.* 93: 963-968.
- van Kerkhof, P., Lee, J., McCormick, L., Tetrault, E., Lu, W., Schoenfish, M., Oorschot, V., Strous, G.J., Klumperman, J., and Bu, G. 2005. Sorting

nexin 17 facilitates LRP recycling in the early endosome. *Embo J* 24: 2851-2861.

- Wilhelmsen, K., J., C., Glenn, G., Hoffman, R.C., Tucker, P., and van der Geer, P. 2004. Purification and identification of protein-tyrosine kinase-binding proteins using synthetic phosphopeptides as affinity reagents. *Mol Cell Proteomics*. 3: 887-895. .
- Williamson, R., Scales, T., Clark, B.R., Gibb, G., Reynolds, C.H., Kellie, S., Bird, I.N., Varndell, I.M., Sheppard, P.W., Everall, I., et al. 2002. Rapid tyrosine phosphorylation of neuronal proteins including tau and focal adhesion kinase in response to amyloid-beta peptide exposure: involvement of Src family protein kinases. *J Neurosci* 22: 10-20.
- Wolters, D.A., Washburn, M.P., and Yates, J.R.r. 2001. An automated multidimensional protein identification technology for shotgun proteomics. *Analytical Chemistry* 73: 5683-5690.
- Wu, L., and Gonias, S.L. 2005. The low-density lipoprotein receptor-related protein-1 associates transiently with lipid rafts. *J Cell Biochem*. 96: 1021-1033.
- Xie, Z., Dong, Y., Maeda, U., Xia, W., and Tanzi, R.E. 2007. RNA interference silencing of the adaptor molecules ShcC and Fe65 differentially affect amyloid precursor protein processing and Abeta generation. *J Biol Chem*. 282: 4318-4325. .
- Yamamoto, H., Yamauchi, E., Taniguchi, H., Ono, T., and Miyamoto, E. 2002. Phosphorylation of microtubule-associated protein tau by Ca²⁺/calmodulin-dependent protein kinase II in its tubulin binding sites. *Arch Biochem Biophys* 408: 255-262.
- Yoon, I.-S., Pietrzik, C.U., Kang, D.E., and Koo, E.H. 2005. Sequences from the Low Density Lipoprotein Receptor-related Protein (LRP) Cytoplasmic Domain Enhance Amyloid {beta} Protein Production via the {beta}-Secretase Pathway without Altering Amyloid Precursor Protein/LRP Nuclear Signaling. *J. Biol. Chem*. 280: 20140-20147.

This chapter is, in part, a reprint of a submitted manuscript in press:

Interactions of the NPXY microdomains of the LDL Receptor-Related Protein 1.

Guttman, M., Betts, G.N., Barnes, H., Ghassemian, M., van der Geer, P. and

Komives, E.A. (2009) *Proteomics, in press*. The dissertation author was the primary researcher and author of this manuscript.